ABSTRACT

Title of dissertation: COOPERATIVE NETWORKING
AND RELATED ISSUES:
STABILITY, ENERGY HARVESTING,
AND NEIGHBOR DISCOVERY

Jeongho Jeon, Doctor of Philosophy, 2013

Dissertation directed by: Professor Anthony Ephremides
Department of Electrical and Computer Engineering

This dissertation deals with various newly emerging topics in the context of cooperative networking. The first part is about the cognitive radio. To guarantee the performance of high priority users, it is important to know the activity of the high priority communication system but the knowledge is usually imperfect due to randomness in the observed signal. In such a context, the stability property of cognitive radio systems in the presence of sensing errors is studied. General guidelines on controlling the operating point of the sensing device over its receiver operating characteristics are also given. We then consider the hybrid of different modes of operation for cognitive radio systems with time-varying connectivity. The random connectivity gives additional chances that can be utilized by the low priority communication system.

The second part of this dissertation is about the random access. We are specifically interested in the scenario when the nodes are harvesting energy from the environment. For such a system, we accurately assess the effect of limited, but renewable, energy availability on the stability region. The effect of finite capacity batteries is also studied. We

next consider the exploitation of diversity amongst users under random access framework. That is, each user adapts its transmission probability based on the local channel state information in a decentralized manner. The impact of imperfect channel state information on the stability region is investigated. Furthermore, it is compared to the class of stationary scheduling policies that make centralized decisions based on the channel state feedback.

The backpressure policy for cross-layer control of wireless multi-hop networks is known to be throughput-optimal for i.i.d. arrivals. The third part of this dissertation is about the backpressure-based control for networks with time-correlated arrivals that may exhibit long-range dependency. It is shown that the original backpressure policy is still throughput-optimal but with increased average network delay. The case when the arrival rate vector is possibly outside the stability region is also studied by augmenting the backpressure policy with the flow control mechanism.

Lastly, the problem of neighbor discovery in a wireless sensor network is dealt. We first introduce the realistic effect of physical layer considerations in the evaluation of the performance of logical discovery algorithms by incorporating physical layer parameters. Secondly, given the lack of knowledge of the number of neighbors along with the lack of knowledge of the individual signal parameters, we adopt the viewpoint of random set theory to the problem of detecting the transmitting neighbors. Random set theory is a generalization of standard probability theory by assigning sets, rather than values, to random outcomes and it has been applied to multi-user detection problem when the set of transmitters are unknown and dynamically changing.

COOPERATIVE NETWORKING AND RELATED ISSUES: STABILITY, ENERGY HARVESTING, AND NEIGHBOR DISCOVERY

by

Jeongho Jeon

Dissertation submitted to the Faculty of the Graduate School of the
University of Maryland, College Park in partial fulfillment
of the requirements for the degree of
Doctor of Philosophy
2013

Advisory Committee:
Professor Anthony Ephremides, Chair/Advisor
Professor Sennur Ulukus
Professor Richard J. La
Professor Prakash Narayan
Professor Aravind Srinivasan

Dedication

To Bukyung

Acknowledgments

I would like to appreciate my advisor Professor Ephremides for giving me the opportunity to work with him. This thesis would not have been possible without his guidance, encouragement, and generous support.

Table of Contents

Chapter 1

Introduction

1.1 Motivation

The cognitive radio, a means of opening up licensed bands to unlicensed users, has the potential to become a solution to the current spectrum underutilization problem [1–4]. Exploiting renewable energy resources from the environment, often termed energy harvesting, permits unattended operation of infrastructureless distributed wireless networks [5–7]. The diversity amongst users due to constructive/destructive effect of multipath signal propagation can be exploited to increase the data rate [8]. The cross-layer approach can significantly leverage the overall network performance when compared to the conventional layered approach [9]. The wireless sensor networks have great versatility in civilian/military applications such as environmental monitoring and target detection/tracking in a cost-effective manner [10]. This dissertation deals with such newly emerging topics in wireless communications and networking.

There is an increasing demand for variety of wireless devices and applications for our daily lives, but the usable electromagnetic radio spectrum is of limited physical extend. Recent studies on the spectrum usage have revealed that substantial portion of the licensed spectrum is underutilized, which arouses a pressing need for developing a new technique for improved spectrum utilization [1]. The cognitive radio communication is a promising solution to the spectrum underutilization problem [2–4]. The high-priority

user, often called as the primary (or licensed), is allowed to access the spectrum whenever it needs, while the low-priority user, called as the secondary, is required to make a decision on its transmission based on what the primary user does. Thus, knowing the activity of the primary user is an important part of operating the cognitive radio systems. In reality, such knowledge is acquired through a certain decision process at the secondary user, which is subject to errors. In such a context, we study the effect of practical spectrum sensing on the stability of cognitive radio systems. Furthermore, the problem of controlling the operating point of the sensing device over its receiver operating characteristic is dealt.

On the other hand, there have been different communication models proposed for cognitive radio, which are broadly classified into *overlay*, *underlay*, and *interweave* modes [11]. The overlay approach allows concurrent primary and secondary transmissions, but the secondary users are required to use part of their power to assist primary transmissions and the remainder of the power for its own communication. The enabling premise is that the secondary user knows the primary message non-casually, which makes the implementation of the overlay mode practically challenging. The underlay mode also allows concurrent primary and secondary transmissions, but the primary communication is protected via regulating the power of the secondary user such that the induced amount of interference at the primary destination is kept below the acceptable noise floor. In both the underlay and overlay modes, concurrent primary and secondary user operation is invariably associated with interference at the primary destination, which is not desired. The interweave approach is based on the idea of opportunistic communication exploiting the idleness of the primary user. In this thesis, the hybrid of interweave and underlay

modes of operation for cognitive radio systems with time-varying connectivity is considered. Note that the random connectivity of links gives additional chances that can be utilized by the secondary communication system. That is, although the primary system is active, the secondary system can operate in the interweave mode when the link between the secondary transmitter and the primary receiver is disconnected.

The ALOHA protocol, the simple scheme of attempting transmission randomly, independently, distributively, and based on simple ACK/NACK feedback from the receiver, has gained continued popularity since its creation by Abramson [12, 13]. It is especially suitable for distributed multi-access communication systems due to its simplicity and the independence of the centralized controller. It also serves as a cornerstone benchmark for assessment of performance of more elaborate schemes. On the other hand, exploiting renewable energy resources such as thermal, vibration, solar, acoustic, wind, and even ambient radio power allows unattended operation of infrastructureless distributed wireless networks [5–7]. Despite the rapid advancement of hardware technologies, the study of communication systems comprised of nodes that have energy harvesting capability are still in a very early stage. Note that when dealing with nodes equipped with non-rechargeable batteries, the common objectives were usually short-term such as maximizing the finite *network lifetime* [14, 15]. The functionality of harvesting energy permits our assessment of the system long-term performance such as throughput, fairness and stability. In such a context, we revisit the canonical problem of the random access stability when nodes are powered by batteries recharging from randomly time-varying renewable energy sources.

Increasing demand for high data rate to support a wide range of services in wireless

data networks has led to the exploitation of diversity amongst users [8]. The diversity gain arises from the fact that wireless links experience random fading due to the constructive/destructive effect of multipath signal propagation and, thereby, there is always a user having better channel quality than the others at any time [16]. A downlink scheduler exploiting such diversity gain is called the opportunistic scheduler [17–19]. Similar concept can be applied to the uplink communication but it is needed to have a centralized controller gathering channel state information (CSI) from distributed users, making a centralized decision, and distributing the decision information back to the distributed users. There is a recent line of work on exploiting CSI under random access framework, which is called channel-aware random access (CARA) [20–23]. The CARA allows the distributed nodes to adjust their random access probability based on the local CSI. However, most of the previous work on CARA was performed based on the ideal assumption that the perfect local CSI is available at each user [20–23]. In reality, however, the CSI is imperfect due to randomness in the observed signal and the performance of CARA would highly depend on the accuracy of CSI. In such a context, the performance of CARA in the presence of channel estimation errors is studied and the impact of imperfect CSI on the achieved stability region is identified.

In [24], the problem of optimal control for general wireless multi-hop networks was studied and a maximum throughput policy that supports the entire stability region was proposed, although the region is unknown a priori. The maximum throughput policy is comprised of two parts: maximum differential backlog routing and max-weight scheduling. Since the policy selects paths dynamically according to the differential backlog between neighboring nodes (rather than requiring them to be specified in advance), it is often

referred to as the *backpressure* policy. After the original work of [24], there has been a lot of effort on its generalization and extension [25–32]. A notable achievement concerned the case where the arrival rate vector is possibly outside the stability region [26, 27]. This was accomplished by augmenting the backpressure policy with the flow control mechanism that is designed to maximize the network utility [9, 33–36]. Despite the significance of the original work and its extensions, one weakness might be the fact that they were derived under the assumption that the number of packet arrivals at each node is independent and identically distributed (i.i.d.) over time slots. Several measurement-based studies have revealed that scale-invariant burstiness, often called as *self-similarity*, exists in local/wide-area network and Internet traffic [37–39]. Possible explanation includes heavy-tailed file size distribution, human interactions, and protocol-level dynamics. It was also shown that the variable-bit-rate video traffic is long-range dependent [40]. Self-similarity and long-range dependence are two distinct concepts and, hence, one does not necessarily imply the other. However, when both are viewed at the asymptotically large scale, they are identical [41]. In such a context, we revisit the backpressure-based stochastic control for wireless multi-hop networks with time-correlated arrivals. Specifically, the considered arrival process is fairly general in the sense that it may exhibit short/long-range dependence depending on the asymptotic shape of the autocorrelation function.

In a wireless sensor network, a large number of sensors are randomly deployed over the region of interest and, presumably, neighbor discovery is the first and foremost process to run after the deployment to form a network whose connectivity greatly affects the performance of subsequent network operations over the entire life span [42]. The challenge is compounded by the fact that neighbor discovery has to be done without any a priori

knowledge on the random deployment or any communication infrastructures. The problem of neighbor discovery is considered in this thesis by incorporating the physical layer parameters in contrast to the most of the previous work [42–45]. In [42], which assumed a collision channel. Specifically, the pilot signals that nodes transmit are successfully decoded if the strength of the received signal relative to the interference is sufficiently high. Thus, each node must extract signal parameter information from the superposition of an unknown number of received signals. This problem falls naturally in the purview of random set theory (RST) which generalizes standard probability theory by assigning *sets*, rather than values, to random outcomes [46]. First, we introduce the realistic effect of physical layer considerations in the evaluation of the performance of *logical* discovery algorithms; such an introduction is necessary for the accurate assessment of how an algorithm performs. Secondly, given the *double* uncertainty of the environment (that is, the lack of knowledge of the number of neighbors along with the lack of knowledge of the individual signal parameters), we adopt the viewpoint of RST and demonstrate its advantage relative to classical matched filter detection method.

1.2 Thesis Outline

This thesis is organized as follows. In Chapter 2, we explain the model for the success of packet transmissions, revisit the notion of stability, and describe the stochastic dominance technique used in the subsequent chapters, which is a useful tool to deal with systems of interacting queues. Chapter 3 is about the cognitive radio systems comprised of a set of source-destination pairs having different priorities in accessing the shared

medium. Specifically, in Chapter 3.2, the stability property of cognitive radio systems in the presence of sensing errors is studied. In Chapter 3.3, we consider the hybrid cognitive access for systems with time-varying connectivity. Chapter 4 is about the random access systems. The scenario when the nodes are harvesting energy from the environment is studied in Chapter 4.2. We then move to the channel-aware random access in the presence of channel estimation errors in Chapter 4.3. Chapter 5 extends the backpressure-based stochastic control for general wireless multi-hop networks to the case when the arrivals are time-correlated. Specifically, in Chapter 5.3, we consider the case when the arrival rate vector is inside the stability region, and Chapter 5.4 deals with the case when the arrival rate vector is possibly outside the stability region. In Chapter 6, we study the problem of neighbor discovery in a wireless sensor network. The performance of chosen neighbor discovery algorithm is precisely analyzed in Chapter 6.4 by incorporating physical layer parameters. In Chapter 6.5, the problem of detecting the transmitting neighbors is considered using random set theory. Finally, we draw conclusions in Chapter 7 with summary on additional contributions and collaborations.

Chapter 2

Stability of Constrained Queueing Systems

2.1 SINR-Based Model for Packet Transmissions

A queueing system is constrained in the sense that the services are interdependent such as the activation of links in wireless networks. A simplistic form describing such dependency might be the collision channel model, in which if more than one nodes transmit at the same time, none of them are successful. However, it is too pessimistic in the sense that a transmission may succeed even in the presence of interference, which is called *capture effect* [47–51]. Throughout this thesis, we consider interfering channels and nodes whose transmissions are successful if the received signal-to-interference-plus-noise-ratio (SINR) exceeds a certain threshold. This reflects the effect of fading, attenuation and interference at the physical layer, along with the capability of multi-user detection at the receiver [51–54]. Denote with $q_{i|\mathcal{M}}$ the success probability of node i when a set $\mathcal{M}$ of nodes are transmitting simultaneously. The success probability $q_{i|\mathcal{M}}$ is a function of the received SINR as

$$q_{i|\mathcal{M}} = \Pr[\gamma_{i|\mathcal{M}} \geq \theta] \tag{2.1}$$

where $\gamma_{i|\mathcal{M}}$ denotes node i's SINR at the receiver given set $\mathcal{M}$ of transmitters and θ is the threshold for the successful decoding of the received packets, which depends on the modulation scheme, target bit-error-rate, and the number of bits in the packet, i.e., the transmission rate. The use of matched filters was implicitly assumed in writing Eq. (2.1)

for decoding the signal at the receiver, which fundamentally treats interference as white Gaussian noise. Although techniques such as the successive interference cancellation [55] can improve the probability of success, comparing different physical layer techniques is outside the scope of our work here.

The SINR of the signal transmitted from node i at the receiver is described as

$$\gamma_{i|\mathcal{M}} = \frac{P_{\mathrm{rx},i}}{N + \sum_{j \in \mathcal{M} \setminus \{i\}} P_{\mathrm{rx},j}}$$

where $\mathcal{M}$ is the set of nodes transmitting simultaneously, N is the background noise power, and $P_{\mathrm{rx},i}$ is the received signal power from node i at the receiver which is modeled by

$$P_{\mathrm{rx},i} = \psi_i^2 K r_i^{-\nu} P_{\mathrm{tx},i}$$

where ψ_i is a Rayleigh random variable with $E[\psi_i^2] = 1$, K is a constant, ν is the propagation loss exponent, r_i is the distance between node i and the receiver, and $P_{\mathrm{tx},i}$ is the transmission power of node i. Let $f_{\psi_i^2}$ be the probability density function of ψ_i^2, which is exponential with unit mean [56]. Then, the success probability of a transmission by node i when it transmits alone is computed as

$$\begin{aligned} q_{i|\{i\}} &= \Pr\left[\frac{\psi_i^2 K r_i^{-\nu} P_{\mathrm{tx},i}}{N} \geq \theta\right] \\ &= \int_0^\infty \Pr\left[\omega \geq \frac{\theta N r_i^\nu}{K P_{\mathrm{tx},i}}\right] f_{\psi_i^2}(\omega) d\omega \\ &= \exp\left(-\frac{\theta N r_i^\nu}{K P_{\mathrm{tx},i}}\right) \end{aligned}$$

Similarly, the success probability of a transmission by node i when it transmits along with

the other node j is given by

$$\begin{aligned} q_{i|\{i,j\}} &= \Pr\left[\frac{\psi_i^2 K r_i^{-\nu} P_{\text{tx},i}}{N + \psi_j^2 K r_j^{-\nu} P_{\text{tx},j}} \geq \theta\right] \\ &= \int_0^\infty \int_0^\infty \Pr\left[\omega_i \geq \frac{\theta(N + \omega_j K r_j^{-\nu} P_{\text{tx},j})}{K r_i^{-\nu} P_{\text{tx},i}}\right] f_{\psi_i^2}(\omega_i) f_{\psi_j^2}(\omega_j) d\omega_i d\omega_j \\ &= \int_0^\infty \exp\left(-\frac{\theta(N + \omega_j K r_j^{-\nu} P_{\text{tx},j})}{K r_i^{-\nu} P_{\text{tx},i}}\right) f_{\psi_j^2}(\omega_j) d\omega_j \\ &= \left(1 + \theta \frac{P_{\text{tx},j}}{P_{\text{tx},i}} \left(\frac{r_i}{r_j}\right)^\nu\right)^{-1} \exp\left(-\frac{\theta N r_i^\nu}{K P_{\text{tx},i}}\right) \end{aligned}$$

where $i, j \in \{1, 2\}$, $j \neq i$, and ψ_i and ψ_j were assumed mutually independent. Similarly, it can be extended to the case when multiple interfering signals exist and the computation involves multiple integrals over the fading distributions.

Note from Eq. (2.1) that, if $\theta < 1$, it is possible for two or more signals to simultaneously satisfy the criterion, and if $\theta \geq 1$, at most one signal having the highest SINR may satisfy the criterion. If θ goes to ∞ and the noise effect is neglected, the criterion in Eq. (2.1) is equivalent to the collision channel model, and if θ goes to 0, all transmissions will be successful, but at the same time, the data rate also goes to 0.

2.2 Revisiting the Notion of Stability

We adopt the notion of stability used in [57] in which the stability of a queue is equivalent to the existence of a proper limiting distribution. In other words, a queue is said to be *stable* if

$$\lim_{n\to\infty} \Pr[Q_i(n) < x] = F(x) \text{ and } \lim_{x\to\infty} F(x) = 1$$

If a weaker condition holds, namely,

$$\lim_{x\to\infty} \liminf_{n\to\infty} \Pr[Q_i(n) < x] = 1$$

the queue is said to be *substable* or bounded in probability. Otherwise, the queue is *unstable*. A stable queue is necessarily substable, but a substable queue is stable if the distribution tends to a limit. If $Q_i(n)$ is an aperiodic and irreducible Markov chain defined on a countable space, substability is equivalent to the stability and it can be understood as the recurrence of the chain. Both the positive and null recurrence imply stability because a limiting distribution exists for both cases although the latter may be degenerate.

Loynes' theorem plays a central role in the stability analysis [58]. It states that if the arrival and service processes of a queue are strictly jointly stationary and the average arrival rate is less than the average service rate, the queue is stable. If the average arrival rate is greater than the average service rate, the queue is unstable and the value of $Q_i(n)$ approaches infinity almost surely. If they are equal, the queue can be either stable or substable.

2.3 Stochastic Dominance Technique

Consider two-node random access having bursty packet arrivals. Even with the collision channel model, the stability analysis is non-trivial due to the interaction between queues. That is, the service process of a queue depends on the status of the other and, thus, the rates of the individual departure processes cannot be computed directly without knowing the stationary probability of the joint queue length process. One way to bypass this difficulty is the stochastic dominance technique for two-node systems, which was

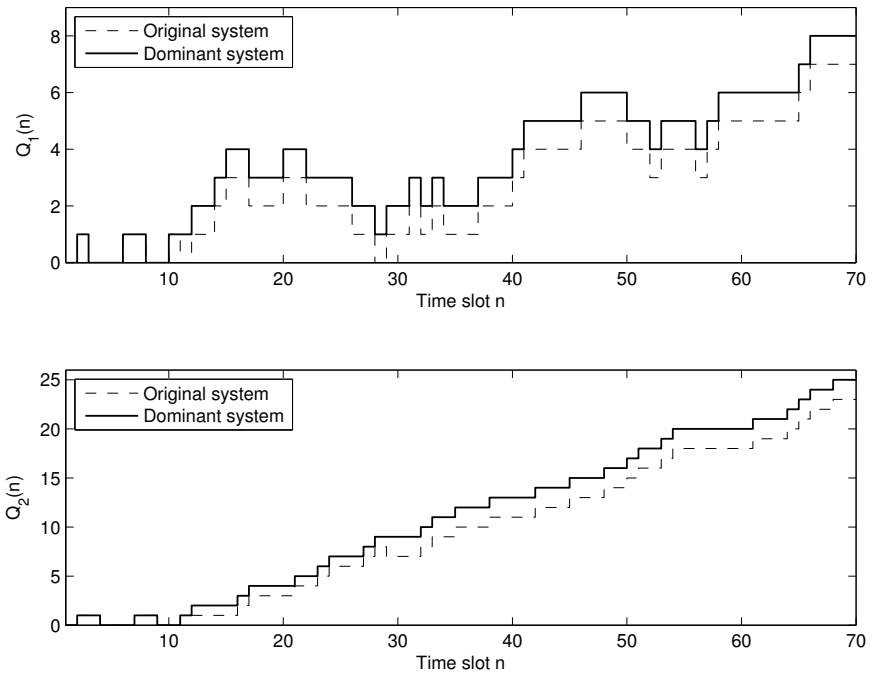

Figure 2.1: Example queue length sample path of the cognitive radio system in Chapter 3.2

introduced in [59] and further utilized to deal with such interacting queueing systems [53, 60–63]. The essence of the stochastic dominance technique is to decouple the interaction between queues via the construction of a hypothetical system which operates as follows: i) the packet arrivals at each node occur at *exactly* the same instants as in the original system, ii) the *coin tosses* that determine the random access of nodes have *exactly* the same outcomes in both systems, iii) however, one of the nodes in the system continues to transmit dummy packets even when its packet queue is empty. Sending dummy packets is only aimed to cause constant interference to the other node regardless of the emptiness of its own queue and does not contribute to throughput. It is obvious that sample-pathwise the queue sizes in this dominant system will never be smaller than their counterparts in

the original system, provided the queues start with identical initial conditions, which is depicted in Fig. 2.1. Thus, the stability condition obtained for the dominant system is a sufficient condition for the stability of the original system. It turns out, however, that it is indeed sufficient and necessary. The reason is this: if for some input rate vector, the queue at the node transmitting dummy packets is unstable in the hypothetical system, then the size of the corresponding queue approaches infinity almost surely. Note that as long as the queue does not empty, the behavior of the hypothetical system and the original system are identical, provided they start from the same initial conditions, since dummy packets will never have to be used. A sample-path that goes to infinity without visiting the empty state, which is a feasible one for a queue that is unstable, will be identical for both the hypothetical and the original systems. Therefore, the instability of the hypothetical system implies the instability of the original system. For more details, please refer [59].

Chapter 3

Cognitive Radio

3.1 Background

We begin with some background study on cognitive radio. In [64], an opportunistic scheduling policy for cognitive access systems was developed based on the collision channel model. Furthermore, the activity of the primary user was modeled as a random process which evolves independent of the secondary users. In other words, even if the primary user's packet is lost due to the collision caused by a secondary user, the primary user does not attempt to retransmit the lost packet; this cannot be validated in the majority of data networks. Unless the primary user is servicing a certain loss-tolerant application, the lost packets must be retransmitted through a medium access control (MAC) protocol such as the automatic-repeat-request (ARQ) and those retransmissions would surely affect the primary user's activity. In [65], the unrealistic assumption made in the previous work [64] mentioned above was corrected for a reduced system model consisting of a single primary and secondary user. In such an effort, an active period that the primary user transmits successively until it becomes idle was defined as an interval that the primary user's packet queue is non-empty. This is based on the assumption that the primary user transmits whenever its queue is non-empty. Consequently, the primary user's activity is affected by the secondary user through the queueing dynamics because the interference caused by concurrent transmissions lowers the service rate of the queue. For the considered model, a

joint flow control and power allocation policy was obtained, but the derivation is based on the assumption that the primary user is always stable. In the absence of the knowledge on the network stability region, however, it is infeasible to judge the stability of the primary user's queue a priori, and the characterization of the stability region is usually not an easy problem especially when the network nodes are *interacting*. In [66], the interaction between users was fully taken into account for a similar network model with that considered in [65]. In contrast to the traditional notion of cognitive radio, in which the secondary user is required to relinquish the channel as soon as the primary user is detected, the secondary user is allowed to not only exploit the idle slots of the primary user but also to transmit along with the primary user with some probability to attain full utilization of the shared channel with capture. Such abolition of strong primacy, however, requires the secondary user to properly control its multi-access probability in the way that it does not hamper the stability of the primary user at any given input rate whenever it is stabilizable. In [60], the approach in [66] was further extended to the scenario when the primary user is powered from a randomly time-varying renewable energy source and has a battery for storing the harvested energy. The limited energy availability imposed by the battery status results in a reduced stability region, which is precisely quantified in the paper.

3.2 Cognitive Radio with Imperfect Sensing

3.2.1 Motivation

Most of the previous work on cognitive radio, e.g., [60, 64–66], was performed based on the ideal assumption that the secondary user always knows the exact activity of

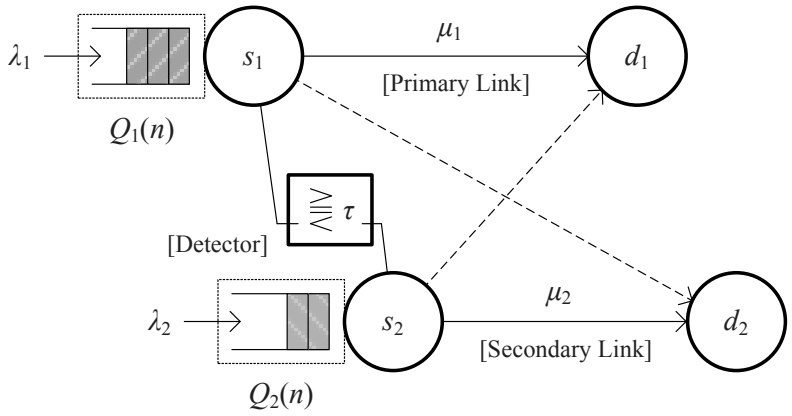

Figure 3.1: The cognitive access system model with sensing at the secondary source

the primary user without an error. In reality, however, such knowledge is acquired through a certain decision process at the secondary user, and it is partial knowledge because the occurrence of errors in the decision process is inevitable as long as there exists randomness in the observed signal. In [67], the performance of the energy detector, which is popular due to its generosity and low complexity [68], was derived in terms of the probabilities of *false alarm* and *miss*, which are functions of the sensing duration, the sampling rate, and the received signal-to-noise-ratio (SNR). After that, the sensing duration is optimized in order to maximize the secondary user's throughput at given target error probabilities, but the primary user's activity was abstracted as in [64] as a random process with fixed a priori probability. In [69], the approach in [67] was extended to the multi-channel scenario, and a cooperative sensing scheduling policy was proposed to detect the activities over the channels.

In this chapter, we focus attention on the effect of practical spectrum sensing on which the overall performance of the cognitive access system depends. The opportunistic cognitive access protocol proposed in [66] is considered again for the system consisting

of a single primary and secondary source-destination pair as shown in Fig. 4.9. The primary user transmits uninterruptedly whenever its queue is non-empty which is independent of actions made by the secondary user. On the other hand, the transmission by the secondary user is chosen in a careful manner that does not hamper the primary user's stability guarantee. The secondary user first observes the activity of the primary user and, if it is sensed to be idle, the secondary user transmits with probability 1 if its packet queue is non-empty. Otherwise, if the primary user is sensed to be active, the secondary user transmits with some probability p to take advantage of the capture effect although, at the same time, it risks impeding the primary user's success. Our design objective is, therefore, to optimally choose the multi-access probability p by the secondary user so as to maximize its own stable throughput while ensuring the stability of the primary user at given input rate demand in the presence of sensing errors at the secondary user.

Our contributions can be summarized as follows. First, we introduce a practical model for cognitive access systems. Specifically, when compared to the previous work that oversimplified the primary user's activity [64, 67, 69], the primary user's activity in this work is precisely modeled through the queueing dynamics which is also subject to the interference caused by the secondary user. Furthermore, the imperfect spectrum sensing, one of the most practical aspects of cognitive access systems but generally overlooked in most of the related previous work [60, 64–66], is also incorporated in the model. Secondly, the impact of imperfect sensing on the stability of the cognitive access systems is precisely analyzed. The remarkable result is that there exists a condition for which we can achieve identical stability region that is achieved with perfect sensing, which fundamentally eliminates the need for the spectrum sensing itself. This is the case when relatively

strong capture effect exists and the condition is expressed in terms of value of physical layer parameters. For the case when the condition does not hold, we quantify the loss due to the imperfect sensing in terms of the size of the stability region when compared against the case when perfect sensing is performed. Finally, we study the problem of controlling the operating point of the sensing device over its receiver operating characteristic (ROC) and summarize some key aspects observed in the control.

3.2.2 System Model

We consider a system consisting of two source-destination pairs, the primary pair (s_1, d_1) and the secondary pair (s_2, d_2), as shown in Fig. 4.9. Each source s_i, $i \in \{1, 2\}$, has an infinite size queue for storing the arriving packets of fixed length. Time is slotted and the slot duration is equal to a packet transmission time. As illustrated in Fig. 3.2, the primary user's transmission consists of the preamble symbols followed by the encoded data symbols of a packet, if the primary user transmits during time slot n. Otherwise, if the primary user does not transmit, the entire slot is unused. It is assumed that the secondary user knows the exact timing of the primary user's frame and performs sensing during the preamble symbol duration. Once the secondary user decides to transmit, it transmits over the primary user's data symbol duration in a synchronous manner. It is assumed that the acknowledgments (ACKs) on the success of transmissions are sent back from the destinations to the corresponding sources instantaneously and error-free.

Let $Q_i(n)$ denote the number of packets buffered at s_i at the beginning of the n-th

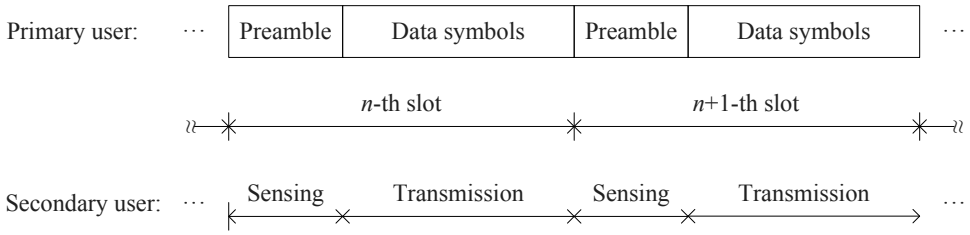

Figure 3.2: Frame structure for cognitive access systems with periodic sensing

slot which evolves according to

$$Q_i(n+1) = \max[Q_i(n) - \mu_i(n), 0] + A_i(n)$$

where the stochastic processes $\{\mu_i(n)\}_{n=0}^{\infty}$ and $\{A_i(n)\}_{n=0}^{\infty}$ are sequences of binary random variables representing the number of arrivals and services at s_i during time slot n, respectively. The arrival process $\{A_i(n)\}_{n=0}^{\infty}$ is modeled as an independent and identically distributed (i.i.d.) Bernoulli process with $E[A_i(n)] = \lambda_i$, and the processes at different nodes are assumed to be independent of each other. The service process $\{\mu_i(n)\}_{n=0}^{\infty}$ depends jointly on the transmission protocol, sensing errors, and the underlying channel model, which governs the success of transmissions. In the considered cognitive access protocol, s_1 transmits whenever $Q_1(n) \neq 0$, whereas s_2 adapts its transmission based on the observation made on the activity of s_1. Given that $Q_2(n) \neq 0$, s_2 transmits with probability 1 if s_1 is observed to be idle. Although s_1 is observed to be active, s_2 transmits with probability p to take advantage of the capture. Note that s_1 can be falsely perceived to be active by s_2 when indeed it is idle or falsely perceived to be idle when it is active, which are called *false alarm* and *miss*, and their rates are denoted by ϵ_f and ϵ_m, respectively.

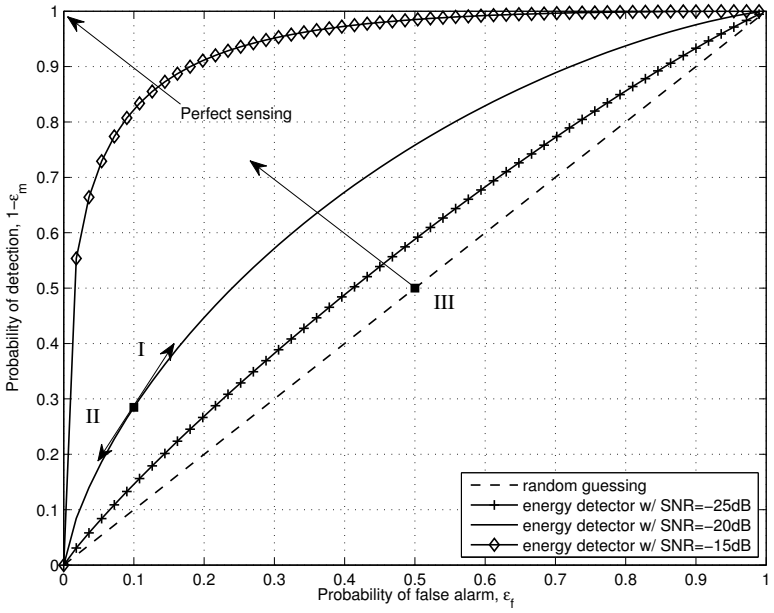

Figure 3.3: Receiver operating characteristic curves under energy detection scheme

3.2.3 Stability in the Presence of Sensing Errors

3.2.3.1 Background on the Spectrum Sensing

Spectrum sensing is the task of obtaining awareness about the existence of the primary user's transmission over the shared channel. It is mandatory by IEEE 802.22 that the secondary user must perform sensing before making any transmission decision over the licensed spectrum [70]. The goal of this chapter is to point out some fundamental aspects of the spectrum sensing. Please refer [3], [68], and references therein for more details on various spectrum sensing techniques. Among many others, the energy detector is the most popular because of its low computational and implementation complexity. In addition, it is more generic as receivers do not need any a priori knowledge on the primary user's signal waveform [68]. The output of the energy detector, which is the sum

of the sampled received signal power, is compared to a certain threshold τ to decide the existence of the primary user's signal as illustrated in Fig. 4.9. The performance of a detector can be specified in terms of the probability of miss ϵ_m and the probability of false alarm ϵ_f. Let $\bar{\epsilon}_m = 1 - \epsilon_m$ and $\bar{\epsilon}_f = 1 - \epsilon_f$, which are the probabilities of detection and correct rejection, respectively. With phase-shift keying (PSK) modulation and circular symmetric Gaussian noise modeling, the probability of detection with the energy detector was derived as [67]

$$\bar{\epsilon}_m = \mathcal{Q}\left(\frac{1}{\sqrt{2\gamma+1}}\left(\mathcal{Q}^{-1}(\epsilon_f) - \sqrt{T_s f_s}\gamma\right)\right) \tag{3.1}$$

where $\mathcal{Q}(\cdot)$ is the Q-function, i.e., the tail probability of the standard Gaussian distribution, γ is the received SNR of the signal transmitted from s_1 at the detector at s_2, T_s denotes the sensing time, and f_s is the sampling frequency. In Fig. 3.3, the receiver operating characteristic (ROC) curve, i.e., Eq. (3.1), is plotted for different received SNR values. In general, ϵ_m and ϵ_f are in a trade-off relationship, as observed in the figure, since one can always be made arbitrarily small at the expense of the other [71]. Specifically, any point on a given curve can be attained by controlling the threshold τ for the detection. It is assumed throughout this chapter that $\bar{\epsilon}_m > \epsilon_f$, which simply indicates that the equipped detector performs better than the pure random guessing[1] whose ROC curve is the diagonal line connecting $(0, 0)$ and $(1, 1)$ in the figure.

[1]The random guessing, which completely ignores the observation, can be done by running coin tossing, and each point on the diagonal line can be achieved by altering the probability of *head*.

3.2.3.2 Main Result on the Stability Region

In this chapter, we describe the stability region of the cognitive access system in the presence of sensing errors. This enables us to judge the stability of the system at any given input rate vector. As noted earlier, the queues in the system are interacting, which makes the analysis challenging. The proof of the main results described in this chapter is presented in Chapter 3.2.4 which can be outlined as follows: we first obtained the stability region for given multi-access probability p using the stochastic dominance technique explained in Chapter 2.3. Since an input rate vector that is outside of the stability region at a certain multi-access probability may be stably supported by another feasible multi-access probability, determination of the closure of the stability region is necessary and important. Thus, we take the closure of the stability region over all feasible values of p, which is what is described in this chapter.

Define $\Delta_i = q_{i|\{i\}} - q_{i|\{1,2\}}$, $i \in \{1, 2\}$, which is the difference between the success probabilities when s_i transmits alone and when it transmits along with s_j ($j \neq i$). The quantity Δ_i is strictly positive since interference only reduces the probability of success. Let us further define

$$\eta \triangleq q_{1|\{1\}}q_{2|\{1,2\}} + q_{2|\{2\}}q_{1|\{1,2\}} - q_{1|\{1\}}q_{2|\{2\}}$$

which can be viewed as an indicator of the degree of the capture effect. In the case of the collision channel, for instance, it is given by $q_{i|\{i\}} = 1$ and $q_{i|\{1,2\}} = 0$, $\forall i \in \{1, 2\}$ and, thus, $\eta = -1$. On the contrary, in the case of the perfect orthogonal channel with $q_{i|\{i\}} = q_{i|\{1,2\}} = 1$, $\forall i \in \{1, 2\}$, we have $\eta = 1$.

Described below is our main finding, which is a sufficient and necessary condition

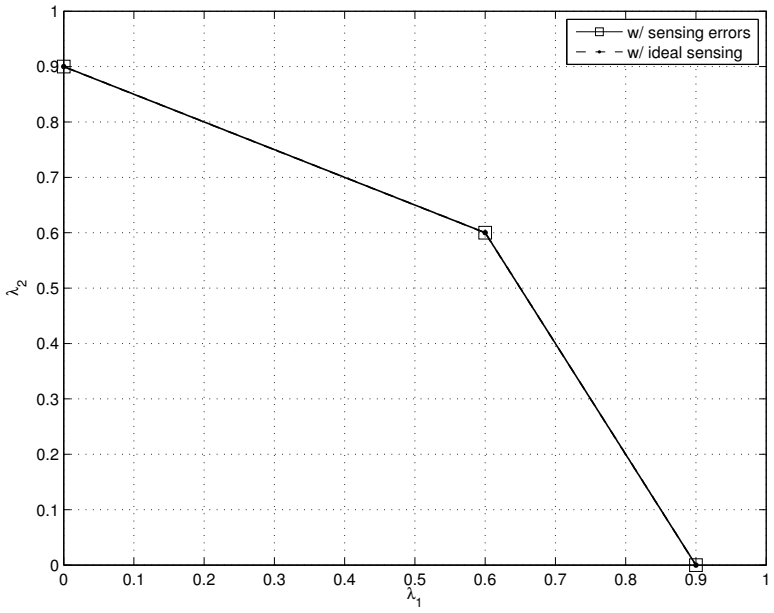

Figure 3.4: Illustration of the stability region for Case A (parameter setting: $q_{1|\{1\}} = q_{2|\{2\}} = 0.9$, $q_{1|\{1,2\}} = q_{2|\{1,2\}} = 0.6$ with any positive values of ϵ_m and ϵ_f)

for the stability of the considered cognitive access system.

- Case A: If $\eta \geq 0$, the stability region of the system is given by the union of the following subregions:

$$\mathcal{R}_1^A = \left\{(\lambda_1, \lambda_2) : \lambda_2 \leq q_{2|\{2\}} - \frac{\Delta_2}{q_{1|\{1,2\}}}\lambda_1, 0 \leq \lambda_1 \leq I_1^A\right\}$$
$$\mathcal{R}_2^A = \left\{(\lambda_1, \lambda_2) : \lambda_2 \leq \frac{q_{2|\{1,2\}}}{\Delta_1}(q_{1|\{1\}} - \lambda_1), I_1^A < \lambda_1 \leq q_{1|\{1\}}\right\}$$

  where $I_1^A = q_{1|\{1,2\}}$. The region is depicted in Fig. 3.4, which is a convex polygon. The entire boundary of the region can be achieved with multi-access probability $p^* = 1$. Note that the stability region does not depend on sensing error rates.

- Case B: If $-q_{2|\{2\}}\epsilon_f\Delta_1 \leq \eta < 0$, the stability region is given by the union of the

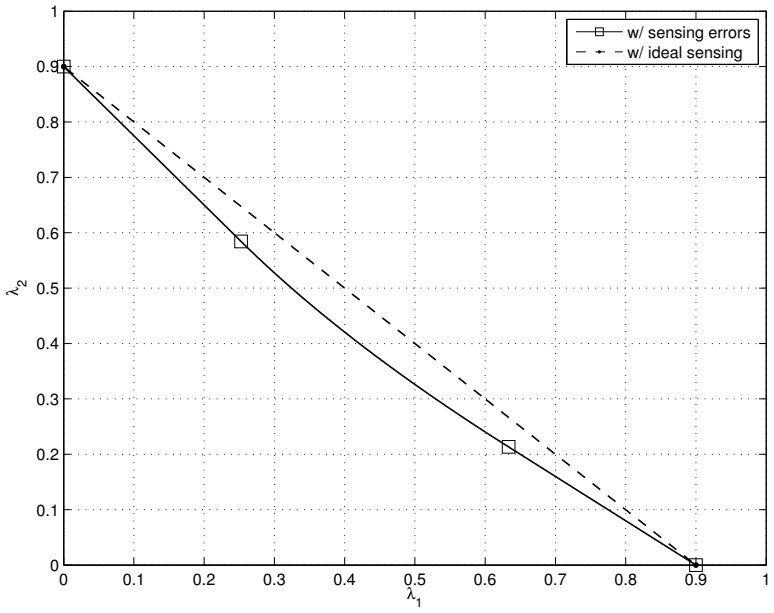

Figure 3.5: Illustration of the stability region for Case B (parameter setting: $q_{1|\{1\}} = q_{2|\{2\}} = 0.9$, $q_{1|\{1,2\}} = q_{2|\{1,2\}} = 0.4$, $\epsilon_m = \epsilon_f = 0.3$)

following subregions:

$$\mathcal{R}_1^B = \left\{(\lambda_1, \lambda_2) : \lambda_2 \leq q_{2|\{2\}} - \frac{\Delta_2}{q_{1|\{1,2\}}}\lambda_1, 0 \leq \lambda_1 \leq I_1^B\right\}$$

$$\mathcal{R}_2^B = \left\{(\lambda_1, \lambda_2) : \lambda_2 \leq \frac{(\sqrt{-\eta'} - \sqrt{q_{2|\{2\}}\epsilon_f\lambda_1})^2}{\bar{\epsilon}_m\Delta_1} + \frac{q_{2|\{1,2\}}(q_{1|\{1\}} - \lambda_1)}{\Delta_1}, \right.$$
$$\left. I_1^B < \lambda_1 \leq I_2^B\right\}$$

$$\mathcal{R}_3^B = \left\{(\lambda_1, \lambda_2) : \lambda_2 \leq \frac{q_{2|\{1,2\}}}{\Delta_1}(q_{1|\{1\}} - \lambda_1), I_2^B < \lambda_1 \leq q_{1|\{1\}}\right\}$$

where $\eta' = \bar{\epsilon}_m\eta - q_{1|\{1,2\}}q_{2|\{2\}}\epsilon_f$, $I_1^B = \frac{q_{1|\{1,2\}}^2 q_{2|\{2\}}\epsilon_f}{-\eta'}$, and $I_2^B = \frac{-\eta'}{q_{2|\{2\}}\epsilon_f}$. Note that $\eta < 0$ implies $\eta' < 0$ but the converse is not true. The boundary of the subregion $\mathcal{R}_1^B$ is achieved with $p^* = 1$, that of $\mathcal{R}_2^B$ is achieved with

$$p^* = \frac{q_{1|\{1\}} - \epsilon_m\Delta_1 - \sqrt{\frac{-\eta'\lambda_1}{q_{2|\{2\}}\epsilon_f}}}{\bar{\epsilon}_m\Delta_1} \tag{3.2}$$

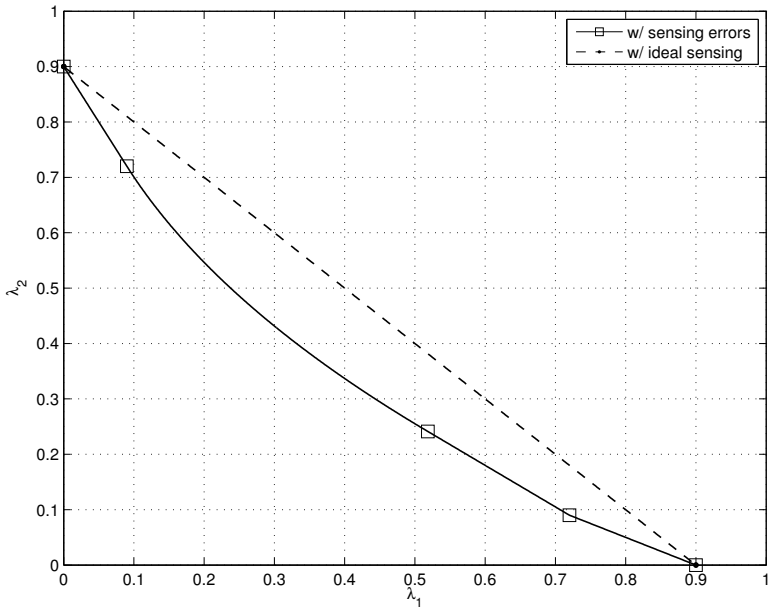

Figure 3.6: Illustration of the stability region for Case C (parameter setting: $q_{1|\{1\}} = q_{2|\{2\}} = 0.9$, $q_{1|\{1,2\}} = q_{2|\{1,2\}} = 0.3$, $\epsilon_m = \epsilon_f = 0.3$)

and that of $\mathcal{R}_3^B$ is achieved with p^* given by Eq. (3.2) evaluated at $\lambda_1 = I_2^B$. The region is non-convex as illustrated in Fig. 3.5. This follows from the non-convexity of the region described by $\mathcal{R}_2^B$. Also, the slope of the boundary of the subregion $\mathcal{R}_1^B$ is steeper than that of $\mathcal{R}_3^B$ for the considered case.

- Case C: If $\eta < -q_{2|\{2\}}\epsilon_f\Delta_1$, the stability region is given by the union of the fol-

lowing subregions:

$$\mathcal{R}_1^C = \left\{(\lambda_1,\lambda_2) : \lambda_2 \le q_{2|\{2\}} - \frac{\Delta_2}{q_{1|\{1,2\}}}\lambda_1, 0 \le \lambda_1 \le I_1^C\right\}$$

$$\mathcal{R}_2^C = \left\{(\lambda_1,\lambda_2) : \lambda_2 \le \frac{(\sqrt{-\eta'} - \sqrt{q_{2|\{2\}}\epsilon_f\lambda_1})^2}{\bar{\epsilon}_m\Delta_1} + \frac{q_{2|\{1,2\}}(q_{1|\{1\}} - \lambda_1)}{\Delta_1}, \right.$$
$$\left. I_1^C < \lambda_1 \le I_2^C\right\}$$

$$\mathcal{R}_3^C = \left\{(\lambda_1,\lambda_2) : \lambda_2 \le q_{2|\{2\}}\bar{\epsilon}_f - \frac{q_{2|\{2\}}\bar{\epsilon}_f - q_{2|\{1,2\}}\epsilon_m}{q_{1|\{1\}} - \epsilon_m\Delta_1}\lambda_1, I_2^C < \lambda_1 \le I_3^C\right\}$$

$$\mathcal{R}_4^C = \left\{(\lambda_1,\lambda_2) : \lambda_2 \le \frac{q_{2|\{1,2\}}}{\Delta_1}(q_{1|\{1\}} - \lambda_1), I_3^C < \lambda_1 \le q_{1|\{1\}}\right\}$$

where $I_1^C = \frac{q_{1|\{1,2\}}^2 q_{2|\{2\}}\epsilon_f}{-\eta'}$, $I_2^C = \frac{q_{2|\{2\}}\epsilon_f(q_{1|\{1\}} - \epsilon_m\Delta_1)^2}{-\eta}$, and $I_3^C = q_{1|\{1\}} - \epsilon_m\Delta_1$. As in Case B, the boundary of subregion $\mathcal{R}_1^C$ is achieved with $p^* = 1$, and that of $\mathcal{R}_2^C$ is achieved with p^* given in Eq. (3.2) which diminishes from one to zero as λ_1 increases from I_1^C to I_2^C. For the boundary of subregions $\mathcal{R}_3^C$ and $\mathcal{R}_4^C$, it is given by $p^* = 0$. The entire region is non-convex as in Case B.

Remark 3.2.1. *Consider the case with perfect sensing whose operating point is the upper left corner on the ROC space as shown in Fig. 3.3. By substituting $\epsilon_f = \epsilon_m = 0$ into the descriptions of the stability region given above, we find the stability region for the case with perfect sensing, which reconfirms the previous result obtained in [66]. For comparison's sake, it is also depicted in Fig. 3.4 to 3.6 along with the case of imperfect sensing. Most importantly, it is observed from Fig. 3.4 that the stability region is not affected by the sensing errors when $\eta \ge 0$. This is because the boundary achieving multi-access probability is $p^* = 1$ regardless of the values of sensing error rates. In other words, when relatively strong capture effect presents which is indicated by η, it is beneficial to let the secondary node access the channel persistently and aggressively regardless of the*

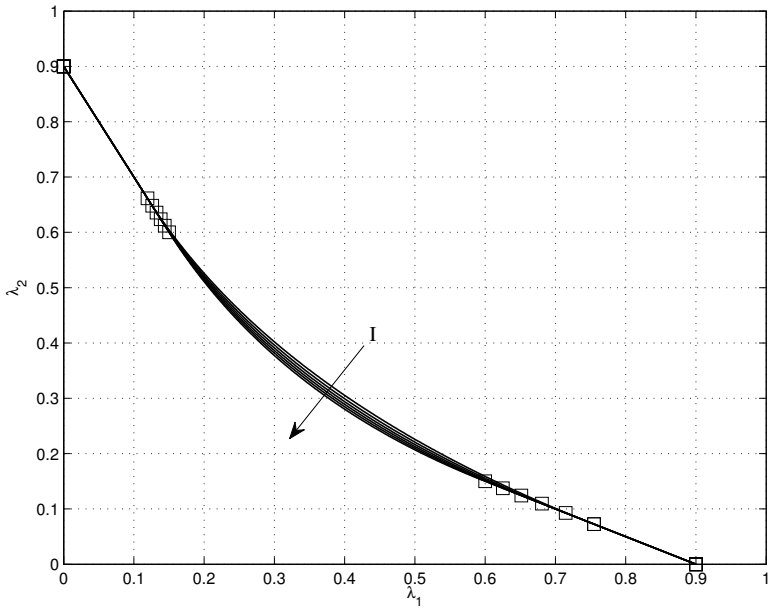

Figure 3.7: Transition of the stability region when moving towards direction I in Fig. 3.3 from $\epsilon_f^\star$ to 1 (energy detector with $\gamma = -20$dB, other parameters: $q_{1|\{1\}} = q_{2|\{2\}} = 0.9$, $q_{1|\{1,2\}} = q_{2|\{1,2\}} = 0.3 \rightarrow \epsilon_f^\star = 0.5$)

sensing outcome, whenever it has non-empty queue. This fundamentally eliminates the need for sensing itself when $\eta \geq 0$. In contrast, from Fig. 3.5 and 3.6, it is observed that when $\eta < 0$, the system suffers from the sensing errors. The difference between the regions, therefore, can be understood as the loss due to the imperfect sensing.

3.2.3.3 Controlling the Operating Point of the Detector

In this chapter, the problem of controlling the operating point of the sensing device is studied. Clearly, Case A in Chapter 3.2.3.2, i.e., when $\eta \geq 0$, is not of our concern because the stability region is not affected by sensing errors. On the other hand, when $\eta < 0$,

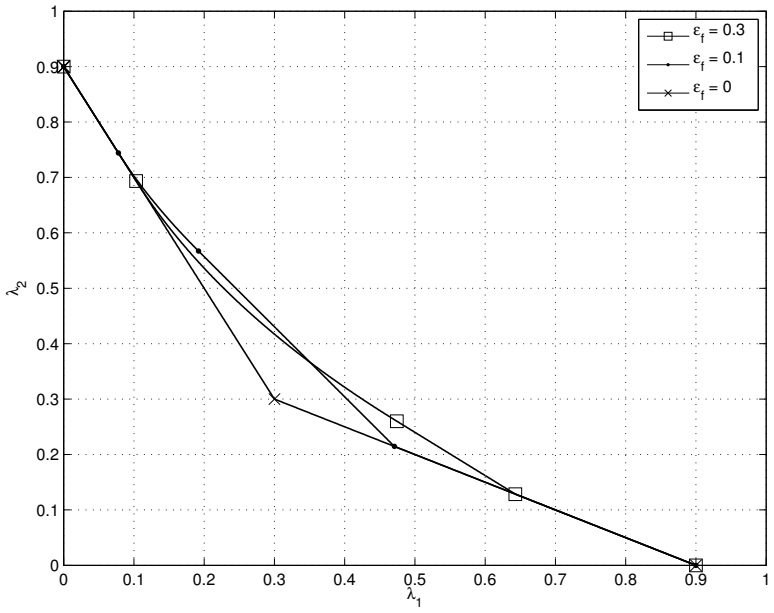

Figure 3.8: Transition of the stability region when moving towards direction II in Fig. 3.3 from $\epsilon_f^\star$ to 0 (identical setting with Fig. 3.7)

which includes both Case B and Case C, there arises a need for optimally choosing the operating point of the sensing device. It is not easy, however, to find certain decisive rules on the control from the descriptions given in Chapter 3.2.3.2, which is complicated with sensing error rates and packet reception probabilities. Moreover, at $\epsilon_f^\star = -\eta/q_{2|\{2\}}\Delta_1$, the stability region experiences a transition from Case B to Case C, and no simple relationship exists between them such as one region becomes a subset of the other. Instead, we summarize some general aspects observed by changing the operating point of the sensing device. The results are demonstrated specifically for the case of energy detectors introduced in Chapter 3.2.3.1, but the statements made in this chapter hold for any rational detector satisfying the following mild conditions: i) its ROC curve connects the points

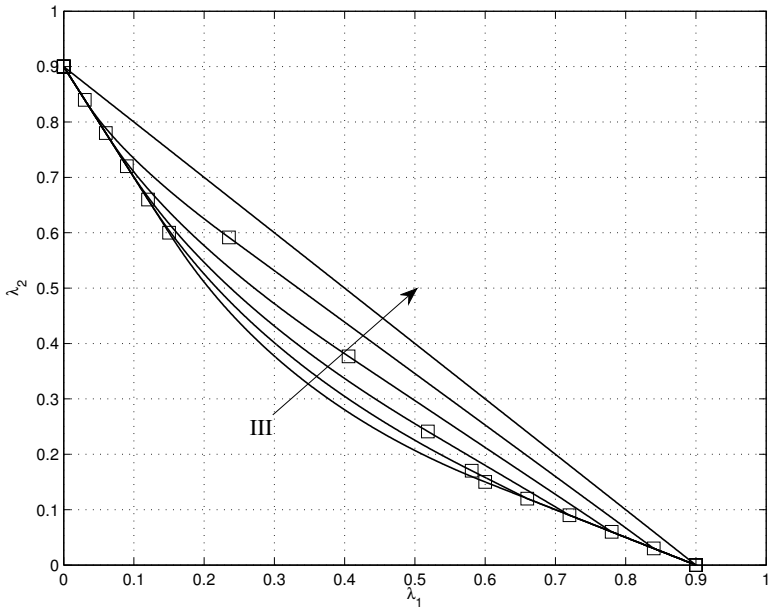

Figure 3.9: Transition of the stability region when moving towards direction III in Fig. 3.3, i.e., from random guessing to ideal sensing (identical parameters with Fig. 3.7)

$(0,0)$ and $(1,1)$ in Fig. 3.3, ii) the superiority over the random guessing, i.e., $\bar{\epsilon}_m > \epsilon_f$, and iii) the monotonicity in the trade-off between ϵ_m and ϵ_f.

We first observe that increasing ϵ_f over $\epsilon_f^\star$ only reduces the stability region as shown in Fig. 3.7. Thus, it is better to lower ϵ_f up to $\epsilon_f^\star$ which directly increases the probability of correct rejection and, thereby, improves the chance to utilize the idle slots, although, at the same time, it risks the success of the primary user by increasing the probability of miss. We next observe that when ϵ_f is further lowered below $\epsilon_f^\star$, the inclusion relation does not hold anymore. As illustrated in Fig. 3.8, each operating point results in a different shape that is not a proper subset of the others at different operating points. We finally consider the case when the accuracy of the sensing device itself is improved from the random guessing to the ideal sensing. It is obvious that the stability region becomes larger as

observed in Fig. 3.9, in which the sensing operating point is moved from $(0.5, 0.5)$ to $(0, 1)$ on the ROC plane with the step size of 0.1. The stability region may or may not experience the transition from Case B to Case C depending on the channel parameter values. Note that in the case of the ideal sensing, the stability region becomes a right triangle as shown in the figure which agrees with the previous result in [66]. On the other hand, we can derive the stability region for the case with random guessing by substituting $\bar{\epsilon}_m = \epsilon_f$ into the descriptions in Chapter 3.2.3.2. Interestingly, it turns out to be identical with that obtained for the two-node random access system [53]. This indicates that if the cognitive access system is based on the sensing information that is nothing but randomly guessed, its performance is not better than that of the random access system.

3.2.4 Stability Analysis

In this chapter, we provide details on the derivation of our main results presented in the previous chapter. In the considered protocol, primary user s_1 transmits a packet whenever its queue is non-empty, independent of the actions made by the secondary user s_2. Secondary user s_2, on the other hand, makes use of the ability to sense before transmitting. If s_1 is observed to be idle, s_2 transmits with probability 1 given that its queue is non-empty. Otherwise, if s_1 is observed to be active, s_2 transmits with probability p. The probability that s_1 is sensed to be idle is $\bar{\epsilon}_f$ when s_1 is indeed idle and ϵ_m when s_1 is actually active. Similarly, the probability that s_1 is sensed to be active is $\bar{\epsilon}_m$ when it is indeed active and ϵ_f when it is actually idle. Taking these into account, the average

service rates of the users can be written as

$$\mu_1 = q_{1|\{1\}} \left(\Pr[Q_2 = 0] + \Pr[Q_2 \neq 0]\bar{\epsilon}_m(1-p)\right) + q_{1|\{1,2\}}\Pr[Q_2 \neq 0]\left(\epsilon_m + \bar{\epsilon}_m p\right) \tag{3.3}$$

$$\mu_2 = q_{2|\{2\}}\Pr[Q_1 = 0](\bar{\epsilon}_f + \epsilon_f p) + q_{2|\{1,2\}}\Pr[Q_1 \neq 0]\left(\epsilon_m + \bar{\epsilon}_m p\right) \tag{3.4}$$

where Q_i denotes the steady-state number of packets in the queue at s_i. In the previous work, it is often required that the probability of detection must be above a certain value as a protection for the primary user. However, this is based on the assumption that the secondary user is always backlogged and, therefore, the occurrence of the missed detection directly results in the interference to the primary user. In the practical system with bursty packet arrivals, however, it is unclear how users interfere with each other since they transmit only when having non-empty queues, and this is the reason why we focus on the queueing stability of the system. Note that the rates of the individual departure processes cannot be computed directly, as they are interdependent, without knowing the stationary probability of the joint queue length process. We bypass this difficulty by using the stochastic dominance technique described in Chapter 2.3.

3.2.4.1 First Dominant System

Construct a hypothetical system which is identical to the original system except that the secondary user s_2 transmits dummy packets when it decides to transmit but when its packet queue is empty. Thus, s_2 transmits with probability 1 if s_1 is sensed to be idle and with probability p if s_1 is sensed to be active, regardless of the emptiness of its queue.

Hence, from Eq. (3.3), the average service rate of s_1 is obtained as

$$\mu_1 = q_{1|\{1\}}\bar{\epsilon}_m(1-p) + q_{1|\{1,2\}}\left(\epsilon_m + \bar{\epsilon}_m p\right)$$

which can be rewritten as

$$\mu_1 = q_{1|\{1\}} - \epsilon_m\Delta_1 - \bar{\epsilon}_m\Delta_1 p \tag{3.5}$$

By Loynes' Theorem, the queue at s_1 is stable if $\lambda_1 \leq \mu_1$, and the content size follows a discrete-time $M/M/1$ model with the arrival rate λ_1 and the service rate μ_1. For a stable input rate λ_1, the queue at s_1 empties out with probability given by

$$\Pr[Q_1 = 0] = 1 - \frac{\lambda_1}{\mu_1} = 1 - \frac{\lambda_1}{q_{1|\{1\}} - \epsilon_m\Delta_1 - \bar{\epsilon}_m\Delta_1 p} \tag{3.6}$$

By substituting Eq. (3.6) into Eq. (3.4), the average service rate of the queue at s_2 is obtained as

$$\mu_2 = q_{2|\{2\}}\left(\bar{\epsilon}_f + \epsilon_f p\right) + \frac{q_{2|\{1,2\}}\epsilon_m - q_{2|\{2\}}\bar{\epsilon}_f + (q_{2|\{1,2\}}\bar{\epsilon}_m - q_{2|\{2\}}\epsilon_f)p}{q_{1|\{1\}} - \epsilon_m\Delta_1 - \bar{\epsilon}_m\Delta_1 p}\lambda_1 \tag{3.7}$$

and the queue at s_2 is stable if $\lambda_2 \leq \mu_2$. Consequently, for a given multi-access probability p, stable input rate pairs (λ_1, λ_2) are those componentwise less than (μ_1, μ_2). In Fig. 3.10, we illustrate the obtained stability region at given p, where the stability region of the second dominant system is obtained in the subsequent chapter. The stability region obtained for the dominant system is indeed the stability region of the original system due to the stochastic dominance and the indistinguishability argument discussed in Chapter 2.3.

We now take the closure of the stability region over the multi-access probability p. This can be equivalently done by solving the following boundary optimization problem

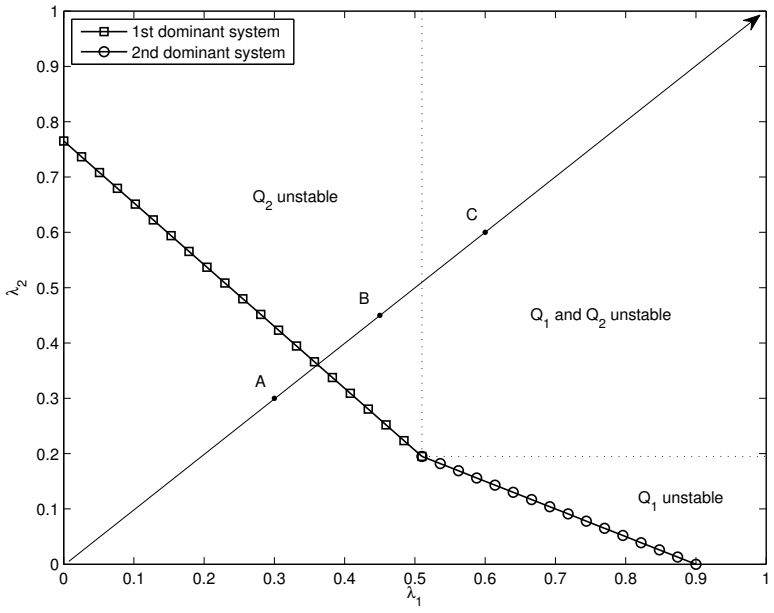

Figure 3.10: Stability region at fixed multi-access probability p (parameter setting: $q_{1|\{1\}} = q_{2|\{2\}} = 0.9$, $q_{1|\{1,2\}} = q_{2|\{1,2\}} = 0.3$, $\epsilon_m = \epsilon_f = 0.3$, $p = 0.5$)

in which we maximize μ_2 over p for a given value of λ_1 while guaranteeing the stability of the queue at s_1, that is

$$\max_{p} \ \mu_2 = q_{2|\{2\}}\left(\bar{\epsilon}_f + \epsilon_f p\right) + \frac{q_{2|\{1,2\}}\epsilon_m - q_{2|\{2\}}\bar{\epsilon}_f + (q_{2|\{1,2\}}\bar{\epsilon}_m - q_{2|\{2\}}\epsilon_f)p}{q_{1|\{1\}} - \epsilon_m\Delta_1 - \bar{\epsilon}_m\Delta_1 p}\lambda_1 \tag{3.8}$$

$$\text{subject to } \ 0 \le \lambda_1 \le q_{1|\{1\}} - \epsilon_m\Delta_1 - \bar{\epsilon}_m\Delta_1 p \tag{3.9}$$

$$0 \le p \le 1 \tag{3.10}$$

To maximize μ_2 over p, we need to understand their relationship. Differentiating μ_2 with respect to p gives

$$\frac{\partial \mu_2}{\partial p} = q_{2|\{2\}}\epsilon_f + \frac{\eta'\lambda_1}{\left(q_{1|\{1\}} - \epsilon_m\Delta_1 - \bar{\epsilon}_m\Delta_1 p\right)^2}$$

where η' was defined as $\eta' = \bar{\epsilon}_m \eta - q_{1|\{1,2\}} q_{2|\{2\}} \epsilon_f$. When $\eta \geq 0$, which is equivalent to the case when $\eta' \geq -q_{1|\{1,2\}} q_{2|\{2\}} \epsilon_f$, we observe that

$$\begin{aligned}
\frac{\partial \mu_2}{\partial p} &\geq q_{2|\{2\}} \epsilon_f - \frac{q_{1|\{1,2\}} q_{2|\{2\}} \epsilon_f \lambda_1}{\left(q_{1|\{1\}} - \epsilon_m \Delta_1 - \bar{\epsilon}_m \Delta_1 p\right)^2} \\
&\geq q_{2|\{2\}} \epsilon_f \left(1 - \frac{q_{1|\{1,2\}}}{q_{1|\{1\}} - \epsilon_m \Delta_1 - \bar{\epsilon}_m \Delta_1 p}\right) \\
&\geq 0
\end{aligned}$$

where the last inequality follows from

$$\begin{aligned}
q_{1|\{1\}} - \epsilon_m \Delta_1 - \bar{\epsilon}_m \Delta_1 p &\geq q_{1|\{1\}} - \epsilon_m \Delta_1 - \bar{\epsilon}_m \Delta_1 \\
&= q_{1|\{1\}} - \Delta_1 \\
&= q_{1|\{1,2\}}
\end{aligned}$$

Thus, if $\eta \geq 0$, μ_2 is a non-decreasing function of p. Note, however, that having $\eta < 0$ does not necessarily mean that μ_2 is a non-increasing function of p. By differentiating μ_2 once again, we have

$$\frac{\partial^2 \mu_2}{\partial p^2} = \frac{2\bar{\epsilon}_m \Delta_1 \eta' \lambda_1}{\left(q_{1|\{1\}} - \epsilon_m \Delta_1 - \bar{\epsilon}_m \Delta_1 p\right)^3}$$

Since the denominator is strictly positive, if $\eta' \geq 0$, μ_2 is convex with respect to p. Otherwise, it is concave with respect to p. These properties of μ_2 is described in Fig. 3.11.

The case when $\eta \geq 0$: In this case, μ_2 is a non-decreasing function of p. Thus, the maximizing p^* is the largest value satisfying both constraints in Eqs. (3.9) and (3.10), that is

$$p^* = \min\left[1, \frac{q_{1|\{1\}} - \epsilon_m \Delta_1 - \lambda_1}{\bar{\epsilon}_m \Delta_1}\right]$$

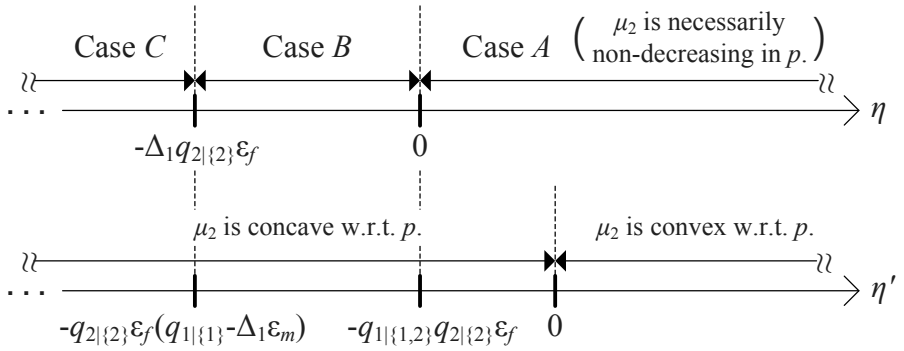

Figure 3.11: Properties of μ_2 with respect to p

Note that the role of Eq. (3.9) is to impose an upper limit on p^* so that the stability of s_1 is guaranteed. For $0 \leq \lambda_1 \leq q_{1|\{1,2\}}$, it is given by $p^* = 1$, and the corresponding maximum function value is obtained as

$$\mu^*_{2,\text{line}_1} = q_{2|\{2\}} - \frac{\Delta_2}{q_{1|\{1,2\}}}\lambda_1 \tag{3.11}$$

For $q_{1|\{1,2\}} < \lambda_1 \leq q_{1|\{1\}} - \epsilon_m\Delta_1$, it is given by $p^* = (q_{1|\{1\}} - \epsilon_m\Delta_1 - \lambda_1)/\bar{\epsilon}_m\Delta_1$, and the corresponding maximum function value is obtained as

$$\mu^*_{2,\text{line}_2} = \frac{q_{2|\{1,2\}}}{\Delta_1}(q_{1|\{1\}} - \lambda_1) \tag{3.12}$$

Note that if $\lambda_1 > q_{1|\{1\}} - \epsilon_m\Delta_1$, the constraint in Eq. (3.9) cannot be met with any feasible $p \in [0, 1]$ and, thus, μ_2 is not defined.

The case when $-q_{2|\{2\}}\epsilon_f\Delta_1 \leq \eta < 0$: In this case, μ_2 is concave with respect to p and, thus, equating the first derivative to zero gives the maximizing p^* as

$$p^* = \frac{q_{1|\{1\}} - \epsilon_m\Delta_1 - \sqrt{\frac{-\eta'\lambda_1}{q_{2|\{2\}}\epsilon_f}}}{\bar{\epsilon}_m\Delta_1} \tag{3.13}$$

and the corresponding maximum function value is obtained as

$$\mu^*_{2,\text{curve}} = \frac{(q_{2|\{2\}}\epsilon_f - q_{2|\{1,2\}}\bar{\epsilon}_m)\lambda_1 - 2\sqrt{-q_{2|\{2\}}\epsilon_f\eta'\lambda_1} - \eta' + q_{1|\{1\}}q_{2|\{1,2\}}\bar{\epsilon}_m}{\bar{\epsilon}_m\Delta_1}$$

which can be rearranged to

$$\mu^*_{2,\text{curve}} = \frac{(\sqrt{-\eta'} - \sqrt{q_{2|\{2\}}\epsilon_f\lambda_1})^2}{\bar{\epsilon}_m\Delta_1} + \frac{q_{2|\{1,2\}}(q_{1|\{1\}} - \lambda_1)}{\Delta_1}$$

Note that $\mu^*_{2,\text{curve}}$ is feasible when both constraints in Eqs. (3.9) and (3.10) are satisfied. For used p^*, Eq. (3.9) becomes

$$\lambda_1 \leq \frac{-\eta'}{q_{2|\{2\}}\epsilon_f} \tag{3.14}$$

and Eq. (3.10) becomes

$$\frac{q^2_{1|\{1,2\}}q_{2|\{2\}}\epsilon_f}{-\eta'} \leq \lambda_1 \leq \frac{q_{2|\{2\}}\epsilon_f(q_{1|\{1\}} - \epsilon_m\Delta_1)^2}{-\eta'} \tag{3.15}$$

which is obtained by rearranging Eq. (3.13) and substituting the extreme values of p. For the considered case when $-q_{2|\{2\}}\epsilon_f\Delta_1 \leq \eta < 0$, the intersection of the ranges of values of λ_1 determined by Eqs. (3.14) and (3.15) is given by

$$\frac{q^2_{1|\{1,2\}}q_{2|\{2\}}\epsilon_f}{-\eta'} \leq \lambda_1 \leq \frac{-\eta'}{q_{2|\{2\}}\epsilon_f} \tag{3.16}$$

On the other hand, if λ_1 lies on the left-hand side (LHS) of the range of Eq. (3.16), we observe that

$$\frac{\partial\mu_2}{\partial p} \geq q_{2|\{2\}}\epsilon_f\left(1 - \left(\frac{q_{1|\{1,2\}}}{q_{1|\{1\}} - \epsilon_m\Delta_1 - \bar{\epsilon}_m\Delta_1 p}\right)^2\right) \geq 0$$

where we used the facts that η' is negative for the considered case and $q_{1|\{1\}} - \epsilon_m\Delta_1 - \bar{\epsilon}_m\Delta_1 p \geq q_{1|\{1,2\}}$ as observed in the previous case. Since μ_2 is a non-decreasing function of p, $p^* = 1$ and the maximum function value is given by μ^*_{2,line_1} in Eq. (3.11). Note that the constraint in Eq. (3.9) is automatically satisfied when λ_1 is on the LHS of the range of Eq. (3.16).

Next consider the case when λ_1 lies on the right-hand side (RHS) of the range of Eq. (3.16). This is the case that, if p^* is set according to Eq. (3.13), the stability of s_1 is lost. For the stability of s_1, it is required that the multi-access probability p is bounded above as

$$p \leq \frac{q_{1|\{1\}} - \epsilon_m \Delta_1 - \lambda_1}{\bar{\epsilon}_m \Delta_1} < \frac{q_{1|\{1\}} - \epsilon_m \Delta_1 + \frac{\eta'}{q_{2|\{2\}}\epsilon_f}}{\bar{\epsilon}_m \Delta_1}$$

For p satisfying the above inequality, we observe that

$$\frac{\partial \mu_2}{\partial p} > q_{2|\{2\}}\epsilon_f \left(1 - \left(\frac{-\eta'}{q_{2|\{2\}}\epsilon_f (q_{1|\{1\}} - \epsilon_m \Delta_1 - \bar{\epsilon}_m \Delta_1 p)}\right)^2\right) > 0$$

In other words, μ_2 is an increasing function of p and, hence, we have

$$p^* = \frac{q_{1|\{1\}} - \epsilon_m \Delta_1 - \lambda_1}{\bar{\epsilon}_m \Delta_1}$$

for λ_1 on the RHS of the range of Eq. (3.16). The corresponding maximum function value is given by μ^*_{2,line_2} in Eq. (3.12). Again, if $\lambda_1 > q_{1|\{1\}} - \epsilon_m \Delta_1$, the constraint in Eq. (3.9) cannot be met with any feasible $p \in [0, 1]$ and, thus, μ_2 is not defined.

The case when $\eta < -q_{2|\{2\}}\epsilon_f \Delta_1$: In this case, μ_2 is still concave with respect to p, but the range of $\mu^*_{2,\text{curve}}$, which was the intersection of the ranges of values of λ_1 determined by Eqs. (3.14) and (3.15), would be identical with the range specified by Eq. (3.15). Again, for λ_1 on the LHS of the range of Eq. (3.15), μ_2 is a non-decreasing function of p, and the maximum function value is given by μ^*_{2,line_1} as in the previous case. On the other hand, if λ_1 lies on the RHS of Eq. (3.15), we observe that

$$\frac{\partial \mu_2}{\partial p} < q_{2|\{2\}}\epsilon_f \left(1 - \left(\frac{q_{1|\{1\}} - \epsilon_m \Delta_1}{q_{1|\{1\}} - \epsilon_m \Delta_1 - \bar{\epsilon}_m \Delta_1 p}\right)^2\right) < 0$$

Therefore, μ_2 is a decreasing function of p and, hence, by substituting $p^* = 0$ into Eq. (3.8), we have

$$\mu^*_{2,\text{line}_3} = q_{2|\{2\}}\bar{\epsilon}_f - \frac{q_{2|\{2\}}\bar{\epsilon}_f - q_{2|\{1,2\}}\epsilon_m}{q_{1|\{1\}} - \epsilon_m\Delta_1}\lambda_1$$

For $\lambda_1 > q_{1|\{1\}} - \epsilon_m\Delta_1$, μ_2 is not defined.

3.2.4.2 Second Dominant System

By reversing the roles of the two users in the previous dominant system, we can construct another parallel dominant system in which the primary user s_1 is now transmitting dummy packets, instead of the secondary node s_2, when its packet queue is empty. Since s_1 transmits with probability 1 in this dominant system, the average service rate of s_2 in Eq. (3.4) becomes

$$\mu_2 = q_{2|\{1,2\}}(\epsilon_m + \bar{\epsilon}_m p)$$

By Loynes' theorem, the queue at s_2 is stable if $\lambda_2 \leq \mu_2$, and it empties out with probability given by

$$\Pr[Q_2 = 0] = 1 - \frac{\lambda_2}{q_{2|\{1,2\}}(\epsilon_m + \bar{\epsilon}_m p)} \tag{3.17}$$

Substituting Eq. (3.17) into Eq. (3.3) and after some manipulation, the stability condition for the queue at s_1 is obtained as

$$\lambda_1 \leq \mu_1 = q_{1|\{1\}} - \frac{\Delta_1}{q_{2|\{1,2\}}}\lambda_2 \tag{3.18}$$

which is depicted in Fig. 3.10 for the range of $\lambda_2 \leq \mu_2$. Observe that Eq. (3.18) can be rearranged to

$$\lambda_2 \leq \frac{q_{2|\{1,2\}}}{\Delta_1}(q_{1|\{1\}} - \lambda_1) \tag{3.19}$$

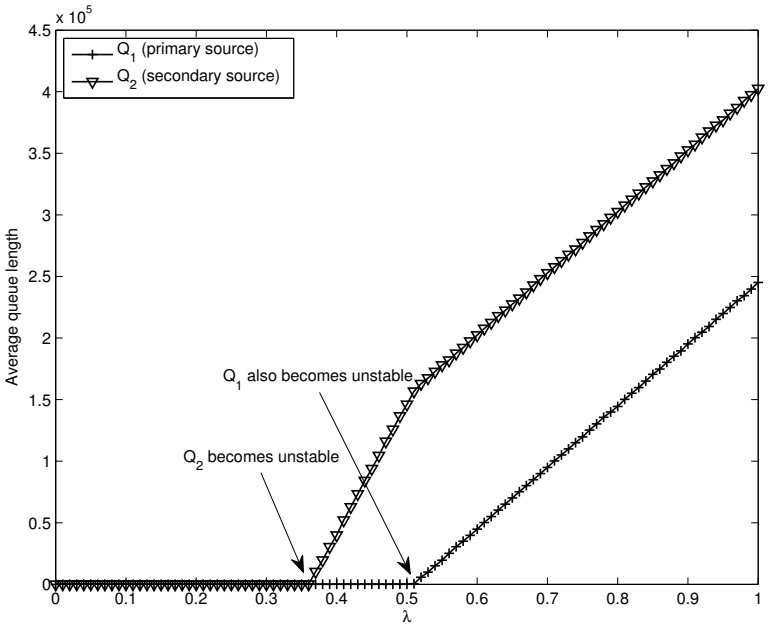

Figure 3.12: Average queue length over 10^6 slots along the diagonal arrow in Fig. 3.10, i.e., $\lambda = \lambda_1 = \lambda_2$, with the same parameter setting used for Fig. 3.10

whose boundary is identical with μ^*_{2,line_2} in Eq. (3.12) for the range of $\lambda_1 \geq q_{1|\{1\}} - \Delta_1(\epsilon_m + \bar{\epsilon}_m p)$. Since Eq. (3.19) does not depend on p, there is no need to optimize over p, and p only has the effect of changing the range of λ_1. This together with the descriptions obtained for the first dominant system completes the proof of our main results presented in Chapter 3.2.3.

3.2.5 Simulation

Here we focus on the validation of the stability result obtained using the stochastic dominance technique, which is illustrated in Fig. 3.10. The simulation results reconfirm that the stability region in Fig. 3.10 is indeed the stability region of the original system.

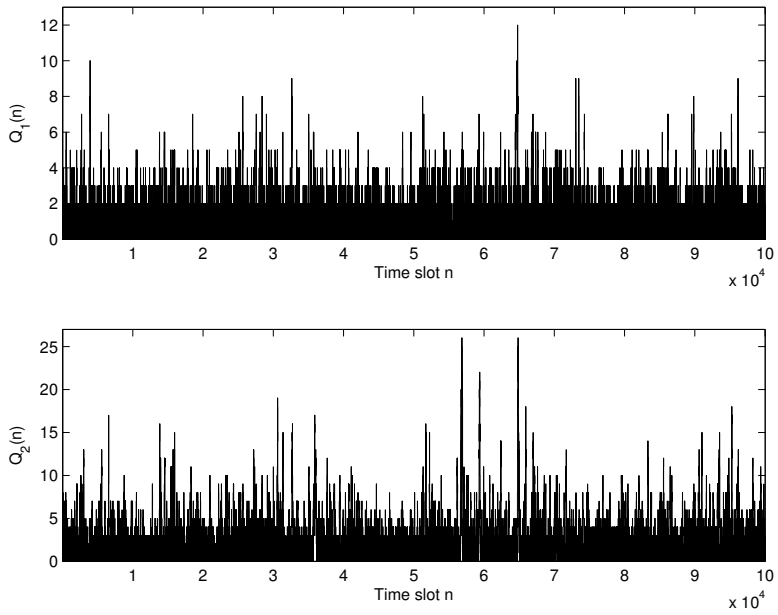

Figure 3.13: Queue length samplepath at point A in Fig. 3.10

Results illustrated from Fig. 3.4 to Fig. 3.9 are consequences of the stability region in Fig. 3.10 by taking the closure over the multi-access probability p by the secondary transmitter.

We first observe the behavior of the average queue sizes as the traffic load increases. For simplicity of exposition, we consider symmetric Bernoulli arrivals, so that $\lambda_i = \lambda$ for all i in $\{ 1, 2 \}$. We simulated the system over 10^6 slots with the same parameter setting used for Fig. 3.10. That is, $q_{1|\{1\}} = q_{2|\{2\}} = 0.9$, $q_{1|\{1,2\}} = q_{2|\{1,2\}} = 0.3$, $\epsilon_m = \epsilon_f = 0.3$, and $p = 0.5$. The resulting simulated queue averages are shown in Fig. 3.12. It can be observed that as we cross the boundary of the stability region, which is at $\lambda = 0.3613$ from Eq. (3.7), the size of the queue at s_2 starts growing. As the input rate is further increased such that it exceeds $\lambda = 0.51$, which is obtained from Eq. (3.5), we observe that the size of the queue at s_1 also starts growing.

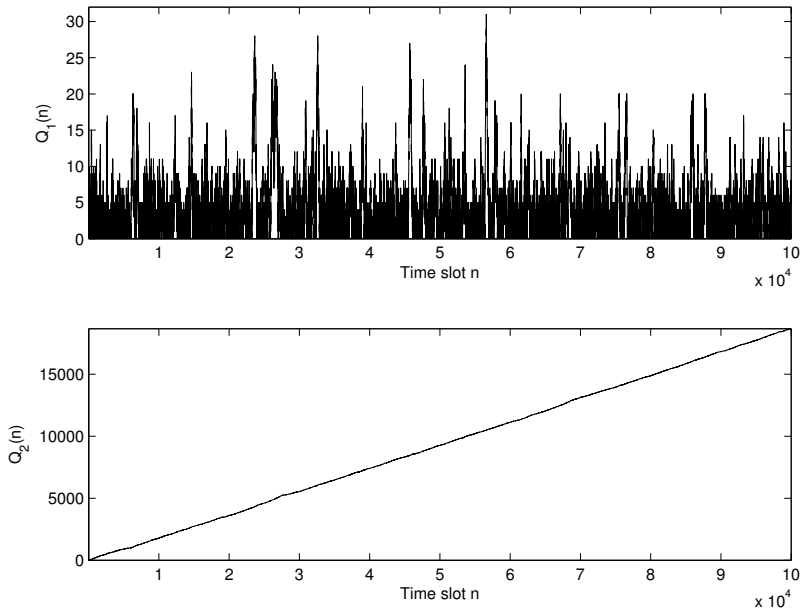

Figure 3.14: Queue length samplepath at point B in Fig. 3.10

However, this result is still insufficient because stability is an asymptotic property of a system but the queue length averages were taken over the finite time interval. Although the simulation interval can be further increased, it is nevertheless finite. Thus, the best we can do is to observe the tendency of queue sizes over the course of time. From Fig. 3.13 to Fig. 3.15, we illustrate queue length sample-paths at input traffic load at points A, B, and C depicted in Fig. 3.10. At point A, the queues at both s_1 and s_2 are expected to be stable, whereas at points B and C, the queue at s_2 and the queues at both s_1 and s_2 are expected to be unstable, respectively. From Fig. 3.13, it can be seen that the queue sizes at both nodes do not increase as time goes on, albeit bursty. From Fig. 3.14 and Fig. 3.15, it can be observed that there is an increasing tendency in the queue size at s_2 and the queue sizes at both s_1 and s_2, respectively. This increasing tendency in the queue size allows us to conjecture the instability of the corresponding queues.

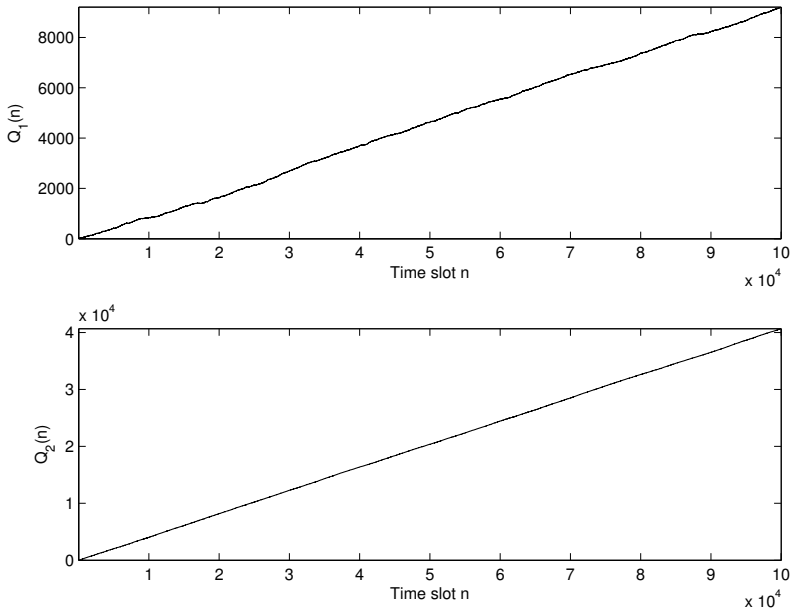

Figure 3.15: Queue length samplepath at point C in Fig. 3.10

3.2.6 Discussion

We studied the effect of imperfect sensing on the stability region of the cognitive access system. Surprisingly, we observed that when there exists relatively strong capture effect, we can achieve the identical stability region that is achieved with perfect sensing, even with positive sensing error rates. This is remarkable because the spectrum sensing itself becomes unnecessary in terms of the achieved stability region, although other performance measures such as the average queueing delay may suffer from the occurrence of errors. When it is not the case that we can achieve identical stability region that is achieved with perfect sensing, the loss due to the imperfect sensing was precisely quantified in terms of the size of the stability region.

3.3 Hybrid Access for Systems with Random Connectivity

3.3.1 Motivation

In this chapter, we are interested in a hybrid of interweave and underlay modes of operation for the system consisting of the primary and the secondary communication systems. The considered system is dynamic in the sense that all the links from sources to destinations have time-varying random *connectivity*. It is assumed that the primary source transmits uninterruptedly whenever the link from itself to the primary destination is connected and its queue is non-empty. The secondary source, on the other hand, transmits opportunistically by observing the primary source's activity and taking into account the connectivity of the links from itself to both the primary and the secondary destinations[2]. That is, the secondary communication system runs in the interweave mode when it is guaranteed that its operation has no effect on the primary communication. This is when the primary source is idle or the interference link from the secondary source to the primary destination is disconnected, which can be viewed as an example of the spatial resource reuse [72]. In addition to the interweave mode, the secondary communication system can optionally operate in the underlay mode, even when it is unavoidable to interfere with the primary communication. The underlay mode is activated with some probability, which we call a *hybrid rate*. Our design objective is, thus, to optimally choose the hybrid rate to maximize the stable throughput of the secondary communication system while ensuring the stability of the primary communication system at given input demand. In [73]

[2]It is assumed that the secondary source knows the connectivity of the link from itself to the primary destination by overhearing the pilot signal broadcasted from the primary destination.

and [74], a similar hybrid access policy was proposed as in our work, but the channel model with static multipacket reception (MPR) capability was assumed [52]. It was also assumed that the secondary source is always backlogged. In [66], a complete stability analysis was performed for a similar hybrid access policy when both the primary and the secondary sources have bursty arrivals. However, the analysis is again based on the static MPR model as in [73]. In [75], it was considered that the secondary source adjusts its hybrid rate according to the channel state alternating between *good* and *bad* states. However, both the primary and the secondary sources communicate with a common destination, and only the link between the secondary source and the common destination is assumed time-varying. Moreover, how to adjust the hybrid rate according to the channel state is missing.

Our contributions can be summarized as follows. First, the stability of the hybrid access policy is precisely analyzed for a dynamic system with time-varying connectivity. Secondly, we observe that the hybrid access policy is not always beneficial when compared against to the interweave-only mode and, consequently, the condition for which the hybrid access policy can outperform is obtained. Finally, the static MPR model, or equivalently the system with time-varying connectivity but with no channel connectivity information, is revisited as a special case of our general model.

3.3.2 System Model

We consider a system consisting of two source-destination pairs, the primary pair (s_1, d_1) and the secondary pair (s_2, d_2), as shown in Fig. 3.16. The assumptions on

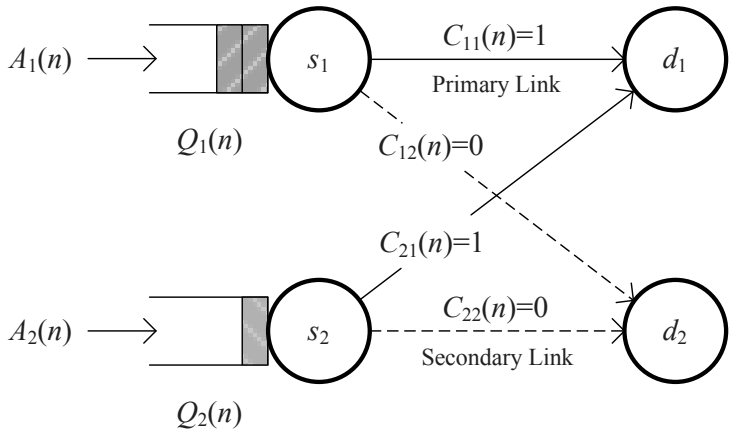

Figure 3.16: The cognitive radio system model with time-varying connectivity (the solid and dotted lines denote that a link is connected and disconnected, respectively.)

arrival processes, time-slotted system model, and transmission acknowledgement follows those of Chapter 3.2.2. The queueing model in Eq. (5.1) is used here as well. Unlike Chapter 3.2, the link between s_i and d_j, $\forall i, j \in \{1, 2\}$, may be either *connected* or *disconnected* due to such as the shadowing effect [56]; that is denoted by the binary variable $C_{ij}(n)$, which is equal to 1 and 0, respectively. The fact that an interference link such as those from s_1 to d_2 and from s_2 to d_1 is disconnected implies that a transmission over a designated link such as those from s_1 to d_1 and from s_2 to d_2 is not affected by the interference signal. The connectivity process $\{C_{ij}(n)\}_{n=0}^{\infty}$ is i.i.d. with $E[C_{ij}(n)] = c_{ij}$. In complying with widely accepted requirements on cognitive radio systems, that is, the primary communication system is oblivious of the existence of any additional systems, it is assumed that the primary source s_1 knows only the connectivity of its own link, i.e., $C_{11}(n)$, based on the pilot signal sent from d_1. On the other hand, the secondary source s_2 is assumed to know the connectivity of not only its own link, i.e., $C_{22}(n)$, but also the interference link from itself to the primary destination, i.e, $C_{21}(n)$, by overhearing the

the pilot signal sent from d_1. Note that neither s_1 nor s_2 knows the connectivity of the link from s_1 to d_2, i.e., $C_{12}(n)$. Thus, the random connectivity over that interference link only reduces the success probability of the secondary transmission in the average sense. To focus on the effect of channel dynamics, it is assumed that the sensing at secondary source on the activity of the primary system is accurate and error-free.

In the following, we describe the transmission policy of each sources. At time slot n, the primary source s_1 transmits with probability 1 at some fixed power if $Q_1(n) \neq 0$ and $C_{11}(n) = 1$. Otherwise, it remains silent. The secondary source s_2, on the other hand, makes decision on its transmission based on the activity of s_1 and the connectivity of both its own link and the interference link from itself to d_1. The interweave mode is enabled only when the transmission by s_2 has no effect on the primary communication. That is, if either s_1 does not transmit at time slot n (i.e., either due to $Q_1(n) = 0$ or $C_{11}(n) = 0$) or s_1 does transmit but the interference link from s_2 to d_1 is disconnected, i.e., $C_{21}(n) = 0$, s_2 transmits with probability 1 at some fixed power if $Q_2(n) \neq 0$ and $C_{22}(n) = 1$. The underlay mode is optionally enabled, although when it is inevitable to cause interference to the primary communication, but at lower power than the interweave mode. That is, even when s_1 transmits at time slot n and the interference link is connected, i.e., $C_{21}(n) = 1$, s_2 transmits with probability p_h, which is called hybrid rate, if $Q_2(n) \neq 0$ and $C_{22}(n) = 1$. This can be viewed as a stationary randomized policy for triggering the underlay mode of operation.

The success of transmissions jointly depend on the actions made by both sources and the underlying connectivity of the links. Also note that a transmission over a connected link can fail even without interference due to fast fading and/or background noise.

The followings are the probabilities of success at given set of actions and configuration of channel connectivity, which also take into account the effect of random failure.

- $q_{1|\{1\}}$: the probability of success of a transmission by s_1 when s_2 does not transmit or it does transmit but $C_{21}(n) = 0$.

- $q_{1|\{1,2\}}$: the probability of success of a transmission by s_1 when both s_1 and s_2 transmit and $C_{21}(n) = 1$, i.e., s_2 operates in the underlay mode.

- $q^i_{2|\{2\}}$: the probability of success of a transmission by s_2 when it operates in the interweave mode and either s_1 does not transmit or it does transmit but $C_{12}(n) = 0$.

- $q^i_{2|\{1,2\}}$: the probability of success of a transmission by s_2 when it operates in the interweave mode, s_1 transmits and $C_{12}(n) = 1$.

- $q^u_{2|\{2\}}$: the probability of success of a transmission by s_2 when it operates in the underlay mode and $C_{12}(n) = 0$.

- $q^u_{2|\{1,2\}}$: the probability of success of a transmission by s_2 when it operates in the underlay mode and $C_{12}(n) = 1$.

In the above probabilities, although not mentioned specifically, if s_i transmits, the corresponding designated channel is connected, i.e., $C_{ii}(n) = 1$. Once transmit power levels and other physical characteristics such as the distance, propagation loss exponent, statistics of fading are known, those probabilities can be readily computed as in Chapter 2.1.

3.3.3 Stability of Hybrid Access

Let $\Delta_1 = q_{1|\{1\}} - q_{1|\{1,2\}}$, which is the difference in the success probabilities of s_1 when it transmits alone and when s_2 transmits along with s_1 in the underlay mode. Similarly, let $\Delta_2^i = q_{2|\{2\}}^i - q_{2|\{1,2\}}^i$ and $\Delta_2^u = q_{2|\{2\}}^u - q_{2|\{1,2\}}^u$. Further define

$$\Psi(p_h) \triangleq q_{2|\{2\}}^i c_{21} + \Delta_2^i c_{12}\bar{c}_{21} + c_{21}p_h(\Delta_2^u c_{12} - q_{2|\{2\}}^u) \tag{3.20}$$

where $\bar{c} = 1 - c$ and this notation is used throughout the paper.

Theorem 3.3.1. *The system is stable under the hybrid access policy with hybrid rate p_h if and only if $\boldsymbol{\lambda} \in \bigcup_{i\in\{1,2\}} \boldsymbol{\Lambda}_i$ where*

$$\boldsymbol{\Lambda}_1 = \left\{ \boldsymbol{\lambda} : \lambda_1 \le c_{11}\left(q_{1|\{1\}} - \Delta_1 c_{21}c_{22}p_h\right), \lambda_2 \le c_{22}\left(q_{2|\{2\}}^i - \frac{\Psi(p_h)\lambda_1}{q_{1|\{1\}} - \Delta_1 c_{21}c_{22}p_h}\right)\right\}$$

$$\boldsymbol{\Lambda}_2 = \left\{ \boldsymbol{\lambda} : \lambda_1 \le c_{11}\left(q_{1|\{1\}} - \frac{\Delta_1 c_{21}p_h\lambda_2}{q_{2|\{2\}}^i - c_{11}\Psi(p_h)}\right), \lambda_2 \le c_{22}\left(q_{2|\{2\}}^i - c_{11}\Psi(p_h)\right)\right\}$$

Proof. Under the hybrid access protocol described in Chapter 3.3.2, the average service rates of the queues at the sources can be expressed as

$$\mu_1 = q_{1|\{1\}}c_{11}\left\{\Pr[Q_2 = 0] + \Pr[Q_2 \neq 0](\bar{c}_{22} + \bar{c}_{21}c_{22} + c_{21}c_{22}\bar{p}_h)\right\}$$
$$+ q_{1|\{1,2\}}c_{11}c_{21}c_{22}p_h\Pr[Q_2 \neq 0]$$

and

$$\mu_2 = q_{2|\{2\}}^i c_{22}\left\{\Pr[Q_1 = 0] + \Pr[Q_1 \neq 0]\left(\bar{c}_{11} + c_{11}\bar{c}_{12}\bar{c}_{21}\right)\right\}$$
$$+ \Pr[Q_1 \neq 0]\left\{q_{2|\{1,2\}}^i c_{11}c_{12}\bar{c}_{21}c_{22} + q_{2|\{2\}}^u c_{11}\bar{c}_{12}c_{21}c_{22}p_h + q_{2|\{1,2\}}^u c_{11}c_{12}c_{21}c_{22}p_h\right\}$$

By substituting $\Pr[Q_1 = 0] = 1 - \Pr[Q_1 \neq 0]$ into the above equations and rearranging the terms, they are further simplified to

$$\mu_1 = q_{1|\{1\}}c_{11} - \Delta_1 c_{11}c_{21}c_{22}p_h\Pr[Q_2 \neq 0] \tag{3.21}$$

and

$$\mu_2 = q^i_{2|\{2\}} c_{22} - c_{11} c_{22} \Psi(p_h) \Pr[Q_1 \neq 0] \tag{3.22}$$

where $\Psi(p_h)$ was defined in Eq. (3.20).

It can be seen from Eq. (3.21) and Eq. (3.22) that the service rate of one depends on the other, i.e., the queues are interacting. Thus, we use the stochastic dominance technique in Chapter 2.3 to resolve the interaction between queues. Consider first a hypothetical system which is identical to the original system except that the secondary source s_2 transmits dummy packets when it decides to transmit but its queue is empty. Since s_2 transmits regardless of the emptiness of its queue, it is equivalent to setting $\Pr[Q_2 \neq 0] = 1$. Hence, from Eq. (3.21), the average service rate of s_1 in this hypothetical system becomes

$$\mu_1 = c_{11}(q_{1|\{1\}} - \Delta_1 c_{21} c_{22} p_h) \tag{3.23}$$

By Loynes' Theorem, the queue at s_1 is stable if $\lambda_1 \leq \mu_1$, and the content size follows a discrete-time $M/M/1$ model. For a stable rate $\lambda_1 (\leq \mu_1)$, the probability that the queue at s_1 is non-empty is given by

$$\Pr[Q_1 \neq 0] = \frac{\lambda_1}{\mu_1} = \frac{\lambda_1}{c_{11}(q_{1|\{1\}} - \Delta_1 c_{21} c_{22} p_h)} \tag{3.24}$$

and, by substituting Eq. (3.24) into Eq. (3.22), we obtain

$$\mu_2 = c_{22} \left(q^i_{2|\{2\}} - \frac{\Psi(p_h)\lambda_1}{q_{1|\{1\}} - \Delta_1 c_{22} c_{21} p_h} \right) \tag{3.25}$$

and the queue at s_2 is stable if $\lambda_2 \leq \mu_2$. For a given hybrid rate p_h, input rate pairs (λ_1, λ_2) that can be stably admitted into the system are those componentwise less than (μ_1, μ_2), where μ_1 and μ_2 are given in Eq. (3.23) and Eq. (3.25), respectively. The stability region of this dominant system is denoted by $\mathbf{\Lambda}_1$ in Theorem 3.3.1.

Construct next a parallel dominant system in which the primary source s_1 transmits dummy packets, instead of the secondary source s_2, when its queue is empty. Then, the average service rate of s_2 in Eq. (3.22) becomes

$$\mu_2 = c_{22}(q^i_{2|\{2\}} - c_{11}\Psi(p_h)) \tag{3.26}$$

and the queue at s_2 is stable if $\lambda_2 \leq \mu_2$. For a stable rate $\lambda_2 (\leq \mu_2)$, the probability that the queue at s_2 is non-empty is given by

$$\Pr[Q_2 \neq 0] = \frac{\lambda_2}{c_{22}(q^i_{2|\{2\}} - c_{11}\Psi(p_h))}$$

and by substituting the above probability into Eq. (3.21), we obtain the average service rate of s_1 as

$$\mu_1 = c_{11}\left(q_{1|\{1\}} - \frac{\Delta_1 c_{21} p_h \lambda_2}{q^i_{2|\{2\}} - c_{11}\Psi(p_h)}\right) \tag{3.27}$$

and the queue at s_1 is stable if $\lambda_1 \leq \mu_1$. The stability region of this dominant system, which is denoted by $\mathbf{\Lambda}_2$ in Theorem 3.3.1, is comprised of input rate pairs (λ_1, λ_2) that are componentwise less than (μ_1, μ_2), where μ_1 and μ_2 are specified in Eqs. (3.27) and (3.26), respectively. □

3.3.4 Interpretation

3.3.4.1 Superiority of the Hybrid Access

We first illustrate in Fig. 3.17 the stability region of the system described in Theorem 3.3.1 for different values of the hybrid rate p_h. The vertex of the region, denoted by P_V, in the figure is the point where the boundaries of the subregions $\mathbf{\Lambda}_1$ and $\mathbf{\Lambda}_2$ meet with

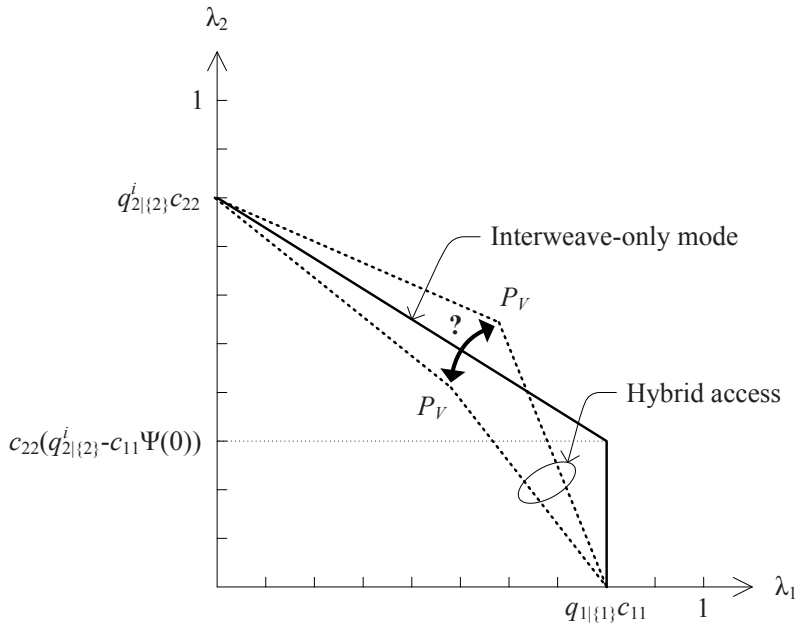

Figure 3.17: Illustration of the stability region: Interweave-only mode vs. hybrid access

each other and is given by

$$P_V = (P_{V,x}, P_{V,y}) = \big(c_{11}(q_{1|\{1\}} - \Delta_1 c_{21} c_{22} p_h), c_{22}(q^i_{2|\{2\}} - c_{11}\Psi(p_h))\big) \tag{3.28}$$

The stability region of the interweave-only mode, which is also depicted in the figure, can be found by setting $p_h = 0$ in Theorem 3.3.1. Let us define

$$\Upsilon \triangleq q_{1|\{1\}}(q^u_{2|\{2\}} - \Delta^u_2 c_{12}) - \Delta_1 c_{22}(q^i_{2|\{2\}} c_{21} + \Delta^i_2 c_{12}\bar{c}_{21})$$

The following corollary answers the question on the necessity of the hybrid access policy. In other words, does the hybrid access policy indeed perform better than the interweave-only mode?

Corollary 3.3.1. *If $\Upsilon \leq 0$, the stability region of the hybrid access policy becomes a proper subset of that of the interweave-only mode for any $p_h \in (0, 1]$. If $\Upsilon > 0$, one is not a subset of the other.*

Proof. The upper boundary of the stability region of the interweave-only mode in Fig. 3.17 is given by

$$\bar{\lambda}_2 = c_{22}\left(q^i_{2|\{2\}} - \frac{\Psi(0)\lambda_1}{q_{1|\{1\}}}\right)$$

for $\lambda_1 \leq c_{11}q_{1|\{1\}}$, which is obtained by substituting $p_h = 0$ into the description of $\mathbf{\Lambda}_1$ in Theorem 3.3.1. For the proof, it suffices to show that if $\Upsilon \leq 0$, the value of $P_{V,y}$ is less than or equal to the value of $\bar{\lambda}_2$ evaluated at $\lambda_1 = P_{V,x}$. The fact that $\Upsilon \leq 0$ is written as

$$q_{1|\{1\}}(q^u_{2|\{2\}} - \Delta^u_2 c_{12}) \leq \Delta_1 c_{22}\left(q^i_{2|\{2\}}c_{21} + \Delta^i_2 c_{12}\bar{c}_{21}\right)$$

Multiplying by a positive number $c_{21}p_h$, $p_h \in (0, 1]$, to both sides, which does not change the inequality, yields

$$q_{1|\{1\}}(\Psi(0) - \Psi(p_h)) \leq \Delta_1 c_{21}c_{22}p_h\Psi(0)$$

By dividing by $q_{1|\{1\}}$, multiplying by $c_{11}c_{22}$ and adding $q^i_{2|\{2\}}c_{22}$ to both sides of the above inequality, which again does not affect the inequality, it follows that

$$c_{22}\left(q^i_{2|\{2\}} - c_{11}\Psi(p_h)\right) \leq c_{22}\left(q^i_{2|\{2\}} - \frac{c_{11}(q_{1|\{1\}} - \Delta_1 c_{21}c_{22}p_h)\Psi(0)}{q_{1|\{1\}}}\right)$$

Finally, we observe that the left-hand side of the above inequality is equal to $P_{V,y}$, whereas the right-hand side is the value of $\bar{\lambda}_2$ at $\lambda_1 = P_{V,x}$. This completes the proof. □

From the above corollary, we see that if $\Upsilon \leq 0$, there is no need for the hybrid mode of operation in terms of the stability region. The following corollary establishes the closure of the stability region over the hybrid rate p_h for the case when $\Upsilon > 0$. Note that when $\Upsilon \leq 0$, the closure is equal to the stability region of the interweave-only mode. Let us define the following points in the two-dimensional Euclidean space to facilitate the

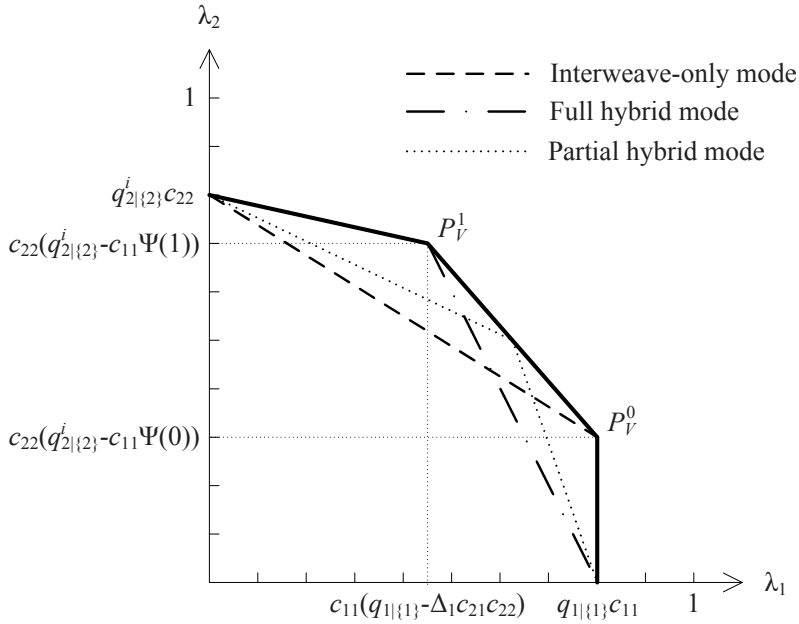

Figure 3.18: Closure of the stability region for the case when $\Upsilon > 0$

description of the next corollary:

$$P_V^1 = \big(c_{11}(q_{1|\{1\}} - \Delta_1 c_{21} c_{22}), c_{22}(q^i_{2|\{2\}} - c_{11}\Psi(1))\big)$$

$$P_V^0 = \big(q_{1|\{1\}}c_{11}, c_{22}(q^i_{2|\{2\}} - c_{11}\Psi(0))\big)$$

where P_V^1 and P_V^0 are the points that P_V in Eq. (3.28) is evaluated at $p_h = 1$ and $p_h = 0$, respectively.

Corollary 3.3.2. *The boundary of the closure of the stability region for the case when* $\Upsilon > 0$ *is described by three segments: (i) the straight line connecting* $(q_{1|\{1\}}c_{11}, 0)$ *and* P_V^0*, (ii) the straight line connecting* P_V^0 *and* P_V^1*, and (iii) the straight line connecting* P_V^1 *and* $(0, q^i_{2|\{2\}}c_{22})$.

Proof. The proof follows from the geometry in Fig. 3.18, which depicts the stability region of the hybrid access policy by varying p_h from zero (interweave-only mode) to one

(full hybrid mode). □

3.3.4.2 Special Case without the Connectivity Information

Let us now consider a special case without the channel connectivity information. It is equivalent to assume that the channels are always connected, i.e., $c_{ij} = 1, \forall i, j$, but each source experiences random disconnection of the links without knowing it a priori. Thus, the success probability of a transmission is now the one that is normalized over the underlying channel conditions. On the other hand, also note that s_2 does not know a priori whether its transmission would interfere with the transmission over the primary link or not without knowing the connectivity of the link from itself to d_1. Hence, it is impossible or unnecessary to differentiate the transmit power level set for the underlay mode from the interweave mode and, thus, we let $q_{2|\{2\}} = q^i_{2|\{2\}} = q^u_{2|\{2\}}$ and $q_{2|\{1,2\}} = q^i_{2|\{1,2\}} = q^u_{2|\{1,2\}}$. Consequently, s_1 transmits whenever its queue is non-empty, whereas s_2 transmits with probability 1 if s_1 is inactive and with probability p_h if s_1 is active with constant power, given that its queue is non-empty. The normalized success probabilities are $\tilde{q}_{1|\{1\}} = c_{11}q_{1|\{1\}}$, $\tilde{q}_{2|\{2\}} = c_{22}q_{2|\{2\}}$, $\tilde{q}_{1|\{1,2\}} = \bar{c}_{21}q_{1|\{1\}} + c_{21}q_{1|\{1,2\}}$, and $\tilde{q}_{2|\{1,2\}} = \bar{c}_{12}q_{2|\{2\}} + c_{12}q_{2|\{1,2\}}$. By setting $c_{ij} = 1, \forall i, j$, and by replacing the success probabilities in Theorem 3.3.1 with the normalized ones, we obtain the stability region of the system as in the following corollary, which reconfirms the previous result obtained in [66] for the system with static MPR capability, i.e., without the notion of channel connectivity.

Corollary 3.3.3. *The stability region of the hybrid access policy for the case without the*

channel connectivity information is given by the union of the following subregions:

$$\tilde{\mathbf{\Lambda}}_1 = \left\{ \boldsymbol{\lambda} : \lambda_1 \leq \tilde{q}_{1|\{1\}} - \tilde{\Delta}_1 p_h,\ \lambda_2 \leq \tilde{q}_{2|\{2\}} - \frac{\tilde{q}_{2|\{2\}} - \tilde{q}_{2|\{1,2\}} p_h}{\tilde{q}_{1|\{1\}} - \tilde{\Delta}_1 p_h} \lambda_1 \right\}$$

$$\tilde{\mathbf{\Lambda}}_2 = \left\{ \boldsymbol{\lambda} : \lambda_1 \leq \tilde{q}_{1|\{1\}} - \frac{\tilde{\Delta}_1}{\tilde{q}_{2|\{1,2\}}} \lambda_2,\ \lambda_2 \leq \tilde{q}_{2|\{1,2\}} p_h \right\}$$

where $\tilde{\Delta}_1 = \tilde{q}_{1|\{1\}} - \tilde{q}_{1|\{1,2\}}$.

In Fig. 3.19, we illustrate the stability region for the case without the channel connectivity information. The vertex of the region in Fig. 3.19(a) is given by $\tilde{P}_V = \left(\tilde{q}_{1|\{1\}} - \tilde{\Delta}_1 p_h, \tilde{q}_{2|\{1,2\}} p_h \right)$ and, similarly as in Fig. 3.17, if $\tilde{P}_V$ is contained inside the stability region of the interweave-only mode for any $p_h \in (0, 1]$, then there is no need for the hybrid mode of operation. This corresponds to the condition that

$$\tilde{\Upsilon} \triangleq \tilde{q}_{1|\{1\}} \tilde{q}_{2|\{1,2\}} + \tilde{q}_{2|\{2\}} \tilde{q}_{1|\{1,2\}} - \tilde{q}_{1|\{1\}} \tilde{q}_{2|\{2\}} \leq 0$$

Fig. 3.19(b) illustrates the closure of the stability region for the case when $\tilde{\Upsilon} > 0$, where $\tilde{P}_V^1$ is the point that $\tilde{P}_V$ is evaluated at $p_h = 1$. From the figure, we observe that the closure is equal to the stability region of the full hybrid mode. In other words, the stability region obtained for any $p_h \in [0, 1)$ becomes a subset of that obtained for $p_h = 1$. Thus, if we are considering a system with static channels or dynamic channels but with no connectivity information, there is no room in which a partial hybrid access policy can play a role. The optimal policy that achieves the maximum stability region is simply a threshold rule: interweave-only mode ($p_h = 0$) if $\tilde{\Upsilon} \leq 0$ or full hybrid mode ($p_h = 1$) if $\tilde{\Upsilon} > 0$.

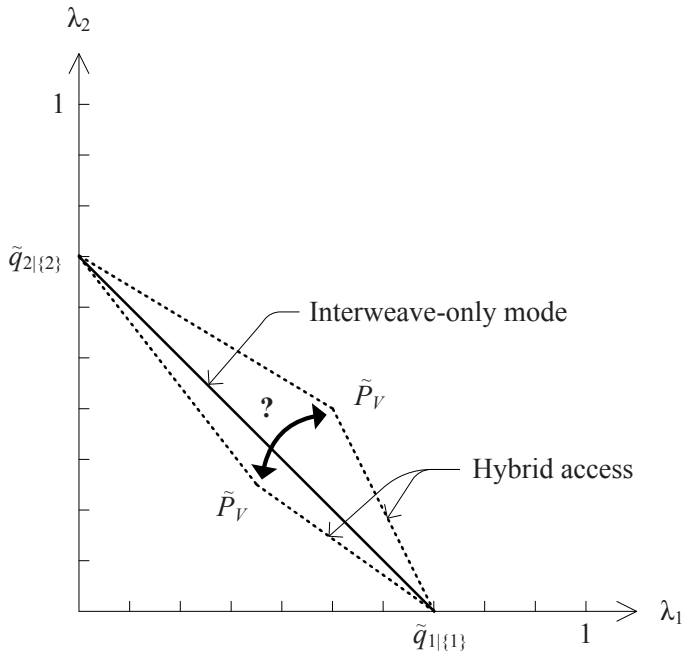

(a) Interweave-only mode vs. hybrid access

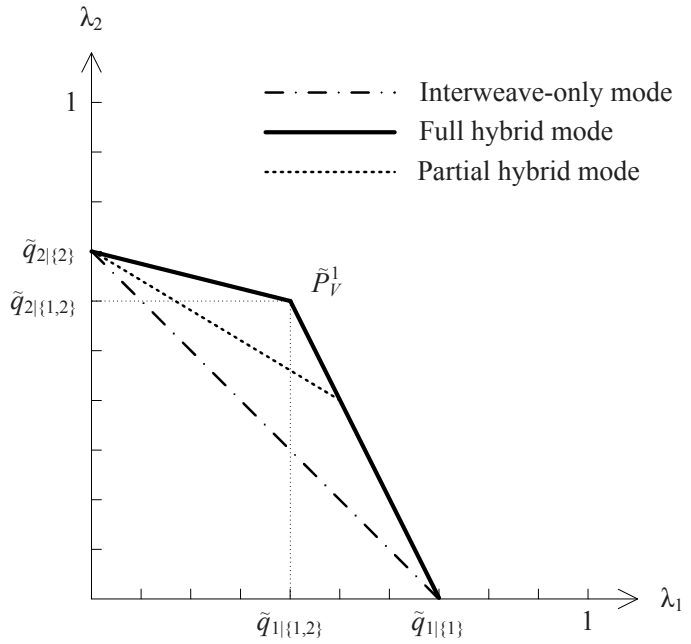

(b) Closure for the case when $\bar{\Upsilon} > 0$

Figure 3.19: Illustration of the stability region for the case without channel connectivity information

3.3.5 Discussion

We studied the hybrid access policy for cognitive radio systems with time-varying connectivity and showed that it is not always the case that the hybrid access policy outperforms the interweave-only mode. Thus, the condition for which there is a gain from using the hybrid access policy is specified. For the special case without the channel connectivity information, it was shown that the optimal policy is either interweave-only or full-hybrid mode depending on the MPR capability. In future work, we plan to study a dynamic hybrid access policy that triggers the underlay mode of operation at the secondary source based on the queue length information using the Lyapunov drift technique.

3.4 Chapter Summary

This chapter attempts to answer some of those important yet unaddressed questions on cognitive radio systems. The first was about the effect of imperfect sensing on the stability region of the cognitive radio systems. Interestingly, we showed that even with non-zero sensing error rates, there exists a condition for which we can achieve the identical stability region that is achieved with perfect sensing. The next was about the hybrid of interweave and underlay modes of operation for cognitive radio systems with random connectivity. We analyzed the stability of the hybrid access policy and showed that it is not always beneficial when compared against the interweave-only mode.

Chapter Appendix 3.A – On the Convexity of the Stability Region in Chapter 3.2.3.2

In this appendix, we interpret the criterion on the convexity of the stability region in terms of values of physical layer parameters. In Chapter 3.2.3.2, it was shown that the convexity is determined by the sign of η, which is equivalent to judge

$$\eta \gtrless 0 \Leftrightarrow \frac{\Delta_1}{q_{1|\{1\}}} + \frac{\Delta_2}{q_{2|\{2\}}} \lessgtr 1 \tag{3.29}$$

where $\Delta_i = q_{i|\{i\}} - q_{i|\{i,j\}}$ for $i, j \in \{\, 1, 2 \,\}$ and $i \neq j$. These packet reception probabilities were derived in Chapter 2.1 and, by substituting these probabilities into the definition of Δ_i, we obtain

$$\Delta_i = \theta \frac{P_{\mathrm{tx},j}}{P_{\mathrm{tx},i}} \left(\frac{r_{ii}}{r_{ji}} \right)^{\nu} \left(1 + \theta \frac{P_{\mathrm{tx},j}}{P_{\mathrm{tx},i}} \left(\frac{r_{ii}}{r_{ji}} \right)^{\nu} \right)^{-1} \exp\left(-\frac{\theta N r_{ii}^{\nu}}{K P_{\mathrm{tx},i}} \right)$$

Then, by substituting Δ_i, $\forall i \in \{1, 2\}$, into (3.29), we express the criterion in terms of the physical layer parameters as

$$\begin{aligned} \eta \gtrless 0 &\Leftrightarrow \frac{\theta P_{\mathrm{tx},2} r_{11}^{\nu}}{P_{\mathrm{tx},1} r_{21}^{\nu} + \theta P_{\mathrm{tx},2} r_{11}^{\nu}} + \frac{\theta P_{\mathrm{tx},1} r_{22}^{\nu}}{P_{\mathrm{tx},2} r_{12}^{\nu} + \theta P_{\mathrm{tx},1} r_{22}^{\nu}} \lessgtr 1 \\ &\Leftrightarrow \theta^2 r_{11}^{\nu} r_{22}^{\nu} \lessgtr r_{12}^{\nu} r_{21}^{\nu} \\ &\Leftrightarrow \Upsilon \triangleq \left(\frac{r_{12}}{r_{11}} \frac{r_{21}}{r_{22}} \right)^{\nu/2} \gtrless \theta \end{aligned} \tag{3.30}$$

Note that Υ is expressed only in terms of the distances between sources and destinations and the propagation loss exponent. Thus, changing the transmission power, for example, does not affect the above comparison. Finally, if $\Upsilon \geq 0$, we can achieve identical stability region that is achieved with perfect sensing even with positive sensing error rates.

Chapter 4

Random Access

4.1 Background

This chapter begins with some background on the stability of random access systems. The characterization of the stability region of random access systems for bursty sources (in contrast to *infinitely backlogged* sources, for which the concept does not make sense) is known to be extremely difficult. This is because each node transmits and thereby interferes with the others only when its queue is non-empty. Such queues are said to be *interacting*, or *coupled*, with each other in the sense that the service process of one depends on the status of the others. Consequently, the individual departure rates of the queues cannot be computed separately without knowing the stationary probability of the joint queue length process, which is intractable [59]. This is the reason why most work has focused on small-sized networks and only bounds or approximations are known for the networks with larger number of nodes [53, 57, 59, 76–78]. In [76], the exact stability region was obtained for the two-node case and for an arbitrary number of nodes with symmetric parameters (that is, equal arrival rates and random access probabilities). In [59], a sufficient stability condition for an arbitrary number of nodes with asymmetric parameters was obtained. In [57], the necessary and sufficient stability condition was derived but it can only be evaluated up to the three-node case. The concept of the *instability rank* was introduced in [77] to further improve the inner bound for the general asymmetric

cases. In [78], an approximate stability region was obtained for an arbitrary number of nodes based on the mean-field asymptotics. All the above results were derived under the collision channel model in which, if more than one nodes transmit simultaneously, none of them are successful. This is too pessimistic assumption today in the sense that a transmission may succeed even in the presence of interference [51–53]. In such a context, the two-node stability result was extended to the channel with the multipacket reception (MPR) capability which enables the probabilistic reception of simultaneously transmitted packets [53]. The advent of the multiuser detection technique for separating signals from the superposition of multiple received signals enables a receiver to correctly decode more than one packets simultaneously transmitted from different users. However, the level of abstraction does not allow the exploitation of the channel variation as the channels are modeled with constant success probabilities over time.

Recently, there is a line of work on exploiting the channel state information (CSI) under random access framework, which is called channel-aware random access (CARA) [20–23]. In [20], it is assumed that each user has perfect local CSI and transmits only when the channel gain exceeds a certain threshold. The main contribution of the work is the characterization of the throughput scaling law for the system with infinitely backlogged users, i.e., users have packets to transmit at any time. Limitations of this work include the collision assumption made for the analysis. Also users were assumed to be symmetric in channel statistics. In [21], a similar problem with that in [20] was considered but with additional MPR capability [51–53]. However, like [20], this work is based on the assumptions that users are always backlogged and symmetric in channel statistics. Note that in the system with bursty input traffic, it is not straightforward to know how users

interfere with each other since they transmit only when having non-empty queues, which is more realistic than assuming always backlogged queues. In [22], the stability region of the system comprised of users having bursty packet arrivals and asymmetric channel statistics was obtained under the collision assumption and further extended in [23] to the case with MPR capability. However, the analysis in both [22] and [23] is limited to the two-user scenario. This limitation is again due to the complex interaction between network queues.

4.2 Random Access of Nodes having Energy Harvesting Capability

4.2.1 Motivation

In this chapter, we focus attention on the effect of limited availability of energy in each node's battery, that can be recharged by harvesting energy from the environment, on the system stability region when a pair of such nodes are randomly accessing a common receiver with static MPR capability as that in [53][1]. Note that the analysis becomes significantly more challenging than in the case with unlimited energy for transmission, because the service process of a node depends not only on the status of its own queue and its battery, but also on the status of the other node's queue and battery. The key fact that makes the analysis tractable in this *doubly* interacting system is that the energy consumption is somewhat simplified as it does not depend on the success of the corresponding transmission. For the characterization of the stability region, we first obtain an inner and an outer bound of the stability region for a given transmission probability vector. Since an

[1] Thus, in this chapter, we do not exploit the time-varying nature of wireless channels.

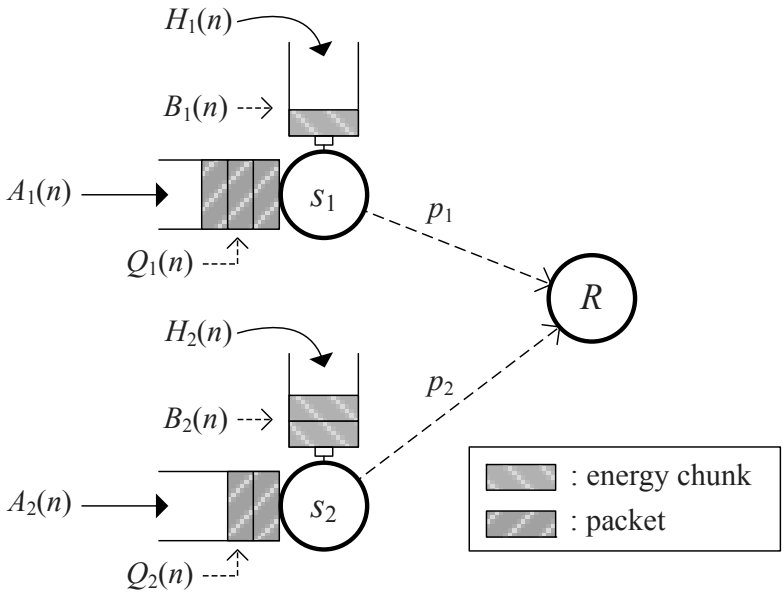

Figure 4.1: Random access of nodes with stochastic energy harvesting

input rate vector that is outside of the stability region at a given transmission probability vector may be stably supported by another transmission probability vector, determination of the closure of the stability region is necessary and important. Consequently, we take the closure of the inner and the outer bound separately over all feasible transmission probability vectors. The remarkable result is that they turn out to be identical. Therefore, our characterization is exact in the sense that the bounds are tight in terms of the closure. Finally, we remark that the results presented in this work generalize those of previous work that assumed unlimited energy for transmission over the collision channel [59, 76] and over the channel with MPR capability [53].

4.2.2 System Model

The system consists of a pair of source nodes randomly accessing a common receiver, each powered by its own battery that can recharge from randomly time-varying

renewable energy sources as shown in Fig. 4.9. Each node has an infinite size queue for storing the arriving packets, that have fixed length, and a battery[2] for storing the harvested energy. Time is slotted and the slot duration is equal to one packet transmission time. Energy is harvested in chunks of fixed size and one chunk of energy is consumed in each transmission. That is, the size of the chunk is equal to the slot duration times the power needed to transmit the fixed size packet over the slot duration. Let $(A_i(n), n \geq 0)$ and $(H_i(n), n \geq 0)$ denote the packet arrival and energy harvesting processes at node i, respectively. They are modeled as independent and identically distributed (i.i.d.) Bernoulli processes with $E[A_i(n)] = \lambda_i$ and $E[H_i(n)] = \delta_i$. The processes at different nodes are also assumed to be independent of each other. Let $Q_i(n)$ and $B_i(n)$ represent the number of buffered packets and the number of stored energy chunks at node i at the beginning of the n-th slot, respectively. Then, $Q_i(n)$ and $B_i(n)$ evolve according to

$$Q_i(n+1) = Q_i(n) - \mu_i(n) + A_i(n) \tag{4.1}$$

and

$$B_i(n+1) = B_i(n) - 1_i(n) + H_i(n) \tag{4.2}$$

where $\mu_i(n) \in \{\, 0, 1 \,\}$ is the actual number of packets that are successfully serviced and, thus, depart from the queue of node i during time slot n, and $1_i(n)$ is the indicator function such that $1_i(n) = 1$ if node i transmits at time slot n, while otherwise $1_i(n) = 0$. Node i is said to be *active* if both its data queue and its battery are non-empty at the same time, so that it can then transmit with probability p_i. If either the queue or the battery is empty, node i is said to be *idle* and remains silent. Since the nodes are accessing a common

[2]The battery capacity is first assumed to be infinite and later relaxed to any finite number.

receiver, the service variable $\mu_i(n)$ depends not only on the status of its own queue and of its battery but also on the status of the other node's queue and battery. Furthermore, it also depends on the underlying channel model.

4.2.3 Main Results on the Stability Region

This chapter presents our main results on the stability of slotted ALOHA for the two-node case with stochastic energy harvesting when the capacity of the batteries is assumed to be infinite. Define $\Delta_i = q_{i|\{i\}} - q_{i|\{1,2\}}$, which is the difference between the success probabilities when node i is transmitting alone and when it transmits along with the other node j ($\neq i$). The quantity Δ_i is strictly positive since interference only reduces the probability of success. Let us define the following points in the two-dimensional Euclidean space to facilitate the description of our main theorem:

$$
\begin{aligned}
P_A &= \big(0, \delta_2 q_{2|\{2\}}\big) \\
P_{B_1} &= \left(\frac{q_{2|\{2\}}(q_{1|\{1\}} - \Delta_1\delta_2)^2}{\Delta_2 q_{1|\{1\}}}, \frac{\Delta_1\delta_2^2 q_{2|\{2\}}}{q_{1|\{1\}}}\right) \\
P_{B_2} &= \left(\frac{\Delta_2\delta_1^2 q_{1|\{1\}}}{q_{2|\{2\}}}, \frac{q_{1|\{1\}}(q_{2|\{2\}} - \Delta_2\delta_1)^2}{\Delta_1 q_{2|\{2\}}}\right) \\
P_{B_3} &= \big(\delta_1(q_{1|\{1\}} - \Delta_1\delta_2), \delta_2(q_{2|\{2\}} - \Delta_2\delta_1)\big) \\
P_C &= \big(\delta_1 q_{1|\{1\}}, 0\big)
\end{aligned}
$$

where P_{B_1}, P_{B_2}, and P_{B_3} are in the first quadrant and P_A and P_C are on y and x-axes, respectively. These points can be seen in Fig. 4.2. Let us further define

$$\Psi \triangleq \frac{\Delta_1\delta_2}{q_{1|\{1\}}} + \frac{\Delta_2\delta_1}{q_{2|\{2\}}}$$

which is non-negative and decreasing as the MPR capability improves.

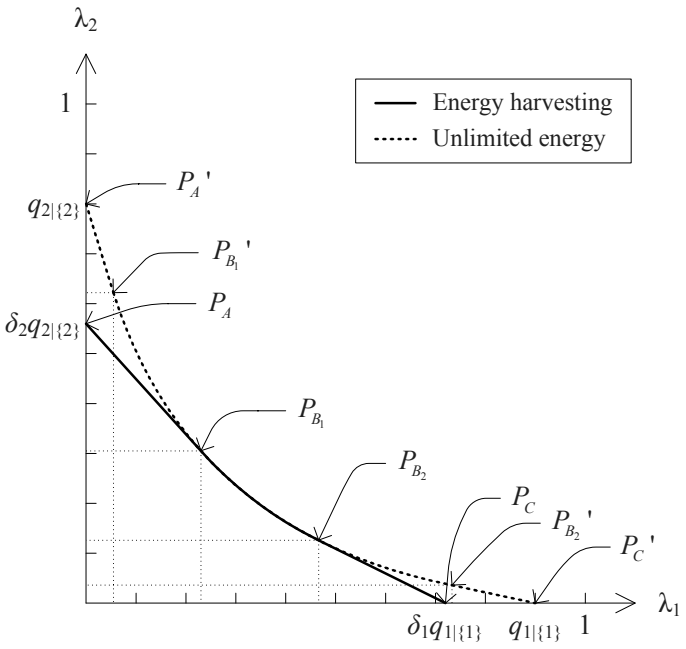

(a) The case with $\Psi \geq 1$ ($q_{1|\{1,2\}} = 0.2, q_{2|\{1,2\}} = 0.15$)

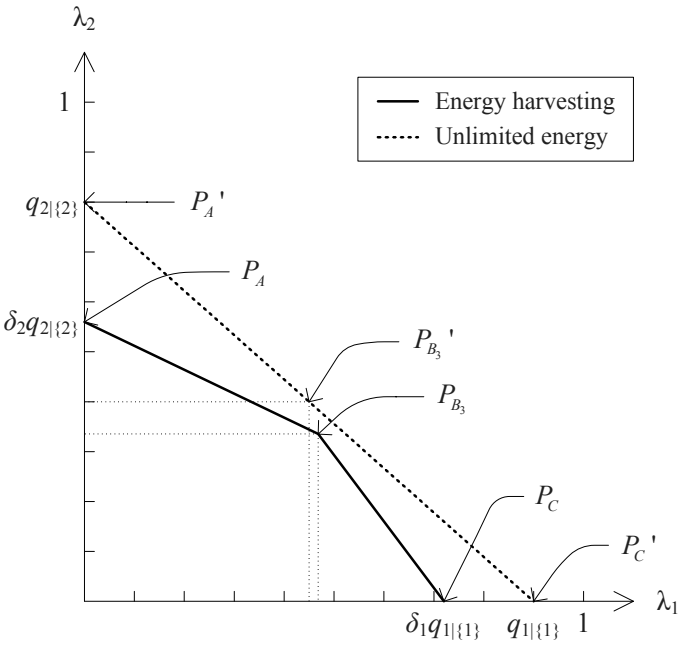

(b) The case with $\Psi < 1$ ($q_{1|\{1,2\}} = 0.45, q_{2|\{1,2\}} = 0.4$)

Figure 4.2: Two-node stability region $\mathfrak{S}(\boldsymbol{\delta})$ at different MPR probabilities where $\boldsymbol{\delta} = (0.8, 0.7)$ and $q_{1|\{1\}} = 0.9, q_{2|\{1\}} = 0.8$

Theorem 4.2.1. *If $\Psi \geq 1$, the boundary of the stability region $\mathfrak{S}(\boldsymbol{\delta})$ of the slotted ALOHA at a given energy harvesting rate $\boldsymbol{\delta}$ is described by three segments: (i) the straight line connecting P_A and P_{B_1}, (ii) the curve*

$$\sqrt{\Delta_2 \lambda_1} + \sqrt{\Delta_1 \lambda_2} = \sqrt{q_{1|\{1\}} q_{2|\{2\}}} \tag{4.3}$$

from P_{B_1} to P_{B_2}, and (iii) the straight line connecting P_{B_2} and P_C. If $\Psi < 1$, it is described by two straight lines: (i) the line connecting P_A and P_{B_3} and (ii) the line connecting P_{B_3} and P_C.

Proof. The proof is presented in Chapter 4.2.4. □

In Fig. 4.2, we illustrate the stability region $\mathfrak{S}(\boldsymbol{\delta})$ for different packet reception probabilities. The boundary of the region is indicated by the solid line. The case with unlimited energy, i.e., $\delta_i = 1, \forall i \in \{1, 2\}$, is also depicted in the figure with the dotted line. The difference between the two regions, therefore, can be understood as the loss due to the limited availability of energy imposed by the variable battery content and the stochastic recharging process.

Corollary 4.2.1. *If $\Psi > 1$, the stability region $\mathfrak{S}(\boldsymbol{\delta})$ is non-convex, whereas if $\Psi \leq 1$, it is a convex polygon. When $\Psi = 1$, the region becomes a right triangle.*

This corollary can be easily verified by comparing the slopes of the lines from P_A to P_{B_1} and from P_{B_2} to P_C and those from P_A to P_{B_3} and from P_{B_3} to P_C. Specifically, when $\Psi = 1$, the curve Eq. (4.3) shrinks to a point whose coordinates are identical to those of P_{B_1} and P_{B_2} and the slopes of the lines from P_A to P_{B_1} and from P_{B_2} to P_C become identical.

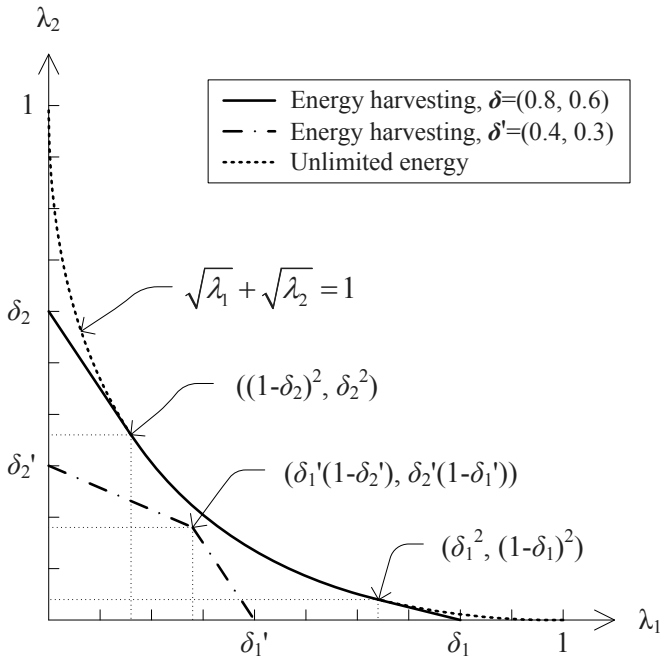

Figure 4.3: Two-node stability region $\mathfrak{S}(\boldsymbol{\delta})$ under the collision channel model, i.e., $q_{i|\{i\}} = 1$ and $q_{i|\{1,2\}} = 0, \forall i \in \{1, 2\}$

When we do not have MPR, i.e., when the channel is described by the classical collision channel model, we can obtain the stable region as described in the following corollary and shown in Fig. 4.3.

Corollary 4.2.2. *The stability region $\mathfrak{S}(\boldsymbol{\delta})$ of the slotted ALOHA under the collision channel model is described as follows. If $\delta_1 + \delta_2 \geq 1$, its boundary is described by three segments: (i) the line segment connecting $(0, \delta_2)$ and $((1-\delta_2)^2, \delta_2^2)$, (ii) the curve $\sqrt{\lambda_1}+\sqrt{\lambda_2} = 1$ from $((1-\delta_2)^2, \delta_2^2)$ to $(\delta_1^2, (1-\delta_1)^2)$, and (iii) the line segment connecting $(\delta_1^2, (1-\delta_1)^2)$ and $(\delta_1, 0)$. If $\delta_1 + \delta_2 < 1$, it is described by two lines: (i) the line segment connecting $(0, \delta_2)$ and $(\delta_1(1-\delta_2), \delta_2(1-\delta_1))$ and (ii) the line segment connecting $(\delta_1(1-\delta_2), \delta_2(1-\delta_1))$ and $(\delta_1, 0)$.*

The corollary is obtained by substituting $q_{i|\{i\}} = 1$ and $q_{i|\{1,2\}} = 0, \forall i \in \{1, 2\}$,

into Theorem 4.2.1.

Corollary 4.2.3. *The stability region $\mathfrak{S}(\mathbf{1})$ of the slotted ALOHA with the unlimited energy for transmission under the collision channel is the region below the curve $\sqrt{\lambda_1} + \sqrt{\lambda_2} = 1$ in the first quadrant of the two-dimensional Euclidean space.*

This last corollary, which is obtained by substituting $\delta_i = 1$, $\forall i \in \{1, 2\}$, into Corollary 4.2.2, reconfirms the well-known result on the stability of the slotted ALOHA obtained in [59].

4.2.4 Stability Analysis

In this chapter, we prove our main result presented in the previous chapter. We first derive a sufficient condition for stability in Chapter 4.2.4.1 and, separately, a necessary condition for stability in Chapter 4.2.4.2 for given energy harvesting rates $\boldsymbol{\delta}$ and transmission probabilities $\boldsymbol{p}$, which yield an inner and an outer bound of $\mathfrak{S}(\boldsymbol{\delta}, \boldsymbol{p})$, respectively, and they are shown in Fig. 4.4. The achievability and the converse of Theorem 4.2.1 is shown in Chapter 4.2.4.3 by taking the closure of the inner and the outer bounds of $\mathfrak{S}(\boldsymbol{\delta}, \boldsymbol{p})$ over $\boldsymbol{p}$ and by observing that these closures turn out to be identical.

4.2.4.1 Sufficient Condition

For the sufficiency, we show that any arrival rate vector $\boldsymbol{\lambda} = (\lambda_1, \lambda_2)$ that is componentwise less than the saturated throughput vector of the system, denoted by $\boldsymbol{\mu}^s = (\mu_1^s, \mu_2^s)$, can be stably supported. An input queue is said to be saturated if, after a head-of-the-line (HOL) packet is transmitted from the queue, there is always a packet queued

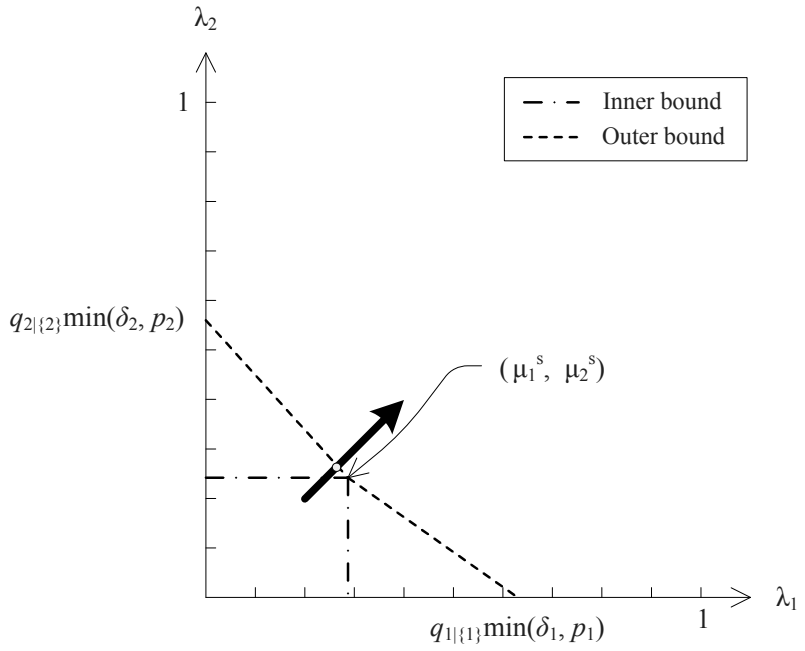

Figure 4.4: An inner and an outer bound of the stability region (parameter setting: $\boldsymbol{p} = (0.7, 0.8)$, $\boldsymbol{\delta} = (0.8, 0.7)$, $q_{1|\{1\}} = 0.9$, $q_{2|\{2\}} = 0.8$, $q_{1|\{1,2\}} = 0.2$, $q_{2|\{1,2\}} = 0.15$)

behind it waiting to take the HOL position, i.e., the input buffer is never empty. Since each node transmits with probability p_i whenever its battery is non-empty and each transmission consumes one chunk of energy, the content size of the battery, $B_i(n)$, forms a decoupled discrete-time $M/M/1$ queue with input rate δ_i and service rate p_i. Consequently, the probability that the battery is non-empty is given by $\min(\frac{\delta_i}{p_i}, 1)$. The probability of success seen by node i is equal to $p_i q_{i|\{i\}}$ if its battery is non-empty while the battery of node $j(\neq i)$ is empty, and equal to $p_i(1-p_j)q_{i|\{i\}} + p_i p_j q_{i|\{1,2\}}$ if both batteries are non-empty. Hence, the saturated throughput of node i is equal to the average service rate

given by

$$\mu_i^s = \left\{ p_i q_{i|\{i\}} \left[1 - \min\left(\frac{\delta_j}{p_j}, 1 \right) \right] + [p_i(1-p_j)q_{i|\{i\}} + p_i p_j q_{i|\{1,2\}}] \min\left(\frac{\delta_j}{p_j}, 1 \right) \right\} \times \min\left(\frac{\delta_i}{p_i}, 1 \right)$$

which can be summarized to

$$\mu_i^s = \min(\delta_i, p_i)(q_{i|\{i\}} - \Delta_i \min(\delta_j, p_j)) \tag{4.4}$$

for $i, j \in \{ 1, 2 \}$ and $i \neq j$.

Lemma 4.2.1. *The system is stable under the slotted ALOHA if the arrival rate vector* $\boldsymbol{\lambda} = (\lambda_1, \lambda_2)$ *is componentwise less than or equal to the saturated throughput vector* $\boldsymbol{\mu}^s = (\mu_1^s, \mu_2^s)$.

Proof. It suffices to show that there is no $\boldsymbol{\lambda} \preceq \boldsymbol{\mu}_s$, where '$\preceq$' denotes componentwise inequality, that makes the system unstable. The intuition is that the behavior of a node with unstable queue is statistically identical to that with saturated queue as time goes to infinity. This is because a queue being unstable, or equivalently transient, implies that its size grows to ∞ without emptying with a nonzero probability. Therefore, if one queue, say queue i, becomes unstable at some $\boldsymbol{\lambda}'$, then the corresponding input rate component λ_i' is greater than the service rate seen in the saturated throughput μ_i^s.

We formally support this argument as follows. Let ϵ_i be any real number satisfying $0 \leq \epsilon_i < \mu_i^s$ and let $\lambda_i = \mu_i^s - \epsilon_i, \forall i \in \{ 1, 2 \}$, such that $\boldsymbol{\lambda} \preceq \boldsymbol{\mu}^s$ and suppose that the system is unstable with the chosen input rate vector. The instability of a system implies that at least one queue in the system is unstable. Let us first suppose that both queues

are unstable such that their queue sizes, $Q_i(n)$, $\forall i \in \{1,2\}$, grow to infinity without emptying with nonzero probability. Since the number of recurrences of the empty-state is finite with probability 1, the probability that each battery is non-empty approaches $\min(\frac{\delta_i}{p_i}, 1)$ as $n \to \infty$, for $i \in \{1,2\}$. Then, the limiting expectation on the actual rate serviced out of queue i, denoted by $\lim_{n\to\infty} E[\mu_i(n)]$, is equal to μ_i^s in Eq.(4.4). On the other hand, from the queueing dynamics in Eq. (4.1), for any $n > 0$, we have

$$Q_i(n) - Q_i(0) = \sum_{k=0}^{n-1} A_i(k) - \sum_{k=0}^{n-1} \mu_i(k)$$

By taking expectations, diving by n, and taking a limit as $n \to \infty$ we have

$$\lim_{n\to\infty} \frac{E[Q_i(n)]}{n} = \lambda_i - \lim_{n\to\infty} \frac{1}{n} \sum_{k=0}^{n-1} E[\mu_i(k)] \tag{4.5}$$

where we use the fact that the effect of the initial queue size disappears as $n \to \infty$ because of the stationarity of the arrival process. The instability of queue i implies that the left-hand-side (LHS) of Eq. (4.5) is strictly positive and, then, it must be the case that

$$\lambda_i = \mu_i^s - \epsilon_i > \lim_{n\to\infty} E[\mu_i(n)] = \mu_i^s$$

which is impossible because ϵ_i is non-negative.

Consider now the case when only one of the queue in the system, say node i, is unstable and the other queue at node $j(\neq i)$ is stable, i.e., the limiting distribution exists only for the queue at node j while the queue at node i is transient. At the steady-state of queue j, the probabilities that the queue and the battery at node i are non-empty are 1 and $\min(\frac{\delta_i}{p_i}, 1)$, respectively. These do not depend on j. In other words, node i randomly interferes with node j with some probability which only has the effect of lowering the average success probability of node j. Since queue j is stable, *the average input rate*

is equal to the average output rate, which can be deduced by setting the LHS of Eq. (4.5) to zero. Additional care should be taken here, because, not all the random variables with a well-defined distribution function have finite expectation, when the distribution is heavy-tailed with tail exponent that is less than 1 [79]. However, in most standard queueing systems including $M/M/1$, $M/G/1$, and $G/M/1$ systems, the queue size exhibits exponential tail [80, 81]. The queue j under consideration is a decoupled discrete-time system that is a variant of $M/M/1$ system whose service is paused when the battery is empty. Since the inter-arrival times of energy chunks follow geometric distribution, and since the energy process is independent of the data process and the channel, the limiting distribution of queue j is also not heavy-tailed. Let us now compute $\mu_{j|\text{active}}$ which is defined as the expected number of packets that is successfully serviced from node j given that node j is active, i.e., given that both its data queue and its battery are non-empty. Since the probability of success seen by node j is $p_j q_{j|\{j\}}$, if node i's battery is empty, and $p_j(1-p_i)q_{j|\{j\}} + p_i p_j q_{j|\{1,2\}}$, if node i's battery is non-empty, we obtain

$$\begin{aligned}\mu_{j|\text{active}} &= p_j q_{j|\{j\}} \left[1 - \min\left(\frac{\delta_i}{p_i}, 1\right)\right] + \left[p_j(1-p_i)q_{j|\{j\}} + p_i p_j q_{j|\{1,2\}}\right] \min\left(\frac{\delta_i}{p_i}, 1\right) \\ &= p_j(q_{j|\{j\}} - \Delta_j \min(\delta_i, p_i))\end{aligned}$$

Since the expected number of packets arriving into the data queue per slot is λ_j, it follows from the property of a stable system, that the input rate is equal to the output rate so that the probability that node j is active at any given time slot is given by

$$\Pr[B_j \neq 0, Q_j \neq 0] = \frac{\lambda_j}{\mu_{j|\text{active}}} \tag{4.6}$$

which does not depend on δ_j. As expectedly, however, if δ_j is decreased, the non-active slots will be more likely to occur due to the emptiness of the battery, rather than that of the

queue. Nevertheless, what it says is that the ratio between the active and non-active slots must remain the same for a given input rate λ_j as long as the queue is stable. By noting that node j transmits with probability p_j only when it is active and node i is unstable, the limiting expectation on the actual rate serviced out of queue i is obtained by

$$\begin{aligned}\lim_{n\to\infty} E[\mu_i(n)] &= \left\{ p_i q_{i|\{i\}} \left(1 - \frac{\lambda_j}{\mu_{j|\text{active}}}\right) + [p_i(1-p_j)q_{i|\{i\}} + p_i p_j q_{i|\{1,2\}}] \frac{\lambda_j}{\mu_{j|\text{active}}} \right\} \\ &\qquad \times \min\left(\frac{\delta_i}{p_i}, 1\right) \\ &= \min(\delta_i, p_i) \left(q_{i|\{i\}} - \frac{\Delta_i \lambda_j}{q_{j|\{j\}} - \Delta_j \min(\delta_i, p_i)} \right) \\ &\overset{\text{(a)}}{\geq} \min(\delta_i, p_i)(q_{i|\{i\}} - \Delta_i \min(\delta_j, p_j)) \\ &= \mu_i^s\end{aligned}$$

where, for (a), we replaced λ_j with $\mu_j^s - \epsilon_j$ and used the fact that ϵ_j is non-negative. Again, the instability of the queue i implies that the LHS of Eq. (4.5) is strictly positive and, then, it must be the case that

$$\lambda_i = \mu_i^s - \epsilon_i > \lim_{n\to\infty} E[\mu_i(n)] \geq \mu_i^s$$

which is impossible because ϵ_i is non-negative.

□

4.2.4.2 Necessary Condition

The necessary condition for the stability of the considered system is derived through the construction of a hypothetical system as in Chapter 2.3; i) the packet and energy chunk arrivals at each node occur at *exactly* the same instants as in the original system, ii) the

coin tosses that determine transmission attempts at each node have *exactly* the same outcomes in both systems, iii) however, one of the nodes in the system continues to transmit dummy packets even when its data queue is empty but its battery is non-empty. The dummy packet transmission continues to consume one chunk of energy in the battery but does not contribute to throughput if the transmission is successful. Such a construction of a hypothetical system with dummy packet transmissions has been widely used to analyze systems of interacting queues as mentioned in Chapter 2.3. However, in the case of a system with batteries, as is considered in this work, there exist sample-paths on which this strict path-wise dominance is violated. This is because dummy packet transmissions alter the dynamics of the batteries through unproductive use of their contents. For example, there are instants when a node is no more able to transmit in the hypothetical system due to the lack of energy while it is able to transmit in the original system. Being not able to transmit may imply a better chance of success for the other node, if the latter attempts to transmit at those instants, which causes a collapse of the sample-path dominance. Instead, here we use the hypothetical system of transmitting dummy packets only to derive a *necessary* condition for the stability of the original system.

Let us define

$$\mathcal{R}_i = \Bigg\{ \boldsymbol{\lambda} : \lambda_i \leq \min(\delta_i, p_i) \left(q_{i|\{i\}} - \frac{\Delta_i \lambda_j}{q_{j|\{j\}} - \Delta_j \min(\delta_i, p_i)} \right), \\ \lambda_j \leq \min(\delta_j, p_j)(q_{j|\{j\}} - \Delta_j \min(\delta_i, p_i)) \Bigg\}$$

where $i \neq j$ and $i, j \in \{ 1, 2 \}$.

Lemma 4.2.2. *If the system is stable under the slotted ALOHA, then* $\boldsymbol{\lambda} \in \bigcup_{i \in \{1,2\}} \mathcal{R}_i$.

Proof. Let us consider a hypothetical system in which node i transmits dummy packets when its packet queue is empty and node $j(\neq i)$ operates as in the original system, where $i, j \in \{\, 1, 2 \,\}$. As mentioned earlier, all other random events including the packet arrivals, energy harvesting, and the decisions for transmissions have the same realizations as in the original system. In the hypothetical system, node i transmits with probability p_i regardless of the emptiness of its data queue, provided its energy queue is non-empty, and each transmission consumes one chunk of energy. Therefore, $B_i(n)$ forms a decoupled discrete-time $M/M/1$ queue whose probability of non-emptiness is given by $\min(\frac{\delta_i}{p_i}, 1)$ and node i behaves independently from node j, i.e., node i only has the effect of lowering the success probability of node j in the average sense. The saturated throughput of node j, therefore, can be computed separately as in Eq. (4.4) and the queue at node j is stable if

$$\lambda_j \leq \min(\delta_j, p_j)(q_{j|\{j\}} - \Delta_j \min(\delta_i, p_i)) \tag{4.7}$$

which follows by applying Lemma 4.2.1 to a single-node case. For λ_j satisfying Eq. (4.7), the probability that node j is active is obtained as in Eq. (4.6) by noting that the probability that battery i is non-empty is given by $\min(\frac{\delta_i}{p_i}, 1)$. Thus, the queue at node i is stable if

$$\begin{aligned}\lambda_i &\leq \left\{ p_i q_{i|\{i\}} \left(1 - \frac{\lambda_j}{\mu_{j|\text{active}}}\right) + [p_i(1-p_j)q_{i|\{i\}} + p_i p_j q_{i|\{1,2\}}] \frac{\lambda_j}{\mu_{j|\text{active}}} \right\} \min\left(\frac{\delta_i}{p_i}, 1\right) \\ &= \min(\delta_i, p_i) \left(q_{i|\{i\}} - \frac{\Delta_i \lambda_j}{q_{j|\{j\}} - \Delta_j \min(\delta_i, p_i)} \right) \end{aligned} \tag{4.8}$$

The pair of equations Eqs. (4.7) and (4.8) describes the stability condition for the hypothetical system in which node i transmits dummy packets, which is a necessary condition for the stability of the original system for the range of values of λ_j specified in Eq. (4.7).

The reason is this: if for some λ_i, queue i is unstable in the hypothetical system, i.e., Eq. (4.8) does not hold, then $Q_i(n)$ approaches infinity almost surely. Note that as long as queue i does not empty, the behavior of the hypothetical system and the original system are identical, provided they start from the same initial conditions, since dummy packets will never have to be used. A sample-path that goes to infinity without visiting the empty state, which is a feasible one for a queue that is unstable, will be identical for both the hypothetical and the original systems. Therefore, the instability of the hypothetical system implies the instability of the original system. □

4.2.4.3 Proof of Theorem 4.2.1

Here we first compute the closure of the outer bound of $\mathfrak{S}(\boldsymbol{\delta}, \boldsymbol{p})$ over all feasible transmission probability vectors $\boldsymbol{p} \in [0, 1]^2$. Therefore, any rate vector that is outside the closure is not attainable. After that, it is proven that the entire interior of the closure can be achieved by showing that the closure of the inner bound is identical with that of the outer bound.

Note that the description on the outer bound of $\mathfrak{S}(\boldsymbol{\delta}, \boldsymbol{p})$ in Lemma 4.2.2 does not depend on $\boldsymbol{\delta}$ for $\boldsymbol{p} \preceq \boldsymbol{\delta}$ and also note that increasing p_i over δ_i has no effect since the value of $\min(\delta_i, p_i)$ is bounded below by δ_i. For the subregion $\mathcal{R}_i$, $i \in \{ 1, 2 \}$, let us consider the following boundary optimization problem in which we maximize the boundary of λ_i,

denoted by $\bar{\lambda}_i$, for a given value of λ_j $(j \neq i)$ as $\boldsymbol{p}$ varies[3], that is

$$\max_{\boldsymbol{p}} \ \bar{\lambda}_i = p_i \left(q_{i|\{i\}} - \frac{\Delta_i \lambda_j}{q_{j|\{j\}} - \Delta_j p_i} \right) \tag{4.9}$$

$$\text{subject to } \ \lambda_j \leq p_j (q_{j|\{j\}} - \Delta_j p_i) \tag{4.10}$$

$$p_i \leq \delta_i, \forall i \in \{\, 1, 2 \,\} \tag{4.11}$$

To maximize $\bar{\lambda}_i$ over $\boldsymbol{p}$, we need to understand their relationship. Note that $\bar{\lambda}_i$ depends only on p_i. Differentiating $\bar{\lambda}_i$ with respect to p_i gives

$$\frac{\partial \bar{\lambda}_i}{\partial p_i} = q_{i|\{i\}} - \frac{\Delta_i q_{j|\{j\}} \lambda_j}{(q_{j|\{j\}} - \Delta_j p_i)^2}$$

and by differentiating once again, we have

$$\frac{\partial^2 \bar{\lambda}_i}{\partial p_i^2} = -\frac{2\Delta_i \Delta_j q_{j|\{j\}} \lambda_j}{(q_{j|\{j\}} - \Delta_j p_i)^3}$$

Since $q_{j|\{j\}} > \Delta_j$, the second derivative is negative and, thus, $\bar{\lambda}_i$ is a concave function of p_i. Equating the first derivative to zero gives the maximizing p_i^* as

$$p_i^* = \frac{1}{\Delta_j} \left(q_{j|\{j\}} - \sqrt{\frac{\Delta_i q_{j|\{j\}} \lambda_j}{q_{i|\{i\}}}} \right) \tag{4.12}$$

and the corresponding maximum function value is obtained by substituting Eq. (4.12) into Eq. (4.9), thus yielding

$$\bar{\lambda}^*_{i,\text{curve}} = \left(1 - \sqrt{\frac{\Delta_i \lambda_j}{q_{i|\{i\}} q_{j|\{j\}}}} \right) \left(\frac{q_{i|\{i\}} q_{j|\{j\}} - \sqrt{\Delta_i q_{i|\{i\}} q_{j|\{j\}}} \lambda_j}{\Delta_j} \right) \tag{4.13}$$

Suppose now that the maximum occurs at a strictly interior point of the feasible region, i.e., $p_i^* \in (0, \delta_i)$, which corresponds to the condition

$$\frac{q_{i|\{i\}} (q_{j|\{j\}} - \Delta_j \delta_i)^2}{\Delta_i q_{j|\{j\}}} < \lambda_j < \frac{q_{i|\{i\}} q_{j|\{j\}}}{\Delta_i} \tag{4.14}$$

[3]Note that optimizing the boundary of a region over $\boldsymbol{p}$ is equivalent to take the closure of the region over $\boldsymbol{p}$.

which is obtained by rearranging Eq. (4.12) and substituting the extreme values of p_i^*. On the other hand, the constraint in Eq. (4.10) should also be satisfied for the derived p_i^*. Hence, by substituting Eq. (4.12) into Eq. (4.10) and using $p_j \leq \delta_j$, we obtain

$$\lambda_j \leq \frac{\Delta_i q_{j|\{j\}} \delta_j^2}{q_{i|\{i\}}} \tag{4.15}$$

Consequently, $\bar{\lambda}_{i,\text{curve}}^*$ in Eq. (4.13) is valid only for the range of values of λ_j that satisfy both Eqs. (4.14) and (4.15). The intersection of the ranges of values of λ_j determined by Eqs. (4.14) and (4.15) would be identical with the range specified by Eq. (4.14) if $\delta_j \geq \frac{q_{i|\{i\}}}{\Delta_i}$, which is impossible because $q_{i|\{i\}} > \Delta_i$ while $\delta_j \leq 1$. Thus, if $\Psi \geq 1$, where Ψ is defined in Chapter 4.2.3, the intersection is given by

$$\frac{q_{i|\{i\}}(q_{j|\{j\}} - \Delta_j \delta_i)^2}{\Delta_i q_{j|\{j\}}} < \lambda_j \leq \frac{\Delta_i q_{j|\{j\}} \delta_j^2}{q_{i|\{i\}}}$$

Otherwise, if $\Psi < 1$, the intersection is an empty set.

Next suppose that either $p_i^* = 0$ or $p_i^* = \delta_i$, which is the case when λ_j lies outside of the range of Eq. (4.14). If λ_j is on the right-hand side of the range, i.e., if $\lambda_j \geq \frac{q_{i|\{i\}} q_{j|\{j\}}}{\Delta_i}$, $\bar{\lambda}_i$ is a non-increasing function of p_i since its first derivative in Eq. (4.3.4) is non-positive. Therefore, $p_i^* = 0$ and $\bar{\lambda}_i^* = 0$. On the other hand, if λ_j is on the left-hand side of the range of Eq. (4.14), $\bar{\lambda}_i$ is a non-decreasing function of p_i and, hence, $p_i^* = \delta_i$ and the corresponding maximum function value is obtained as

$$\bar{\lambda}_{i,\text{line}}^* = \delta_i \left(q_{i|\{i\}} - \frac{\Delta_i \lambda_j}{q_{j|\{j\}} - \Delta_j \delta_i} \right)$$

for

$$\lambda_j \leq \frac{q_{i|\{i\}}(q_{j|\{j\}} - \Delta_j \delta_i)^2}{\Delta_i q_{j|\{j\}}} \tag{4.16}$$

On the other hand, the constraint in Eq. (4.10) at $p_i^* = \delta_i$ becomes

$$\lambda_j \leq \delta_j(q_{j|\{j\}} - \Delta_j \delta_i) \tag{4.17}$$

Thus, $\bar{\lambda}^*_{i,\text{line}}$ is valid for the range of values of λ_j specified as the intersection of the ranges given by Eqs. (4.16) and (4.17). If $\Psi \geq 1$, the intersection coincides with Eq. (4.16) and, if $\Psi < 1$, it coincides with Eq. (4.17). To sum up, $\bar{\lambda}^*_i$ is obtained as follows:

- If $\Psi \geq 1$,

$$\bar{\lambda}^*_i = \begin{cases} \bar{\lambda}^*_{i,\text{curve}}, & \text{for } \frac{q_{i|\{i\}}(q_{j|\{j\}} - \Delta_j\delta_i)^2}{\Delta_i q_{j|\{j\}}} < \lambda_j \leq \frac{\Delta_i q_{j|\{j\}}\delta_j^2}{q_{i|\{i\}}} \\ \bar{\lambda}^*_{i,\text{line}}, & \text{for } \lambda_j \leq \frac{q_{i|\{i\}}(q_{j|\{j\}} - \Delta_j\delta_i)^2}{\Delta_i q_{j|\{j\}}} \end{cases}$$

- If $\Psi < 1$,

$$\bar{\lambda}^*_i = \bar{\lambda}^*_{i,\text{line}}, \text{ for } \lambda_j \leq \delta_j(q_{j|\{j\}} - \Delta_j\delta_i)$$

Substituting $i \in \{\, 1, 2 \,\}$ into the above yields the description for $\bar{\lambda}^*_1$ and $\bar{\lambda}^*_2$ which lead us to the description for the stability region given in Theorem 4.2.1. Specifically, when $\Psi \geq 1$, the end points of $\bar{\lambda}^*_{2,\text{curve}}$ and $\bar{\lambda}^*_{2,\text{line}}$ and those of $\bar{\lambda}^*_{1,\text{curve}}$ and $\bar{\lambda}^*_{1,\text{line}}$ meet at P_{B_1} and P_{B_2} (which are defined in Chapter 4.2.3), respectively. Furthermore, $\bar{\lambda}^*_{1,\text{curve}}$ and $\bar{\lambda}^*_{2,\text{curve}}$ are functions that are inverse of each other and they can be identically rearranged to coincide with Eq. (4.3). These segments together with the axes form a closed region in the two-dimensional Euclidean space as shown in Fig. 4.3.3. If $\Psi < 1$, the end points of $\bar{\lambda}^*_{1,\text{line}}$ and $\bar{\lambda}^*_{2,\text{line}}$ meet at P_{B_3} and, likewise, they define a closed region as shown in Fig. 4.3.3.

What is left to be shown is the achievability of the specified region. From Lemma 4.2.1, we know that $\boldsymbol{\lambda} \preceq \boldsymbol{\mu}^s$ can be stably supported. For some $j \in \{\, 1, 2 \,\}$, if $\boldsymbol{p} \preceq \boldsymbol{\delta}$, μ^s_j

is written as

$$\mu_j^s = p_j(q_{j|\{j\}} - \Delta_j p_i)$$

from which we derive

$$p_j = \frac{\mu_j^s}{q_{j|\{j\}} - \Delta_j p_i} \tag{4.18}$$

By substituting p_j into the expression for μ_i^s $(i \neq j)$, we have

$$\mu_i^s = p_i \left(q_{i|\{i\}} - \frac{\Delta_i \mu_j^s}{q_{j|\{j\}} - \Delta_j p_i} \right)$$

which turns out to be identical to the expression for the outer boundary in Eq. (4.9) by replacing μ_i^s with $\bar{\lambda}_i$ and μ_j^s with λ_j. In other words, the operating point of the saturated system can be controlled to any point on the boundary of $\mathcal{R}_i$ by adjusting p_j according to Eq. (4.18) for $i \in \{1, 2\}$ and $j \neq i$. This implies that the outer bound described by Lemma 4.2.2 can be indeed achieved, which proves the achievability of Theorem 4.2.1.

4.2.5 The Impact of Finite Capacity Batteries

In this chapter, we consider the case where the capacity of the batteries is finite and study the impact of that on the previously obtained stability region. Denote by c_i the capacity of the battery at node i. Then, the number of energy chunks stored in the battery evolves according to

$$B_i(n+1) = \min\left(B_i(n) - 1_i(n) + H_i(n), c_i\right)$$

i.e., the harvested energy chunks now can be stored only if the corresponding battery is not fully recharged. Since most of the analysis overlaps with the case of infinite capacity batteries, the result is demonstrated only for the collision channel model for brevity and

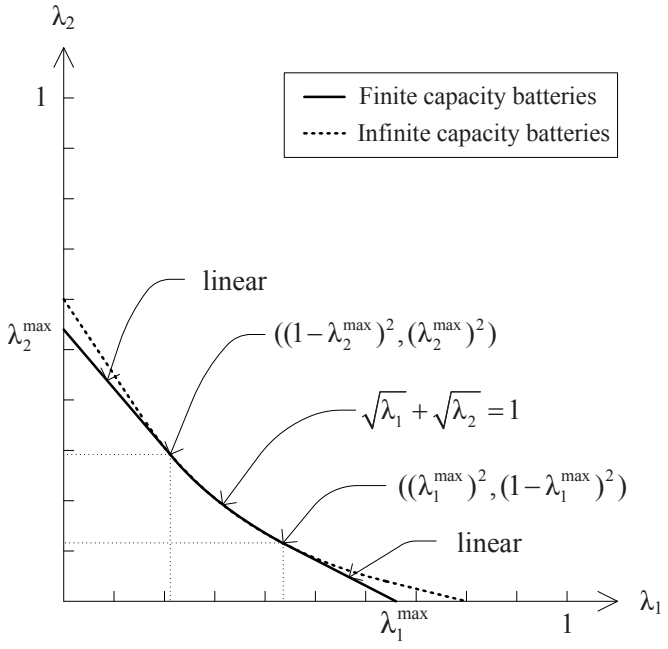

Figure 4.5: Two-node stability region $\mathfrak{S}^{\boldsymbol{c}}(\boldsymbol{\delta})$ with finite capacity batteries where $\boldsymbol{\delta} = (0.8, 0.6)$ and $\boldsymbol{c} = (3, 3)$ (the case when $\lambda_1^{\max} + \lambda_2^{\max} \geq 1$)

to simplify the exposition. It becomes clear from the analysis that the channel with MPR capability can be handled similarly. Denote by c_i the capacity of the battery at node i and let $\lambda_i^{\max} \triangleq \delta_i(1 - \delta_i^{c_i})/(1 - \delta_i^{c_i+1})$.

Theorem 4.2.2. *For a given energy harvesting rate $\boldsymbol{\delta}$, the two-node stability region $\mathfrak{S}^{\boldsymbol{c}}(\boldsymbol{\delta})$ of the collision channel random access with batteries that have finite capacities, denoted by $\boldsymbol{c} = (c_i, i \in \{1, 2\})$, is as follows. If $\lambda_1^{\max} + \lambda_2^{\max} \geq 1$, the boundary of the stability region is composed of three segments: (i) a line segment connecting $(0, \lambda_2^{\max})$ and $((1 - \lambda_2^{\max})^2, (\lambda_2^{\max})^2)$, (ii) the curve $\sqrt{\lambda_1} + \sqrt{\lambda_2} = 1$ from the point with coordinates $((1 - \lambda_2^{\max})^2, (\lambda_2^{\max})^2)$ to the point with coordinates $((\lambda_1^{\max})^2, (1 - \lambda_1^{\max})^2)$, and (iii) a line segment connecting points $((\lambda_1^{\max})^2, (1 - \lambda_1^{\max})^2)$ and $(\lambda_1^{\max}, 0)$. If $\lambda_1^{\max} + \lambda_2^{\max} < 1$, the boundary is described by two straight line segments, namely, (i) the one connecting points*

$(0, \lambda_2^{\max})$ *and* $(\lambda_1^{\max}(1-\lambda_2^{\max}), \lambda_2^{\max}(1-\lambda_1^{\max}))$ *and (ii) the one connecting* $(\lambda_1^{\max}(1-\lambda_2^{\max}), \lambda_2^{\max}(1-\lambda_1^{\max}))$ *and* $(\lambda_1^{\max}, 0)$.

Proof. We begin by noting that when a node, say node i, transmits with probability p_i whenever its battery is non-empty in case it is either saturated or transmits dummy packets if its queue is empty, the size of the battery, $B_i(n)$, follows a decoupled discrete-time $M/M/1/c_i$ model whose probability of being non-empty is given by [80]

$$f_i = \begin{cases} \dfrac{(\delta_i/p_i)\left(1-(\delta_i/p_i)^{c_i}\right)}{1-(\delta_i/p_i)^{c_i+1}}, & \text{if } \delta_i \neq p_i \\ \\ \dfrac{c_i}{c_i+1}, & \text{if } \delta_i = p_i \end{cases}$$

By following similar steps as in the previous chapter, the outer bound of $\mathfrak{S}^{\boldsymbol{c}}(\boldsymbol{\delta}, \boldsymbol{p})$ for the case of the collision channel model is obtained as the union of regions described by

$$\mathcal{R}_i = \left\{ \boldsymbol{\lambda} : \lambda_i \leq p_i f_i \left(1 - \frac{\lambda_j}{1-p_i f_i}\right), \lambda_j \leq p_j f_j (1-p_i f_i) \right\} \tag{4.19}$$

for $i \in \{1, 2\}$ and $i \neq j$. Similarly, the saturated throughput vector of the system, which corresponds to an inner bound of the stability region, is obtained as $\boldsymbol{\mu}^s = (\mu_i^s, i \in \{1, 2\})$ with $\mu_i^s = p_i f_i (1-p_j f_j)$. By substituting $p_j = \mu_j^s/(f_j(1-p_i f_i))$ into the expression for μ_i^s, we observe that the saturated throughput vector $\boldsymbol{\mu}^s$ can achieve any point on the boundary of $\mathcal{R}_i$, i.e., the rate region inside the outer bound of $\mathfrak{S}^{\boldsymbol{c}}(\boldsymbol{\delta}, \boldsymbol{p})$ can be indeed achieved. Let us now compute the closure of the stability region. Observe that the function $p_i f_i$ is an increasing function of p_i and, thus, its maximum occurs at $p_i^* = 1$ and the corresponding maximum function value is obtained as $\delta_i(1-\delta_i^{c_i})/(1-\delta_i^{c_i+1})$, which we denoted by $\lambda_i^{\max}$. Consequently, any non-negative function value that is less than or equal to $\lambda_i^{\max}$ can be attained by appropriately selecting a value for p_i between zero and one. Based on

this observation, replace $p_i f_i$ in Eq. (4.19) with another variable $p_i' \in [0, \lambda_i^{\max}]$. The rest of the proof follows that of Theorem 4.2.1. Specifically, we set up and solve an optimization problem similar to that of Chapter 4.2.4.3 from Eq. (4.9) to Eq. (4.11) with $q_{i|\{i\}} = 1$, $q_{i|\{1,2\}} = 0$, and $p_i \in [0, \lambda_i^{\max}]$, $\forall i \in \{1, 2\}$. Indeed, the result for the channel with the MPR capability can be obtained by solving the same problem as in Chapter 4.2.4.3 but with $p_i \in [0, \lambda_i^{\max}]$, $\forall i \in \{1, 2\}$. The remainder of the proof is omitted for brevity. □

An example two-node stability region $\mathfrak{S}^{\boldsymbol{c}}(\boldsymbol{\delta})$ with finite capacity batteries is depicted in Fig. 4.5 which is the region below the solid line. For comparison's sake, the stability region with infinite capacity batteries for the same parameter values is also depicted in the figure with the dotted line. The difference between the two regions, therefore, represents the loss due to the finite capacity of the batteries.

Corollary 4.2.4. *Denote by $\mathfrak{S}^{\infty}(\boldsymbol{\delta})$ the stability region of the slotted ALOHA with infinite capacity batteries. Then, for any finite capacity batteries, the relation $\mathfrak{S}^{\boldsymbol{c}}(\boldsymbol{\delta}) \subset \mathfrak{S}^{\infty}(\boldsymbol{\delta})$ holds.*

As observed in the proofs of Theorem 4.2.1 and Theorem 4.2.2, we can compute $\mathfrak{S}^{\infty}(\boldsymbol{\delta})$ and $\mathfrak{S}^{\boldsymbol{c}}(\boldsymbol{\delta})$ through a closure operation over $\boldsymbol{p}$ varying in the rectangles $[0, \delta_1] \times [0, \delta_2]$ and $[0, \lambda_1^{\max}] \times [0, \lambda_2^{\max}]$, respectively. The corollary follows from the fact that $\lambda_i^{\max}$ is strictly less than δ_i for any finite c_i.

4.2.6 Simulation

The simulation results presented here suggest that the outer bound obtained in Section 4.2.4 is the stability region of the original system. We simulate the system at the

parameter setting that is identical to that of Fig. 4.4. Note that the main result in Fig. 4.2 is a consequence of the result in Fig. 4.4 by taking the closure of the inner and the outer bounds over the access probability vector $\boldsymbol{p}$. Thus, validating the inner and the outer bounds is necessary and important.

We first observe the average behavior of the system as the traffic load increases. For simplicity of exposition, we consider symmetric Bernoulli arrivals, so that $\lambda_i = \lambda$ for all i in $\{ 1, 2 \}$ as illustrated in Fig. 4.4 with the diagonal arrow. We simulated the system over 10^6 slots and the results are illustrated in Fig. 4.6. It is observed from Fig. 4.6(a) that as we cross the outer bound of the stability region, which is at $\bar{\lambda} = 0.2603$ from Eq. 4.8, the size of the queue at s_2 starts growing. As the input rate is further increased such that it exceeds $\lambda = 0.287$, which is the service rate of s_1 when s_2 transmits dummy packets given in Eq. 4.7, the size of the queue at s_1 also starts growing. The corresponding average battery levels are also shown in Fig. 4.6(b).

Note, however, that the average behavior of the system demonstrated in Fig. 4.6 is not enough to judge the stability of the system because stability is an asymptotic property but the queue length averages were taken over the finite time interval. Although the simulation interval can be further increased, it is nevertheless finite. Thus, the best we can do is to observe the tendency of system dynamics over the course of time. In Fig. 4.7, we illustrate queue length and battery level sample paths at input traffic load at $\lambda = \bar{\lambda} - \epsilon$ with $\epsilon = 0.01$, where $\bar{\lambda}$ is again the point on which in Fig. 4.4 the diagonal arrow meets the outer bound of the stability region. Thus, the chosen loading point is inside the outer bound of the stability region, which is slightly below the boundary. From Fig. 4.7(a), no clear evidence is found to suggest that there is an increasing tendency in the queue size

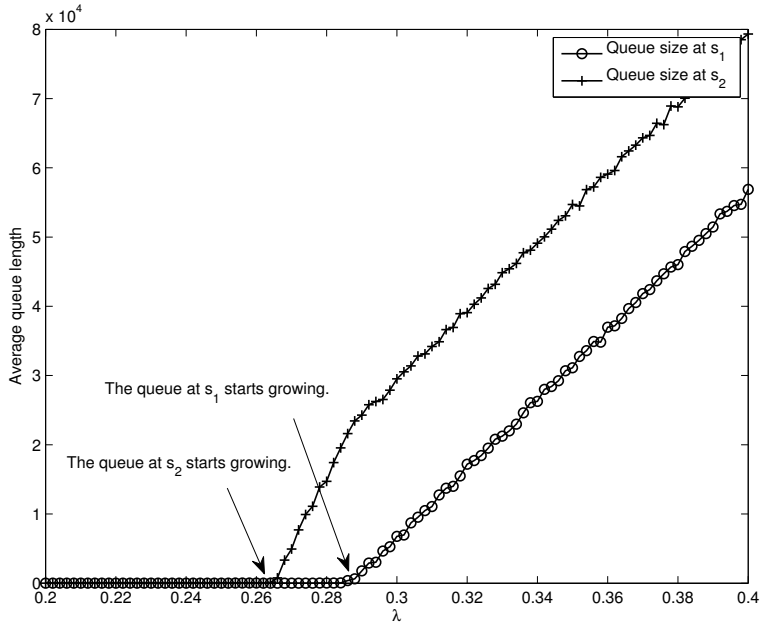

(a) Queue length averages

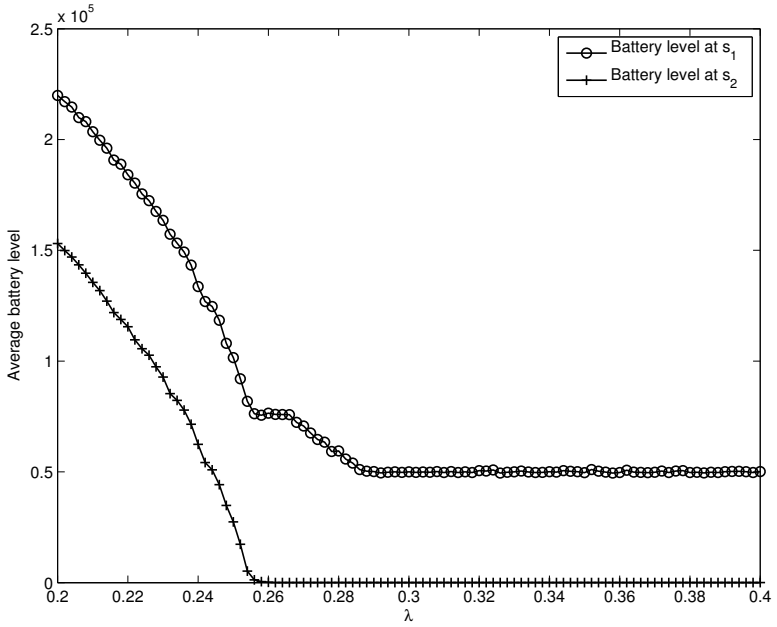

(b) Battery level averages

Figure 4.6: Average behavior of the system over 10^6 slots along the arrow in Fig. 4.4, i.e., $\lambda = \lambda_1 = \lambda_2$ for the range $\lambda \in [0.2, 0.4]$

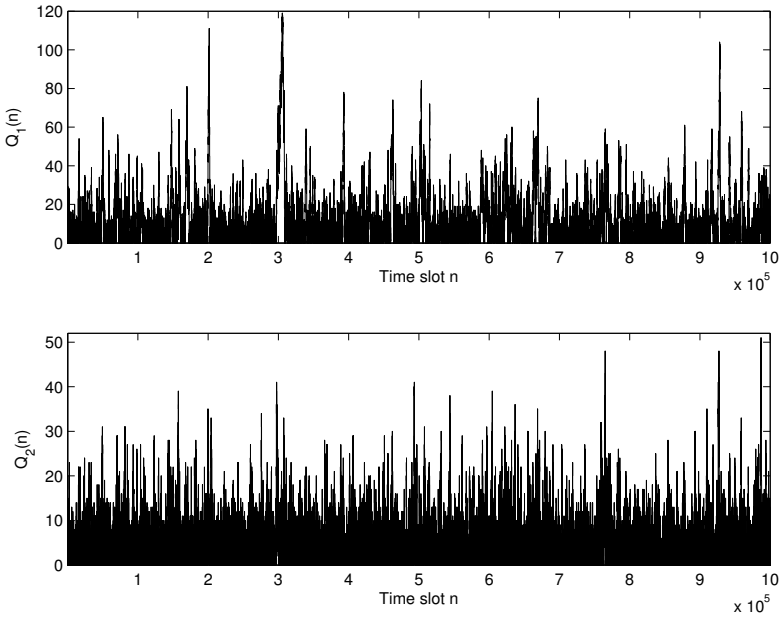

(a) Queue length sample path

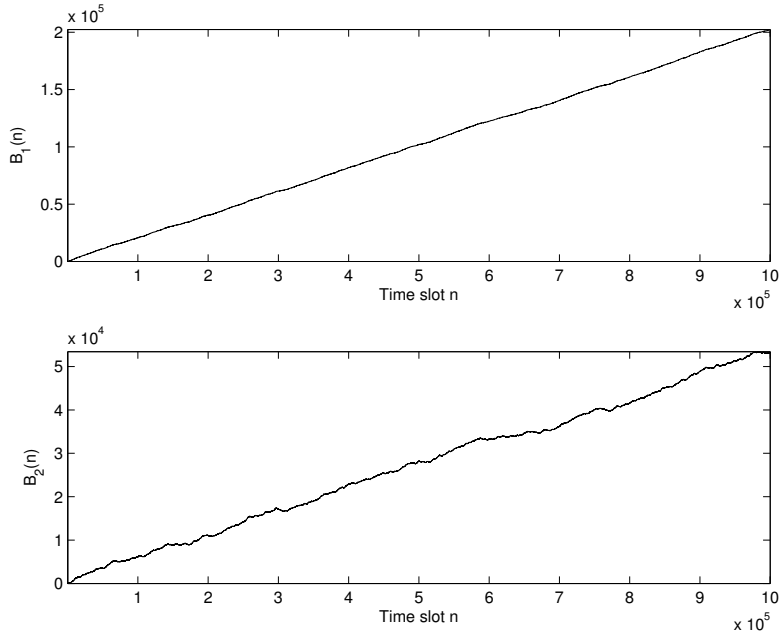

(b) Battery level sample path

Figure 4.7: Sample paths of the system parameters at $\lambda = \bar{\lambda} - \epsilon$ with $\epsilon = 0.01$, where $\bar{\lambda}$ is the point on which in Fig. 4.4 the diagonal arrow meets the outer bound of the stability region

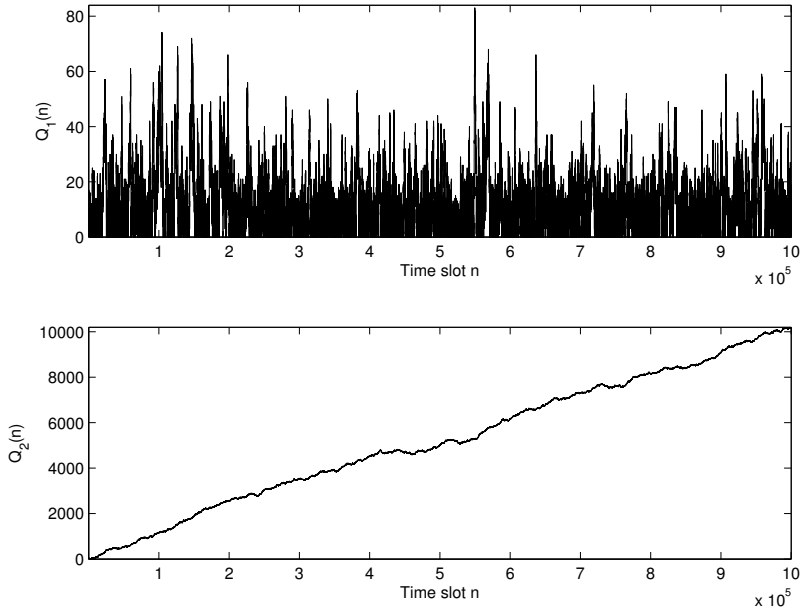

(a) Queue length sample path

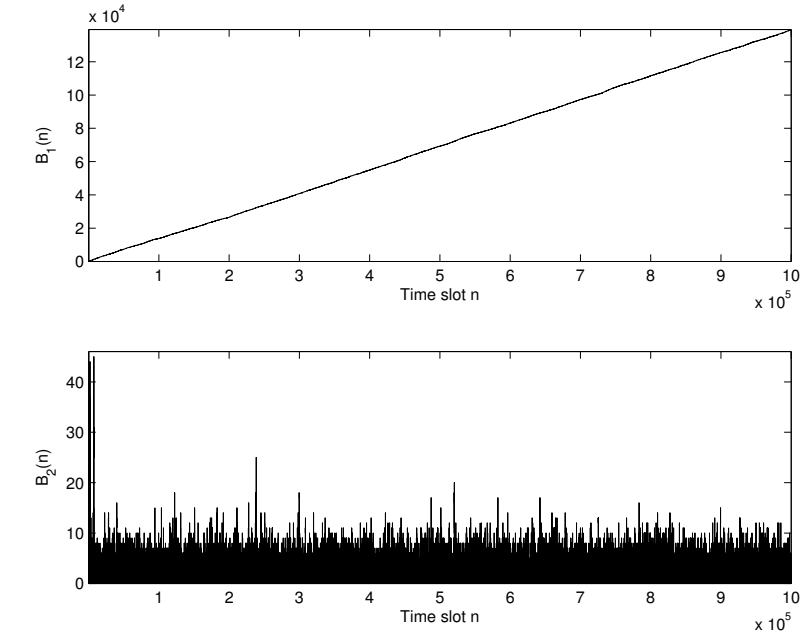

(b) Battery level sample path

Figure 4.8: Sample paths of the system parameters at $\lambda = \bar{\lambda} + \epsilon$ with $\epsilon = 0.01$, where $\bar{\lambda}$ is the point on which in Fig. 4.4 the diagonal arrow meets the outer bound of the stability region

of both nodes, which allows us to conjecture that the system is stable. The corresponding battery level sample paths are shown in Fig. 4.7(b). It is observed that the battery levels at both nodes are increasing. Such an increasing tendency is obvious for the battery at s_1 because δ_1 is greater than p_1, which means that the energy expenditure rate cannot exceeds the energy harvesting rate. It is conjectured that at this loading point, the queue at s_2 is non-empty for less than δ_2/p_2 fraction of time slots and, thus, the battery level at s_2 also increases.

Fig. 4.8 illustrates queue length and battery level sample paths at input traffic load at $\lambda = \bar{\lambda} + \epsilon$, which is slightly outside the outer bound of the stability region. It is observed from Fig. 4.8(a) that there is an increasing tendency in the size of the queue at s_2, which allows us to conjecture the instability of the system. Since the queue at s_2 is keep increasing and does not empty over the simulation interval, the energy expenditure rate is greater than the energy harvesting rate at give δ_2 and p_2, which can be seen in Fig. 4.8(b).

4.2.7 Discussion

We studied the effect of stochastic energy harvesting, which imposes energy availability constraint on each node, on the stability of the slotted ALOHA. An exact characterization of the stability region was carried out for the two-node case under the generalized wireless channel model with MPR capability. By comparing to the case of unlimited energy for transmissions, we identified the loss in terms of the size of the stability region for either infinite or finite battery capacities.

4.3 Channel-Aware Random Access

4.3.1 Motivation

In this chapter, we consider the random access of nodes adapting their transmission probability based on the local channel state information (CSI) in a distributed manner, which is called the channel-aware random access (CARA). It needs to be emphasized that the analysis in all the previous work on CARA discussed in Chapter 4.1 was performed based on the ideal assumption that the perfect local CSI is available at each user [20–23]. In reality, however, the CSI is obtained through an estimation and any kind of estimation is imperfect as long as there is randomness in the observed signal. Consequently, the occurrence of errors in estimation is inevitable and the performance of CARA would certainly depend on the accuracy of channel estimation. To see the effect of imperfect CSI, we allow channel estimation errors in the two-state time-varying channel model considered in [22, 23], in which each user i transmits with probability p_i when its channel state is *good* and the packet queue is non-empty. Note that the errors either deprives the chance to utilize the *good* channel state when falsely estimated to be *bad* or causes unnecessary interference to the other user when its actual channel state is *bad* but falsely estimated to be *good*. There is some related work on CARA with imperfect CSI; in [82], the two-user system was considered under the collision channel model and, in [83], a system with an arbitrary number of users was considered but with always backlogged queues and symmetric channel statistics.

Our contributions can be summarized as follows. We first introduce the realistic effect of practical channel estimation into the stability analysis of CARA. The analysis

also takes into account the compound effect of the MPR capability, which depends not only on the set of transmitters but also on their instantaneous channel states. The derived stability region describes the theoretical limit on rates that can be pushed into the system while maintaining the queues stable at given channel estimation error rates and MPR probabilities. Secondly, by comparing with the case of having perfect CSI, we identify the loss due to the imperfect CSI on the stability region of CARA. Finally, the stability region of the *longest connected queue* (LCQ) policy [24], which is a *throughput-optimal* policy that can stabilize the system whenever the stability is attainable, is derived again in the presence of channel estimation errors. The LCQ policy schedules a user having longest queue among those whose channel is *connected* and, thus, requires queue length and channel state information feedback to the centralized controller. Interestingly, we observed that the stability region of CARA, a fully distributed policy, is not always a proper subset of that of the LCQ policy. This is when relatively strong MPR capability presents.

4.3.2 System Model

We consider a multi-access system consisting of N nodes and a common receiver. The stability analysis of CARA is done for $N = 2$ as illustrated in Fig. 4.9, whereas N is set to an arbitrary positive integer for the analysis of the LCQ policy in Chapter 4.3.5. Each node i has an infinite size queue for storing the arriving packets that have fixed length. Time is slotted and the slot duration is equal to one packet transmission time. Let $Q_i(n)$ denote the number of packets buffered at s_i at the beginning of the n-th slot which

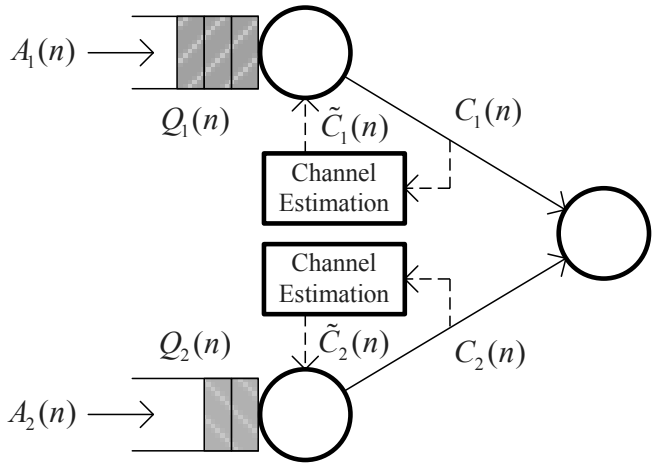

Figure 4.9: Illustration of the system with bursty packet arrivals and channel estimation

evolves according to

$$Q_i(n+1) = \max[Q_i(n) - \mu_i(n), 0] + A_i(n)$$

where the stochastic processes $\{\mu_i(n)\}_{n=0}^{\infty}$ and $\{A_i(n)\}_{n=0}^{\infty}$ are sequences of random variables representing the number of arrivals and services at s_i during time slot n, respectively. The arrival process $\{A_i(n)\}_{n=0}^{\infty}$ is modeled as an independent and identically distributed (i.i.d.) Bernoulli process with $E[A_i(n)] = \lambda_i$, and the processes at different nodes are assumed to be independent of each other. The service process $\{\mu_i(n)\}_{n=0}^{\infty}$ depends jointly on the transmission protocol and the underlying channel model, which governs the success of transmissions.

The channel between node i and the receiver is randomly time-varying and its state at time slot n is denoted by $C_i(n)$ and let $\boldsymbol{C}(n) = \{C_i(n), \ldots, C_N(n)\}$. We assume that channels hold their state for the duration of a slot and potentially change on the slot boundaries[4]. As in the previous work [22, 23], we model the time-varying channel as a

[4]This assumption can be validated when the channel coherence time is relatively longer than the slot

discrete-time stochastic process taking values from $\{G, B\}$, which represents *good* and *bad* states, respectively. The channel processes at different nodes are assumed to be independent of each other but the realizations of a channel at a node at different time slots are not necessarily independent. If fact, a channel process can be arbitrarily correlated over time as long as stationary. We denote by π_i^G and $\pi_i^B (= 1 - \pi_i^G)$ the steady-state probabilities that channel i is in *good* and *bad* states, respectively. The transmission control policy considered in [23] is studied again in which node i transmits with probability p_i when $C_i(n) = G$ and its queue is non-empty. We denoted by $\tilde{C}_i(n)$ the estimated channel state over the link between node i and the receiver, and node i is now transmitting with probability p_i if $\tilde{C}_i(n) = G$ and its queue is non-empty. It is obvious that the performance of this adaptation would highly depend on the accuracy of the channel estimation. Let us define $\epsilon_i^G = \Pr[\tilde{C}_i(n) = B | C_i(n) = G]$ and $\epsilon_i^B = \Pr[\tilde{C}_i(n) = G | C_i(n) = B]$, which are the probabilities of falsely estimating the channel state and let $\bar{\epsilon}_i^G = 1 - \epsilon_i^G$ and $\bar{\epsilon}_i^B = 1 - \epsilon_i^B$.

The success of a transmission depends on the underlying channel model. Unlike the static MPR model used in [51–53], in which the time-varying nature of wireless channels was disregarded, our model captures not only the effect of interference but also the instantaneous channel states of the transmitters. Denote by $\mathcal{N}_{\text{tx}}$ and $\boldsymbol{C}_{\text{tx}}(n)$ the set of transmitting nodes and their channel states, respectively. Then, the probability that a packet transmitted from node i is successfully decoded at the destination is described by

$$q_{i|\boldsymbol{C}_{\text{tx}}(n)} = \Pr[\gamma_{i|\boldsymbol{C}_{\text{tx}}(n)} > \theta]$$

duration.

where $\gamma_{i|\boldsymbol{C}_{\rm tx}(n)}$ is the signal-to-interference-plus-noise-ratio (SINR) of the signal transmitted from node i at the receiver given the channel states of the transmitters $\boldsymbol{C}_{\rm tx}(n)$ and the threshold for the successful decoding θ. We assume throughout the paper that the success probability when a node's own channel state is *bad* is negligible due to such as the deep fading regardless of the interference. This is the situation when the signal-to-noise-ratio (SNR) itself is below the threshold θ for the successful decoding. Thus, for $N = 2$, we are particularly interested in the following reception probabilities[5]

$$q_{1|\{G\}}, q_{1|\{G,B\}}, q_{1|\{G,G\}}, q_{2|\{G\}}, q_{2|\{B,G\}}, q_{2|\{G,G\}}$$

Note that the success probability when a signal is transmitted in the presence of interference cannot exceed the probability when it is transmitted alone. Moreover, since we are considering the multi-access to a common receiver, the fact that a node's channel is in the *good* state implies potentially higher interference level to the other node if they transmit at the same time. Therefore, the following relations hold: $q_{1|\{G\}} > q_{1|\{G,B\}} > q_{1|\{G,G\}}$ and $q_{2|\{G\}} > q_{2|\{B,G\}} > q_{2|\{G,G\}}$.

4.3.3 CARA with Imperfect CSI

This chapter describes the stability region of CARA in the presence of channel estimation errors. As noted earlier, the service process of a queue depends on the status of the other, which makes the analysis challenging. The proof of the results, which is based on the stochastic dominance technique [59], is presented in the next chapter. Let us

[5]For example, $q_{2|\{B,G\}}$ is the probability that the transmission by node 2 is successful when $C_1(n) = B$ and $C_2(n) = G$.

define

$$\Psi_1^{\boldsymbol{\epsilon}} = \pi_2^G \bar{\epsilon}_2^G \left(q_{1|\{G\}} - q_{1|\{G,G\}}\right) + \pi_2^B \epsilon_2^B \left(q_{1|\{G\}} - q_{1|\{G,B\}}\right)$$

$$\Psi_2^{\boldsymbol{\epsilon}} = \pi_1^G \bar{\epsilon}_1^G \left(q_{2|\{G\}} - q_{2|\{G,G\}}\right) + \pi_1^B \epsilon_1^B \left(q_{2|\{G\}} - q_{2|\{B,G\}}\right)$$

which are shorthand notations to simplify the description of our main results.

Lemma 4.3.1. *The stability region $\mathfrak{S}(\boldsymbol{\epsilon}, \boldsymbol{p})$ of CARA at given channel estimation error rate vector $\boldsymbol{\epsilon}$ and transmission probability vector $\boldsymbol{p}$ is the union of the following subregions:*

$$\mathcal{R}_1 = \left\{ (\lambda_1, \lambda_2) : \lambda_1 < \pi_1^G \bar{\epsilon}_1^G p_1 \left(q_{1|\{G\}} - \frac{\Psi_1^{\boldsymbol{\epsilon}} \lambda_2}{\pi_2^G \bar{\epsilon}_2^G \left(q_{2|\{G\}} - \Psi_2^{\boldsymbol{\epsilon}} p_1\right)} \right), \right.$$
$$\left. \lambda_2 < \pi_2^G \bar{\epsilon}_2^G p_2 \left(q_{2|\{G\}} - \Psi_2^{\boldsymbol{\epsilon}} p_1\right) \right\}$$

and

$$\mathcal{R}_2 = \left\{ (\lambda_1, \lambda_2) : \lambda_1 < \pi_1^G \bar{\epsilon}_1^G p_1 \left(q_{1|\{G\}} - \Psi_1^{\boldsymbol{\epsilon}} p_2\right), \right.$$
$$\left. \lambda_2 < \pi_2^G \bar{\epsilon}_2^G p_2 \left(q_{2|\{G\}} - \frac{\Psi_2^{\boldsymbol{\epsilon}} \lambda_1}{\pi_1^G \bar{\epsilon}_1^G \left(q_{1|\{G\}} - \Psi_1^{\boldsymbol{\epsilon}} p_2\right)} \right) \right\}$$

Proof. The proof is presented in the next chapter. □

Let us define the following points in the two-dimensional Euclidean space:

$$P_1 = \left(\frac{\pi_1^G \bar{\epsilon}_1^G q_{2|\{G\}} (q_{1|\{G\}} - \Psi_1^{\boldsymbol{\epsilon}})^2}{\Psi_2^{\boldsymbol{\epsilon}} q_{1|\{G\}}}, \frac{\pi_2^G \bar{\epsilon}_2^G \Psi_1^{\boldsymbol{\epsilon}} q_{2|\{G\}}}{q_{1|\{G\}}} \right) \tag{4.20}$$

$$P_2 = \left(\frac{\pi_1^G \bar{\epsilon}_1^G \Psi_2^{\boldsymbol{\epsilon}} q_{1|\{G\}}}{q_{2|\{G\}}}, \frac{\pi_2^G \bar{\epsilon}_2^G q_{1|\{G\}} (q_{2|\{G\}} - \Psi_2^{\boldsymbol{\epsilon}})^2}{\Psi_1^{\boldsymbol{\epsilon}} q_{2|\{G\}}} \right) \tag{4.21}$$

$$P_3 = (\pi_1^G \bar{\epsilon}_1^G (q_{1|\{G\}} - \Psi_1^{\boldsymbol{\epsilon}}), \pi_2^G \bar{\epsilon}_2^G (q_{2|\{G\}} - \Psi_2^{\boldsymbol{\epsilon}})) \tag{4.22}$$

which are all in the first quadrant.

Theorem 4.3.1. *If* $\frac{\Psi_1^{\boldsymbol{\epsilon}}}{q_{1|\{G\}}} + \frac{\Psi_2^{\boldsymbol{\epsilon}}}{q_{2|\{G\}}} \geq 1$*, the boundary of the stability region* $\mathfrak{S}(\boldsymbol{\epsilon})$ *of CARA at a given channel estimation error rate vector* $\boldsymbol{\epsilon}$ *is described by three segments: (i) the line connecting* $P_Y = (0, \pi_2^G \bar{\epsilon}_2^G q_{2|\{G\}})$ *and* P_1*, (ii) the curve*

$$\sqrt{\frac{\Psi_2^{\boldsymbol{\epsilon}}}{\pi_1^G \bar{\epsilon}_1^G}\lambda_1} + \sqrt{\frac{\Psi_1^{\boldsymbol{\epsilon}}}{\pi_2^G \bar{\epsilon}_2^G}\lambda_2} = \sqrt{q_{1|\{G\}} q_{2|\{G\}}} \tag{4.23}$$

from P_1 *to* P_2*, and (iii) the line connecting* P_2 *and* $P_X = (\pi_1^G \bar{\epsilon}_1^G q_{1|\{G\}}, 0)$*. If* $\frac{\Psi_1^{\boldsymbol{\epsilon}}}{q_{1|\{G\}}} + \frac{\Psi_2^{\boldsymbol{\epsilon}}}{q_{2|\{G\}}} < 1$*, it is described by two lines: (i) the line connecting* P_Y *and* P_3 *and (ii) the line connecting* P_3 *and* P_X*.*

Proof. The proof is presented in the next chapter. □

Corollary 4.3.1. *If* $\frac{\Psi_1^{\boldsymbol{\epsilon}}}{q_{1|\{G\}}} + \frac{\Psi_2^{\boldsymbol{\epsilon}}}{q_{2|\{G\}}} > 1$*, the stability region* $\mathfrak{S}(\boldsymbol{\epsilon})$ *is non-convex. If* $\frac{\Psi_1^{\boldsymbol{\epsilon}}}{q_{1|\{G\}}} + \frac{\Psi_2^{\boldsymbol{\epsilon}}}{q_{2|\{G\}}} \leq 1$*, it is a convex polygon. Specifically, when* $\frac{\Psi_1^{\boldsymbol{\epsilon}}}{q_{1|\{G\}}} + \frac{\Psi_2^{\boldsymbol{\epsilon}}}{q_{2|\{G\}}} = 1$*, the region becomes a right triangle.*

This corollary can be easily verified by comparing the slopes of the lines from P_Y to P_1 and from P_2 to P_X and those from P_Y to P_3 and from P_3 to P_X. Specifically, if $\frac{\Psi_1^{\boldsymbol{\epsilon}}}{q_{1|\{G\}}} + \frac{\Psi_2^{\boldsymbol{\epsilon}}}{q_{2|\{G\}}} = 1$, the curve Eq. (4.23) shrinks to a point whose coordinate is identically described by both P_1 and P_2 and the slopes of the lines from P_Y to P_1 and from P_2 to P_X become identical.

Consider the case when perfect CSI is available. This can be viewed as a special case of our model with $\boldsymbol{\epsilon} = \mathbf{0}$, where $\mathbf{0}$ is the vector of zeros. By substituting $\boldsymbol{\epsilon} = \mathbf{0}$ into Theorem 4.3.1, we can obtain the stability region for the case with perfect CSI, which reconfirms the previous results obtained in [22] and [23]. For the comparison's sake, let us consider the case when CSI is not available and, hence, each node has to make decisions on transmission independent of the underlying channel states. This corresponds

to the original ALOHA in which each node transmits with probability p_i regardless of the underlying channel states whenever its queue is non-empty. Thus, at a given set of transmitters, the success probability of each node is given as a constant, which is obtained by taking the average over the stationary distribution of the channel states. Denote by q_i^{s} and q_i^{m} $(i \in \{1,2\})$ the transmission success probabilities seen by node i when it transmits alone or along with the other node $j(\neq i)$. For the two-node case, it is obtained as $q_1^{\mathrm{s}} = \pi_1^G q_{1|\{G\}}$, $q_1^{\mathrm{m}} = \pi_1^G \pi_2^G q_{1|\{G,G\}} + \pi_1^G \pi_2^B q_{1|\{G,B\}}$, $q_2^{\mathrm{s}} = \pi_2^G q_{2|\{G\}}$, and $q_2^{\mathrm{m}} = \pi_1^G \pi_2^G q_{2|\{G,G\}} + \pi_1^B \pi_2^G q_{2|\{B,G\}}$. Also define $\Delta_i = q_i^{\mathrm{s}} - q_i^{\mathrm{m}}$, which is assumed to be strictly positive without loss of generality. The following theorem obtained in [53] describes the stability region of the original ALOHA for the case with static MPR channels, but it is also applicable to the system with time-varying channels but when the CSI is unavailable. This is because the success probabilities are given as constants over time. We especially denote the stability region for this case by $\mathfrak{S}(\emptyset)$ since the notion of channel estimation errors for the case with no CSI is not valid.

Theorem 4.3.2. *If $\frac{\Delta_1}{q_1^{\mathrm{s}}} + \frac{\Delta_2}{q_2^{\mathrm{s}}} \geq 1$, the boundary of the stability region of ALOHA with no CSI, denoted by $\mathfrak{S}(\emptyset)$, is described by three segments: (i) the line connecting $P_Y = (0, q_2^{\mathrm{s}})$ and $P_1 = (\frac{q_2^{\mathrm{s}}(q_1^{\mathrm{s}}-\Delta_1)^2}{\Delta_2 q_1^{\mathrm{s}}}, \frac{\Delta_1 q_2^{\mathrm{s}}}{q_1^{\mathrm{s}}})$, (ii) the curve $\sqrt{\Delta_2\lambda_1} + \sqrt{\Delta_1\lambda_2} = \sqrt{q_1^{\mathrm{s}} q_2^{\mathrm{s}}}$ from P_1 to $P_2 = (\frac{\Delta_2 q_1^{\mathrm{s}}}{q_2^{\mathrm{s}}}, \frac{q_1^{\mathrm{s}}(q_2^{\mathrm{s}}-\Delta_2)^2}{\Delta_1 q_2^{\mathrm{s}}})$, and (iii) the line connecting P_2 and $P_X = (q_1^{\mathrm{s}}, 0)$. If $\frac{\Delta_1}{q_1^{\mathrm{s}}} + \frac{\Delta_2}{q_2^{\mathrm{s}}} < 1$, it is described by two lines: (i) the line connecting P_Y and $P_3 = (q_1^{\mathrm{s}} - \Delta_1, q_2^{\mathrm{s}} - \Delta_2)$ and (ii) the line connecting P_3 and P_X.*

Proof. Please refer to [53]. □

In Fig. 1 and Fig. 2, we illustrate the stability region of CARA with imperfect

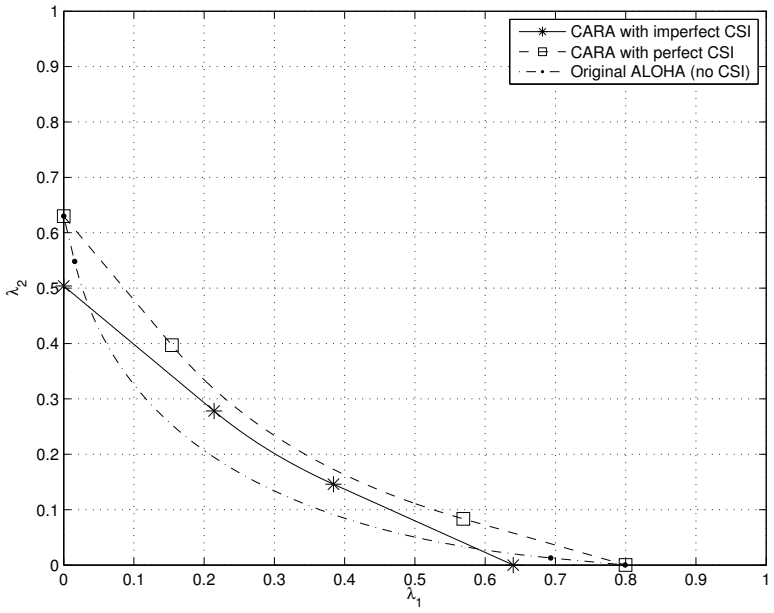

Figure 4.10: Stability region of CARA: the case of non-convex region (parameter setting:$\pi_1^G = 0.8$, $\pi_2^G = 0.7$, $q_{1|\{G\}} = 1$, $q_{2|\{G\}} = 0.9$, $q_{1|\{G,B\}} = q_{2|\{B,G\}} = 0.2$, $q_{1|\{G,G\}} = q_{2|\{G,G\}} = 0.1$, $\epsilon_i^j = 0.2, \forall i, j$)

CSI along with the case with perfect CSI and the original ALOHA with no CSI. It is evident that the stability region of CARA with perfect CSI always includes that of original ALOHA, which complies with the previous results obtained in [22]. It is also obvious that the stability region of CARA with perfect CSI always includes that with imperfect CSI, and the difference between the two regions, therefore, can be understood as the loss due to the errors in channel estimation. However, the stability region of original ALOHA is not a proper subset of that of CARA with imperfect CSI as shown in the figures. The inefficiency of CARA is due to the fact that each node transmits only when the channel is estimated to be *good* and those time slots when the channel is estimated to be *bad* but when it is indeed *good* is not exploited.

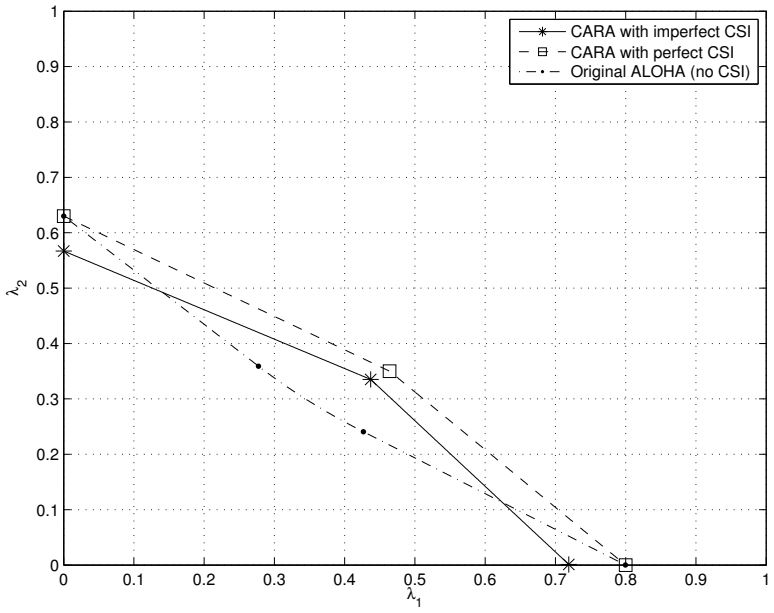

Figure 4.11: Stability region of CARA: the case of convex region (parameter setting:$\pi_1^G = 0.8$, $\pi_2^G = 0.7$, $q_{1|\{G\}} = 1$, $q_{2|\{G\}} = 0.9$, $q_{1|\{G,B\}} = q_{2|\{B,G\}} = 0.5$, $q_{1|\{G,G\}} = q_{2|\{G,G\}} = 0.4$, $\epsilon_i^j = 0.1, \forall i, j$)

4.3.4 Stability Analysis

In this chapter, we provide details on the derivation of our main result presented in the previous chapter. Note that nodes are interfering with each other only when they are transmitting and, under the considered protocol, node i transmits with probability p_i if the estimated channel state is *good* and its queue is non-empty. Since the queues in the system are interacting, we use the stochastic dominance technique introduced in Chapter 2.3.

Construct a hypothetical system which is identical to the original system except that node 2 transmits dummy packets when it decides to transmit but its packet queue is empty.

Define $1_i(n)$ to be an indicator function whose value is one if the transmission by node i is successful, which also necessarily requires that the corresponding node transmits at that time slot. Otherwise, $1_i(n) = 0$. By conditioning on the underlying actual channel states, the average service rate of the queue at node 1 can be expressed as

$$\begin{aligned}\mu_1 &= \sum_{\boldsymbol{C}'} \Pr[1_1|\boldsymbol{C} = \boldsymbol{C}']\Pr[\boldsymbol{C} = \boldsymbol{C}'] \\ &= \Pr[1_1|\boldsymbol{C} = \{G, G\}]\pi_1^G\pi_2^G + \Pr[1_1|\boldsymbol{C} = \{G, B\}]\pi_1^G\pi_2^B \end{aligned} \tag{4.24}$$

where we used the fact that the transmission success probability is zero when a node's own channel state is *bad* and the time index n is suppressed in the steady-state. Note that each node i transmits with probability p_i only when the estimated channel state is *good*. By further conditioning on the estimated channel states, it is expressed as

$$\Pr[1_1|\boldsymbol{C} = \boldsymbol{C}'] = \sum_{\tilde{\boldsymbol{C}}'} \Pr[1_1|\boldsymbol{C} = \boldsymbol{C}', \tilde{\boldsymbol{C}} = \tilde{\boldsymbol{C}}']\Pr[\tilde{\boldsymbol{C}} = \tilde{\boldsymbol{C}}'|\boldsymbol{C} = \boldsymbol{C}']$$

where

$$\Pr[1_1|\boldsymbol{C} = \{G, G\}] = \left[q_{1|\{G\}}p_1(1 - p_2) + q_{1|\{G,G\}}p_1p_2\right] \bar{\epsilon}_1^G\bar{\epsilon}_2^G + q_{1|\{G\}}p_1\bar{\epsilon}_1^G\epsilon_2^G \tag{4.25}$$

and

$$\Pr[1_1|\boldsymbol{C} = \{G, B\}] = q_{1|\{G\}}p_1\bar{\epsilon}_1^G\bar{\epsilon}_2^B + \left[q_{1|\{G\}}p_1(1 - p_2) + q_{1|\{B,G\}}p_1p_2\right] \bar{\epsilon}_1^G\epsilon_2^B \tag{4.26}$$

By substituting Eqs. (4.25) and (4.26) into Eq. (4.24) and, after some manipulations, the average service rate of the queue at node 1 is derived as

$$\mu_1 = \pi_1^G\bar{\epsilon}_1^G p_1 \left(q_{1|\{G\}} - \Psi_1^{\boldsymbol{\epsilon}}p_2\right)$$

where $\Psi_i^{\boldsymbol{\epsilon}}$ is defined in Chapter 4.3.3. By Loynes' Theorem, the queue at node 1 is stable if $\lambda_1 < \mu_1$. Note that the queue size at node 1 in this dominant system can be modeled

as a discrete-time $M/M/1$ system with arrival rate λ_1 and the service rate given above, which does not depend on the status of the queue at node 2. For stable input rate λ_1 that is less than μ_1, the queue at node 1 empties out with probability

$$\Pr[Q_1 = 0] = 1 - \frac{\lambda_1}{\mu_1} = 1 - \frac{\lambda_1}{\pi_1^G \bar{\epsilon}_1^G p_1 \left(q_{1|\{G\}} - \Psi_1^{\boldsymbol{\epsilon}} p_2\right)}$$

Observe that the service process of the queue at node 2 depends on the status of the queue at node 1 since node 1 is able to transmit only when its queue is non-empty and, thereby, interfering with node 2. By conditioning on the emptiness of the queue at node 1, the average service rate of the queue at node 2 can be expressed as

$$\mu_2 = \Pr[1_2|Q_1 \neq 0]\Pr[Q_1 \neq 0] + \Pr[1_2|Q_1 = 0]\Pr[Q_1 = 0] \tag{4.27}$$

The service rate of the queue at node 2 when the queue at node 1 is non-empty can be obtained by following the same procedure used for deriving the service rate of the queue at node 1 and is given by

$$\Pr[1_1|Q_2 \neq 0] = \pi_1^G \bar{\epsilon}_1^G p_1 \left(q_{1|\{G\}} - \Psi_2^{\boldsymbol{\epsilon}} p_1\right) \tag{4.28}$$

The service rate of the queue at node 2 when the queue at node 1 is empty can be obtained quite simply as it does not depend on the action made by node 1 and is given by

$$\Pr[1_1|Q_2 = 0] = \pi_1^G \bar{\epsilon}_1^G p_1 q_{1|\{G\}} \tag{4.29}$$

Substituting Eqs. (4.28) and (4.29) into Eq.(4.27) yields the average service rate of the queue at node 2 which can be summarized to

$$\mu_2 = \pi_2^G \bar{\epsilon}_2^G p_2 \left(q_{2|\{G\}} - \frac{\Psi_2^{\boldsymbol{\epsilon}} \lambda_1}{\pi_1^G \bar{\epsilon}_1^G \left(q_{1|\{G\}} - \Psi_1^{\boldsymbol{\epsilon}} p_2\right)} \right)$$

and by Loyne's Theorem, the queue at node 2 is stable if $\lambda_2 < \mu_2$. Consequently, the stable input rate pairs (λ_1, λ_2) are those less than (μ_1, μ_2) elementwise, and it gives the description of $\mathcal{R}_2$ in Lemma 4.3.1. By reversing the roles of the two nodes, we construct a parallel dominant system in which node 1 transmits dummy packets and, by following the same procedure used for the first dominant system, the stability region for this parallel dominant system is obtained as described in Lemma 4.3.1, which is denoted by $\mathcal{R}_1$.

Importantly, the stability condition obtained using the dominant system technique is not merely a sufficient condition for the stability of the original system but is sufficient and necessary. Consider, for example, the subregion $\mathcal{R}_2$ obtained for the dominant system in which node 2 transmits dummy packets. The sufficient part is trivial which follows from the construction of the dominant system such that the dominant system stochastically dominates the original system in number of packets in the queues at all times. The necessary part can be proved as follows: if for some λ_2, the queue at node 2 is unstable in the hypothetical system, then $Q_2(n)$ approaches infinity almost surely. Note that as long as the queue does not empty, the behavior of the hypothetical system and the original system are identical, provided they start from the same initial conditions, since dummy packets will never have to be used. A sample-path that goes to infinity without visiting the empty state, which is a feasible one for a queue that is unstable, will be identical for both the hypothetical and the original systems. Therefore, the instability of the hypothetical system implies the instability of the original system.

We now obtain the maximum achievable stability region, which is the closure of the stability region $\mathfrak{S}(\boldsymbol{\epsilon}, \boldsymbol{p})$ over the transmission probability vector $\boldsymbol{p}$. An equivalent way of taking the closure operation is to optimize the boundary of the stability region

$\mathfrak{S}(\boldsymbol{\epsilon}, \boldsymbol{p})$ over $\boldsymbol{p}$. For the subregion $\mathcal{R}_2$, for example, we set up the following optimization problem, in which μ_2 is maximized over $\boldsymbol{p}$ at given λ_1 while satisfying the stability of the queue at node 1.

$$\max_{\boldsymbol{p}} \ \mu_2 = \pi_2^G \bar{\epsilon}_2^G p_2 \left(q_{2|\{G\}} - \frac{\Psi_2^{\boldsymbol{\epsilon}} \lambda_1}{\pi_1^G \bar{\epsilon}_1^G \left(q_{1|\{G\}} - \Psi_1^{\boldsymbol{\epsilon}} p_2 \right)} \right) \tag{4.30}$$

$$\text{subject to } \ \lambda_1 < \pi_1^G \bar{\epsilon}_1^G p_1 \left(q_{1|\{G\}} - \Psi_1^{\boldsymbol{\epsilon}} p_2 \right) \tag{4.31}$$

$$\vec{p} \in [0,1]^2 \tag{4.32}$$

Note that μ_2 depends only on p_2 but not on p_1. Differentiating μ_2 with respect to p_2 gives

$$\frac{\partial \mu_2}{\partial p_2} = \pi_2^G \bar{\epsilon}_2^G \left(q_{2|\{G\}} - \frac{\Psi_2^{\boldsymbol{\epsilon}} q_{1|\{G\}} \lambda_1}{\pi_1^G \bar{\epsilon}_1^G \left(q_{1|\{G\}} - \Psi_1^{\boldsymbol{\epsilon}} p_2 \right)^2} \right)$$

By differentiating once again, we have

$$\frac{\partial^2 \mu_2}{\partial p_2^2} = -\frac{2 \Psi_1^{\boldsymbol{\epsilon}} \Psi_2^{\boldsymbol{\epsilon}} \pi_2^G \bar{\epsilon}_2^G q_{1|\{G\}} \lambda_1}{\pi_1^G \bar{\epsilon}_1^G \left(q_{1|\{G\}} - \Psi_1^{\boldsymbol{\epsilon}} p_2 \right)^3}$$

Observe that

$$\begin{aligned} q_{1|\{G\}} - \Psi_1^{\boldsymbol{\epsilon}} p_2 &\geq q_{1|\{G\}} - \Psi_1^{\boldsymbol{\epsilon}} \\ &= (1 - \pi_2^G \bar{\epsilon}_2^G - \pi_2^B \epsilon_2^B) q_{1|\{G\}} + \pi_2^G \bar{\epsilon}_2^G q_{1|\{G,G\}} + \pi_2^B \epsilon_2^B q_{1|\{G,B\}} \\ &\geq (1 - \pi_2^G - \pi_2^B) q_{1|\{G\}} + \pi_2^G \bar{\epsilon}_2^G q_{1|\{G,G\}} + \pi_2^B \epsilon_2^B q_{1|\{G,B\}} \\ &= \pi_2^G \bar{\epsilon}_2^G q_{1|\{G,G\}} + \pi_2^B \epsilon_2^B q_{1|\{G,B\}} \\ &> 0 \end{aligned} \tag{4.33}$$

Therefore, the second derivative is strictly negative and, consequently, μ_2 is a concave function of p_2. Equating the first derivative to zero gives the maximizing p_2^* as

$$p_2^* = \frac{1}{\Psi_1^{\boldsymbol{\epsilon}}} \left(q_{1|\{G\}} - \sqrt{\frac{\Psi_2^{\boldsymbol{\epsilon}} q_{1|\{G\}} \lambda_1}{\pi_1^G \bar{\epsilon}_1^G q_{2|\{G\}}}} \right) \tag{4.34}$$

and the corresponding maximum function value is obtained by substituting Eq. (4.34) into Eq. (4.30) as

$$\mu^*_{2,\mathrm{curve}} = \frac{\pi_2^G \bar{\epsilon}_2^G}{\Psi_1^{\boldsymbol{\epsilon}}} \left(q_{1|\{G\}} - \sqrt{\frac{\Psi_2^{\boldsymbol{\epsilon}} q_{1|\{G\}} \lambda_1}{\pi_1^G \bar{\epsilon}_1^G q_{2|\{G\}}}} \right) \left(q_{2|\{G\}} - \sqrt{\frac{\Psi_2^{\boldsymbol{\epsilon}} q_{2|\{G\}} \lambda_1}{\pi_1^G \bar{\epsilon}_1^G q_{1|\{G\}}}} \right)$$

Suppose that the maximum occurs at a strictly interior point of the feasible region, i.e., $p_2^* \in (0, 1)$, which corresponds to the condition

$$\frac{\pi_1^G \bar{\epsilon}_1^G q_{2|\{G\}} (q_{1|\{G\}} - \Psi_1^{\boldsymbol{\epsilon}})^2}{\Psi_2^{\boldsymbol{\epsilon}} q_{1|\{G\}}} < \lambda_1 < \frac{\pi_1^G \bar{\epsilon}_1^G q_{1|\{G\}} q_{2|\{G\}}}{\Psi_2^{\boldsymbol{\epsilon}}} \tag{4.35}$$

that is obtained by rearranging Eq. (4.34) and substituting the extreme values of p_2^*, i.e., 0 and 1. On the other hand, the constraint Eq. (4.31) should also be satisfied for the derived p_2^*, which gives

$$\lambda_1 < \frac{\pi_1^G \bar{\epsilon}_1^G \Psi_2^{\boldsymbol{\epsilon}} q_{1|\{G\}}}{q_{2|\{G\}}} \tag{4.36}$$

Consequently, $\mu^*_{2,\mathrm{curve}}$ is valid only for the intersection of Eqs. (4.35) and (4.36). By comparing the endpoints, the intersection is specified to be the same with Eq. (4.35) if $\Psi_2^{\boldsymbol{\epsilon}} \geq q_{2|\{G\}}$, which is impossible. This is because, from the relation described in Eq. (4.33), it can be deduced that $\Psi_i^{\boldsymbol{\epsilon}} < q_{i|\{G\}}$. If $\frac{\Psi_1^{\boldsymbol{\epsilon}}}{q_{1|\{G\}}} + \frac{\Psi_2^{\boldsymbol{\epsilon}}}{q_{2|\{G\}}} \geq 1$, the intersection becomes

$$\frac{\pi_1^G \bar{\epsilon}_1^G q_{2|\{G\}} (q_{1|\{G\}} - \Psi_1^{\boldsymbol{\epsilon}})^2}{\Psi_2^{\boldsymbol{\epsilon}} q_{1|\{G\}}} < \lambda_1 < \frac{\pi_1^G \bar{\epsilon}_1^G \Psi_2^{\boldsymbol{\epsilon}} q_{1|\{G\}}}{q_{2|\{G\}}}$$

Otherwise, it is an empty set.

Next suppose that p_2^* is either 0 or 1, which is the case when λ_1 is outside of the range in Eq. (4.35). If λ_1 is on the right-hand side of the range, $\frac{\partial \mu_2}{\partial p_2}$ becomes non-positive and, thus, μ_2 is a non-increasing function of p_2. Therefore, $p_2^* = 0$, which gives $\mu_2^* = 0$. Whereas, if λ_1 is on the left-hand side of the range, μ_2 is a non-decreasing function of p_2

and, thus, $p_2^* = 1$. The corresponding maximum function value is obtained as

$$\mu_{2,\text{line}}^* = \pi_2^G \bar{\epsilon}_2^G \left(q_{2|\{G\}} - \frac{\Psi_2^{\boldsymbol{\epsilon}} \lambda_1}{\pi_1^G \bar{\epsilon}_1^G (q_{1|\{G\}} - \Psi_1^{\boldsymbol{\epsilon}})} \right)$$

By substituting $p_2^* = 1$ into Eq. (4.31), we have

$$\lambda_1 < \pi_1^G \bar{\epsilon}_1^G (q_{1|\{G\}} - \Psi_1^{\boldsymbol{\epsilon}}) \tag{4.37}$$

Given the fact that λ_1 lies on the left-hand side of the range in Eq. (4.35) in addition to the above constraint, it is shown that if $\frac{\Psi_1^{\boldsymbol{\epsilon}}}{q_{1|\{G\}}} + \frac{\Psi_2^{\boldsymbol{\epsilon}}}{q_{2|\{G\}}} \geq 1$, $\mu_{2,\text{line}}^*$ is valid for λ_1 on the entire range of the left-hand side of Eq. (4.35). Otherwise, it is valid for the range specified by Eq. (4.37). Following the similar procedure, we can optimize the boundary of the subregion $\mathcal{R}_1$, which completes the proof of Theorem 4.3.1.

4.3.5 Comparisons with the Centralized Schedulers

In this chapter, we compare the stability region of CARA to that achieved by scheduling policies that make centralized decision based on the CSI feedback. Note that a scheduler allocates each time slot to one of the nodes such that the scheduled node can transmit in an interference-free environment during the allocated slot. In [84], it was shown that queue length information can be utilized to improve the scheduling performance. Specifically, the discovered policy that serves the *longest-connected-queue* (LCQ) among those in '*Good*' channel state stabilizes the system whenever the input rate vector is inside the stability region. Here, the stability region is defined as the set of arrival rate vectors that can be stably supported by considering all possible stationary scheduling policies. This is why the LCQ policy is called a *throughput-optimal* policy. The following

theorem is derived again for the case with channel estimation errors, which was originally derived in [84] for the case with perfect CSI.

Theorem 4.3.3. *The necessary and sufficient stability condition by considering all possible stationary scheduling policies in the presence of channel estimation errors is*

$$\sum_{i\in\mathcal{N}'} \frac{\lambda_i}{q_{i|\{G\}}} < 1 - \prod_{i\in\mathcal{N}'} \left(1 - \pi_i^G \bar{\epsilon}_i^G\right), \quad \forall \mathcal{N}' \in \{\,1, \ldots, N\,\} \tag{4.38}$$

Furthermore, the LCQ policy stabilizes the system as long as it is stabilizable.

Proof. Assume that the system is operating under certain stationary policy and it is stable. Denote by $1_i(n)$ the indicator function that is equal to 1 if the transmission by node i is successful, which necessarily implies that node i is chosen to transmit at that time slot. Also denote by $I_i(n)$ the indicator function that is equal to 1 if the actual channel state between node i and the receiver is *Good* and it is estimated correctly. The expectations are given by $E[1_i(n)] = q_{i|\{C_i(n)\}}$, and $E[I_i(n)] = \pi_i^G \bar{\epsilon}_i^G$. The number of packets at queue i evolves with time according to the queueing dynamics in Eq. (5.1) with $\mu_i(n) = h_i(n) \cdot 1_i(n)$, where $h_i(t) = 1$ if node i is scheduled at time slot n and $I_i(n) = 1$. Thus, the departure rate from queue i is written as

$$E[h_i(t)1_i(t)] = q_{i|\{G\}} E[h_i(t)]$$

Note that if the system is stable, the rate of what comes in must be equal to the rate of what goes out. In other words, for any subset of network nodes $\mathcal{N}'$, the following equality must hold.

$$\sum_{i\in\mathcal{N}'} \frac{\lambda_i}{q_{i|\{G\}}} = \sum_{i\in\mathcal{N}'} E[h_i(t)] \tag{4.39}$$

Consider now the partition of the probability space into the events

$$\Omega_1 = \{\, I_i(t) = 0, i \in \mathcal{N}' \,\}$$

$$\Omega_2 = \{\, I_i(t) = 0, i \in \mathcal{N}' \,\}^c \cap \{\, Q_i(t-1) = 0, i \in \mathcal{N}' \,\}$$

$$\Omega_3 = \{\, I_i(t) = 0, i \in \mathcal{N}' \,\}^c \cap \{\, Q_i(t-1) = 0, i \in \mathcal{N}' \,\}^c$$

where Ω^c is the complementary set of Ω. Notice that $E\left[\sum_{i\in\mathcal{N}'} h_i(t)|\Omega_l\right] = 0$ for $l = 1, 2$ and, therefore, we have

$$\begin{aligned}\sum_{i\in\mathcal{N}'} E[h_i(t)] &= E\left[E\left[\sum_{i\in\mathcal{N}'} h_i(t)|\Omega_3\right]\Pr[\Omega_3]\right] \\ &< 1 - \Pr[\Omega_1] - \Pr[\Omega_2]\end{aligned}$$

Owing to the assumption on the independence of the channel processes between different nodes, we have

$$\Pr[\Omega_1] = \prod_{i\in\mathcal{N}'} (1 - \pi_i^G \bar{\epsilon}_i^G)$$

and $\Pr[\Omega_2] > 0$. Therefore, we have

$$\sum_{i\in\mathcal{N}'} E[h_i(t)] < 1 - \prod_{i\in\mathcal{N}'} (1 - \pi_i^G \bar{\epsilon}_i^G) \tag{4.40}$$

and Eqs. (4.39) and (4.40) implies Eq. (4.38) in the theorem.

For the sufficiency, we use the Lyapunov drift argument similar to that used in [84]. Denote by $L(\vec{Q}(t))$ a Lyapunov function of the queue length process and define the conditional Lyapunov drift as $\Delta(L(\vec{Q}(t))) = E[L(\vec{Q}(t+1)) - L(\vec{Q}(t))|\vec{Q}(t)]$. If there exist some $\epsilon > 0$ and a finite number b such that the conditional Lyapunov drift satisfies $\Delta(L(\vec{Q}(t))) < -\epsilon$ for $L(\vec{Q}(t)) > b$, the queues in the system are stable. This is an application of Foster's criterion for ergodicity of a Markov chain [24]. Let us consider

$L(\vec{Q}) = \sum_{i=1}^{N} q_{i|\{G\}}^{-1} Q_i^2$. Then, for the considered Lyapunov function, it can be shown that the conditional Lyapunov drift satisfies

$$\Delta(L(\vec{Q}(t))) < 1 + \sum_{i=1}^{N} q_{i|\{G\}}^{-1} \left(E[A_i^2(t)] + 2\lambda_i Q_i(t) \right) - 2E \left[\sum_{i=1}^{N} Q_i(t) h_i(t+1) | \vec{Q}(t) \right] \tag{4.41}$$

The details on the derivation of the above inequality can be found in [84].

Define now a permutation e_i for $i = 0, \ldots, N$ such that $e_0 = 0$ and $Q_{e_i}(t) \geq Q_{e_{i-1}}(t)$, for $i = 2, \ldots, N$. Consider also a partition of the probability space into the events Φ_i defined by

$$\Phi_i = \{ I_{e_i}(t+1) = 1, I_{e_j}(t+1) = 0, \ N \geq j > i \}$$

for $i = 1, \ldots, N$ and $\Phi_0 = \{ \vec{I}(t+1) = \vec{0} \}$. Notice that from the definition of the LCQ policy, in the event Φ_j, queue e_j is served if it is not empty. Therefore, the last term in the right-hand side of Eq. (4.41) becomes

$$E \left[\sum_{i=1}^{N} Q_i(t) h_i(t+1) | \vec{Q}(t) \right] = \sum_{i=1}^{N} Q_{e_i}(t) \pi_i^G \bar{\epsilon}_i^G \prod_{j=i+1}^{N} (1 - \pi_{e_j}^G \bar{\epsilon}_{e_j}^G)$$

By substituting the above into Eq. (4.41) and after some manipulation, we obtain

$$\Delta(L(\vec{Q}(t))) < 1 + \sum_{i=1}^{N} E[A_i^2(t)] + 2Q_{e_N}(t) \max_{\mathcal{N}' \subset \{1, \ldots, N\}} \left[\sum_{i \in \mathcal{N}'} \frac{\lambda_i}{q_{i|\{G\}}} - 1 + \prod_{i \in \mathcal{N}'} \left(1 - \pi_i^G \bar{\epsilon}_i^G\right) \right]$$

It is not difficult to observe that if the condition in Eq. (4.38) is met, then for sufficiently large $Q_{e_N}(t)$, the right-hand side of the above conditional Lyapunov drift becomes negative. This completes the proof. □

For the two-node case, the stability condition in Eq. (4.38) in the above theorem becomes

$$\frac{\lambda_1}{q_{1|\{G\}}} + \frac{\lambda_2}{q_{2|\{G\}}} < \pi_1^G \bar{\epsilon}_1^G + \pi_2^G \bar{\epsilon}_2^G (1 - \pi_1^G \bar{\epsilon}_1^G)$$

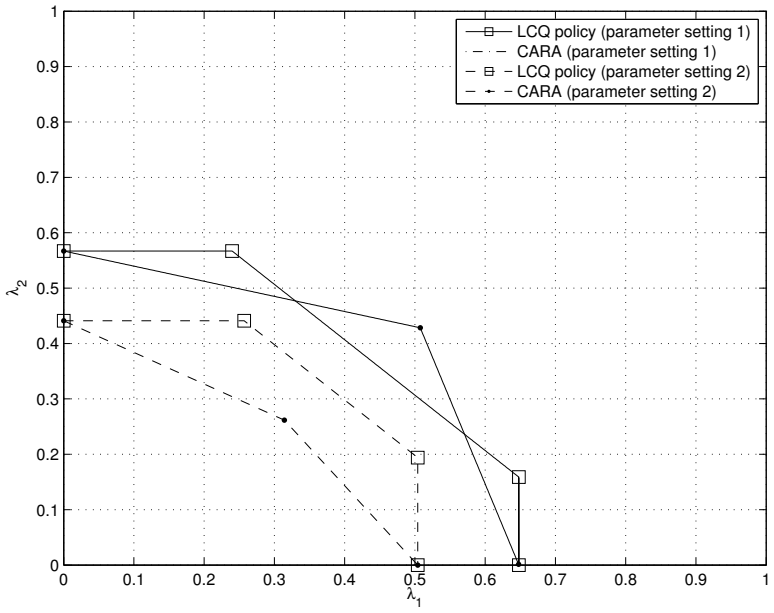

Figure 4.12: Comparison with the LCQ policy (common setting: $\pi_1^G = 0.8$, $\pi_2^G = 0.7$, $q_{1|\{G\}} = q_{2|\{G\}} = 0.9$, parameter setting 1: $q_{1|\{G,B\}} = q_{2|\{B,G\}} = 0.7$, $q_{1|\{G,G\}} = q_{2|\{G,G\}} = 0.6$, $\epsilon_i^j = 0.1, \forall i, j$, parameter setting 2: $q_{1|\{G,B\}} = q_{2|\{B,G\}} = 0.4$, $q_{1|\{G,G\}} = q_{2|\{G,G\}} = 0.3$, $\epsilon_i^j = 0.3, \forall i, j$)

and $\lambda_i < \pi_i^G \bar{\epsilon}_i^G q_{i|\{G\}}$ for $i \in \{1, 2\}$. In Fig. 2, we compare the stability region of CARA to that achieved by LCQ policy, and it can be observed that the former is not necessarily a subset of the latter. Indeed, the relationship between them depends on parameters such as the channel estimation error and the MPR probabilities. Note that the stability region of CARA becomes a subset of that of the LCQ policy when the stability region of CARA is non-convex, or convex but if the vertex P_3 given in Eq. (4.22) is strictly contained in the stability region achieved by LCQ policy. The condition for P_3 to be inside the stability

region of the LCQ policy is given by

$$\frac{\Psi_1^{\epsilon}}{\pi_2^G \bar{\epsilon}_2^G q_{1|\{G\}}} + \frac{\Psi_2^{\epsilon}}{\pi_1^G \bar{\epsilon}_1^G q_{2|\{G\}}} > 1$$

Otherwise, if the stability region of CARA is convex and the above inequality does not hold, the stability region of CARA is not a proper subset of that of the LCQ policy, i.e., there exists a region that can be achieved only by CARA.

4.3.6 Discussion

We studied the stability property of CARA in the presence of channel estimation errors and showed that its stability region may not strictly contain that of original ALOHA. To guarantee the superiority of CARA even with imperfect CSI, we need to modify the protocol itself such that each node transmits with some positive probability, although it believes that the channel is in the *bad* state. Such modification was not considered here. We also compared the stability region of CARA to that achieved by the throughput-optimal LCQ policy and showed that the former is not necessarily a subset of the latter especially as the MPR capability improves.

4.4 Chapter Summary

In this chapter, interesting variants of the random access systems was studied. The first was the random access of nodes having energy harvesting capability. We accurately assessed the effect of limited energy availability due to harvesting on the stability region by comparing against the case of having unlimited energy. We next considered the random

access of nodes adapting their transmission probability based on the local channel state information and studied the impact of imperfect sensing on the achieved stability region.

Chapter 5

Cross-Layer Control for Wireless Multi-Hop Network with Time-Correlated Arrivals

5.1 Background

The performance of the backpressure-based stochastic network control in multi-hop wireless networks with time-correlated arrivals is studied in this chapter using the Lyapunov drift technique [24–27]. The considered arrival process is fairly general in the sense that it may exhibit short/long-range dependence depending on the asymptotic shape of the autocorrelation function. The results are obtained separately for both cases when the arrival rate vector is strictly inside and possibly outside the stability region, which incorporates the statistical information of the arrival processes. To the best of our knowledge, there is no existing work which takes arrivals that are possibly long-range dependent into the analysis of the backpressure-based control for general mult-ihop networks. In [25], it was shown that the original backpressure policy [24] is still throughput-optimal for the system with non-i.i.d. arrivals and channel states. Since, however, it uses the fact that the correlations would be eventually averaged out over sufficiently long time interval, the derived results do not explicitly contain the statistical information of such non-i.i.d. processes. Also, only the case when the arrival rate vector is strictly inside the stability region was considered in the work. In [85], the delay performance of the max-

weight scheduling was studied for both single-hop and multi-hop networks with two-state Markov modulated arrival processes that are certainly short-range dependent. The arrival process considered in [86] is as general as ours but was considered in the context of maximal scheduling for single-hop networks.

This chapter begins with the case when the arrival rate vector is strictly inside the stability region. This is the case when the throughput of each flow is equal to its arrival rate if the network is stable. For this, we show that the backpressure policy stabilizes the network no matter whether the arrivals are i.i.d. or time-correlated as long as the average rate vector is contained in the stability region. The effect of correlations in the network traffic appears in the increased average network delay when compared to the i.i.d. case. We next consider the case when the arrival rate vector is possibly outside the stability region and use the method of joint flow control and backpressure policy developed in [26,27]. The joint policy performs arbitrarily close to the utility-optimal throughput point with a corresponding tradeoff in the average network delay. The effect of correlations in the network traffic appears in the tradeoff relation and we make a comparison with the i.i.d. case.

5.2 Correlation in the Input Traffic

We consider a time-slotted wireless multi-hop network with N nodes and L directed links. An example network topology is shown in Fig. 5.1. We denote by $\mathcal{N}$ and $\mathcal{L}$ the set of nodes and links, respectively. Let $A_{n,c}(t)$ represent the exogenously arriving amount of data at node n during time slot t which is destined to node c in units of bits/slot. At

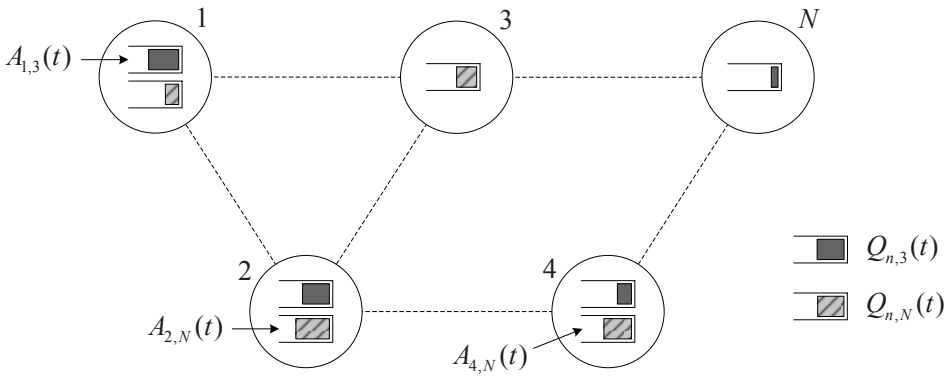

Figure 5.1: Wireless multi-hop network with multiple input streams and per-destination queueing

each node, all the exogenous and endogenous traffic due to relaying is classified and queued according to their destinations. We let $Q_{n,c}(t)$ be the backlog of destination c data that is awaiting transmission in node n at time slot t in units of bits and define $\overrightarrow{Q}(t) \triangleq (Q_{n,c}(t), \forall n, c)$. We assume that the system starts with empty queues, i.e., $Q_{n,c}(0) = 0$ for all (n, c) pairs. Denote by $\mu_l(t)$ and $\mu_{l,c}(t)$ the transmission rate over link l during time slot t and the amount of rate that is offered to destination c traffic in $\mu_l(t)$ in units of bits/slot, respectively. Thus, $\sum_c \mu_{l,c}(t) \leq \mu_l(t)$ for all l. Note that the transmission rate of each link depends not only on the underlying channel state but also on the activation of other interfering links. Denote by Γ_t the feasible region of link transmission rate vector $\overrightarrow{\mu}(t) \triangleq (\mu_l(t), \forall l)$ at time slot t. In each time slot, a control policy chooses $\overrightarrow{\mu}(t)$ from the constrained set Γ_t and allocates rates to the traversing flows.

In this work, the arrival process $A_{n,c}(t)$ does not necessarily to be i.i.d. but only needs to be wide-sense stationary (WSS); that is a process with constant mean $\lambda_{n,c}$, finite variance $\sigma^2_{n,c}$, and an autocorrelation function $\rho_{n,c}(k) \triangleq E[(A_{n,c}(t) - \lambda_{n,c})(A_{n,c}(t-k) - \lambda_{n,c})]/\sigma^2_{n,c}$ that depends only on the time-lag between samples. Denote by $H(t)$ the past

history of all arrivals up to but not including time slot t. If there exists finite number $T \geq 0$ such that $E[A_{n,c}(t)|H(t-k)] = \lambda_{n,c}$ for $k \geq T$, then $\rho_{n,c}(k) = 0$ for $k > T$. Stochastic processes that fall in this category are said to have finite-length memory; an i.i.d. process is a special case with $T = 0$. If there is no such finite T, we further divide the processes according to the asymptotic shape of autocorrelation function $\rho_{n,c}(k)$. For most of the stochastic models including autoregressive moving average processes and Markov modulated processes, the autocorrelation functions are characterized by exponential decay, i.e., $\rho_{n,c}(k) \sim \alpha^k$ as $k \to \infty$, where $0 < \alpha < 1$. The exponential tail of the autocorrelation function implies $\sum_k \rho_{n,c}(k) < \infty$. Stochastic processes belonging to this category are said to be short-range dependent. The burstiness of the input traffic modeled by a short-range dependent process would tend to be smoothed by averaging over a long enough time scale. On the other hand, long-range dependent processes are characterized by power-law decay of the autocorrelation function, i.e., $\rho_{n,c}(k) \sim k^{-\beta}$ as $k \to \infty$, where $0 < \beta < 1$. As a consequence, the autocorrelation function is nonsummable, i.e., $\sum_k \rho_{n,c}(k) = \infty$, which implies that while high-lag correlations are individually small, their cumulative effect gives rise to features which are drastically different from those of short-range dependent processes [40]. Examples of long-range dependent processes are fractional Brownian motion and its discrete-time analog, fractional Gaussian noise. The degree of self-similarity of a series is expressed using a single parameter H, called Hurst parameter. Self-similar processes and long-range dependent processes are related through the relation $H = 1 - \beta/2$; for a self-similar process with long-range dependence, we have $1/2 < H < 1$. Nevertheless, they are two different concepts; self-similarity involves all scales whereas long-range dependence only involves asymptotically large scale. Yet, if we

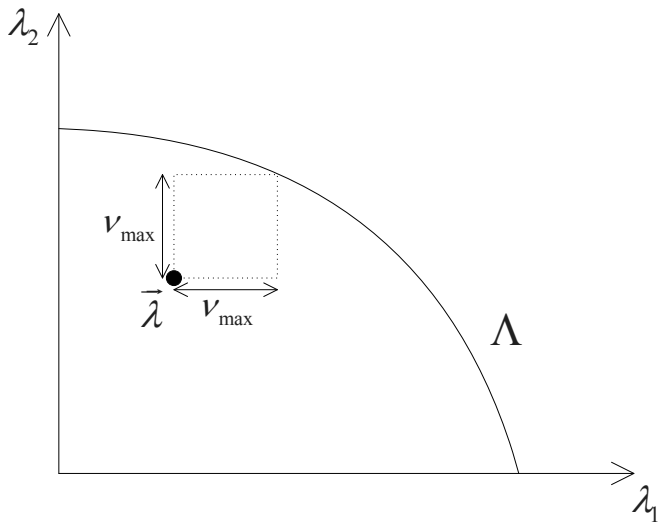

Figure 5.2: Illustration of two-dimensional stability region and the arrival rate vector that is inside the stability region

are only concerned about the steady-state performance measures such as average network delay, the effect of self-similarity is not different from that of long-range dependency.

5.3 Network with Stabilizable Input Traffic

Define $\mathcal{I}_n$ and $\mathcal{O}_n$ as the set of incoming and outgoing links of node n, respectively. In other words, $\mathcal{I}_n = \{\, l : \mathrm{rx}(l) = n \,\}$ and $\mathcal{O}_n = \{\, l : \mathrm{tx}(l) = n \,\}$, where $\mathrm{tx}(l)$ and $\mathrm{rx}(l)$ are the transmitting and receiving nodes of link l, respectively. Then, the queue length process at node n for destination c data evolves as

$$Q_{n,c}(t+1) \leq \max\left[Q_{n,c}(t) - \sum_{l\in\mathcal{O}_n} \mu_{l,c}(t), 0\right] + \sum_{l\in\mathcal{I}_n} \mu_{l,c}(t) + A_{n,c}(t) \qquad (5.1)$$

which is an inequality rather than an equality because the actual endogenous arrivals may be less than the allocated link rates if the corresponding transmitters do not have enough data. The reason for Eq. (5.1) to contain the $\max$ operation is the same. The stability

region Λ of a system is defined as the set of arrival rate vectors $\overrightarrow{\lambda} \triangleq (\lambda_{n,c}, \forall n, c)$ for which all queues in the network are stable by considering all possible stationary policies [24]. Assuming that the arrival rate vector is inside the stability region, i.e., $\overrightarrow{\lambda} \in \Lambda$, as shown in Fig. 5.2, the exact throughput that is equal to the arrival rate is achieved at each flow simply by stabilizing the network. It is well-known that the the backpressure policy in Algorithm 1 stabilizes a network whenever the arrival rate vector is inside the stability region but requires the i.i.d. assumption on the number of arrivals [24, 26].

Algorithm 1 Backpressure Policy [24]

- Differential Backlog Routing/Scheduling: The differential backlog of destination c data over link l is defined as $D_{l,c}(t) \triangleq Q_{\mathrm{tx}(l),c}(t) - Q_{\mathrm{rx}(l),c}(t)$. If the link is directly connected to the destination, i.e, $\mathrm{rx}(l) = c$, $D_{l,c}(t) \triangleq Q_{\mathrm{tx}(l),c}(t)$. The maximum differential backlog over link l is obtained as $D_l(t) = \max_c D_{l,c}(t)$ and the maximizing destination c^* data is chosen for potential transmission over link l.

- Max-Weight Rate Allocation: The link transmission rate vector $\vec{\mu}(t)$ is selected from feasible region Γ_t to maximize the weighted sum rate as

$$\arg \max_{\vec{\mu}(t) \in \Gamma_t} \sum_{l \in \mathcal{L}} D_l(t) \mu_l(t)$$

  where the weight of each link corresponds to the maximum differential backlog of the link.

Note that the policy lets the maximizing commodity c^* use all the allocated rate over the link. Therefore, $\mu_{l,c^*}(t) = \mu_l(t)$ and $\mu_{l,c}(t) = 0$ for all $c \neq c^*$. Before presenting the performance of the backpressure policy with time-correlated arrivals, let us define

the following constants. Denote by $A_{\max}$ the maximum amount of arrivals to any node in any slot, i.e., $\sum_c A_{n,c}(t) \leq A_{\max}$ for all n. Further define $\mu_{\max}^{\text{out}}$ and $\mu_{\max}^{\text{in}}$ as the maximum transmission rate out of, and into, any node in any slot as $\sum_{l\in\mathcal{O}_n} \mu_l(t) \leq \mu_{\max}^{\text{out}}$ and $\sum_{l\in\mathcal{I}_n} \mu_l(t) \leq \mu_{\max}^{\text{in}}$, respectively.

Theorem 5.3.1. *If arrival rate vector $\overrightarrow{\lambda}$ is strictly interior to stability region Λ and there exists finite integer $T > 0$ such that $E[A_{n,c}(t)|H(t-k)] = \lambda_{n,c}$ for $k \geq T$ and for all (n,c) pairs, the backpressure policy stabilizes the network and guarantees bounded average queue backlog as*

$$\limsup_{t\to\infty} \frac{1}{t} \sum_{\tau=0}^{t-1} \sum_{n,c} E[Q_{n,c}(\tau)] \leq \frac{1}{2\nu_{\max}} \left(NB_1 + 2 \sum_{n,c} \phi_{n,c}(T) \right)$$

where

$$\phi_{n,c}(T) \triangleq \sigma_{n,c}^2 \sum_{k=1}^{T} \rho_{n,c}(k) + T\lambda_{n,c} \left(\mu_{\max}^{\text{in}} + \lambda_{n,c} \right)$$

and $B_1 \triangleq (\mu_{\max}^{\text{in}} + A_{\max})^2 + (\mu_{\max}^{\text{out}})^2$ and $\nu_{\max}$ is defined as the maximum of ν such that $\overrightarrow{\lambda} + \nu \overrightarrow{1} \in \Lambda$ where $\overrightarrow{1}$ is a vector of ones whose cardinality is the same with that of $\overrightarrow{\lambda}$.

Proof. Define $L(\overrightarrow{Q}(t)) \triangleq \sum_{n,c} Q_{n,c}(t)^2$ as a Lyapunov function for scalar measure of the network congestion. From the queueing dynamics in Eq. (5.1), it can be verified that

$$\begin{aligned} Q_{n,c}(t+1)^2 \leq Q_{n,c}(t)^2 &+ \left(\sum_{l\in\mathcal{O}_n} \mu_{l,c}(t) \right)^2 + \left(\sum_{l\in\mathcal{I}_n} \mu_{l,c}(t) + A_{n,c}(t) \right)^2 \\ &- 2Q_{n,c}(t) \left(\sum_{l\in\mathcal{O}_n} \mu_{l,c}(t) - \sum_{l\in\mathcal{I}_n} \mu_{l,c}(t) \right) + 2Q_{n,c}(t) A_{n,c}(t) \end{aligned}$$

Summing over all (n,c) pairs and taking conditional expectation given the current queue

backlog $\overrightarrow{Q}(t)$ yields the conditional Lyapunov drift satisfying

$$\begin{aligned}\Delta(\overrightarrow{Q}(t)) &\triangleq E[L(\overrightarrow{Q}(t+1)) - L(\overrightarrow{Q}(t))|\overrightarrow{Q}(t)] \\ &\leq NB_1 - 2\sum_{n,c} Q_{n,c}(t) E\left[\sum_{l\in\mathcal{O}_n}\mu_{l,c}(t) - \sum_{l\in\mathcal{I}_n}\mu_{l,c}(t)\middle|\overrightarrow{Q}(t)\right] \\ &\quad + 2\sum_{n,c} Q_{n,c}(t) E\left[A_{n,c}(t)|\,\overrightarrow{Q}(t)\right] \end{aligned} \tag{5.2}$$

Note that the control variables on the right-hand side (RHS) of the drift expression are link transmission rates $\mu_{l,c}(t)$. By simply converting the corresponding terms containing control variables from node-centric to link-centric expressions, we obtain the following identity:

$$\sum_{n,c} Q_{n,c}(t)\left(\sum_{l\in\mathcal{O}_n}\mu_{l,c}(t) - \sum_{l\in\mathcal{I}_n}\mu_{l,c}(t)\right) = \sum_{l}\sum_{c}\mu_{l,c}(t)\left(Q_{\mathrm{tx}(l),c}(t) - Q_{\mathrm{rx}(l),c}(t)\right) \tag{5.3}$$

which reveals the rationale behind the design of backpressure policy; it is aimed to minimize the RHS of Eq. (5.2) by maximizing Eq. (5.3). The original proof in [24] showed that for sufficiently large values of queue backlogs, the RHS of Eq. (5.2) under the backpressure policy becomes negative, which corresponds to the Forster's criteria for stability of irreducible Markov chains [87]. In [25–27], the Lyapunov drift technique was extended such that an explicit upper bound on the sum of average queue backlogs can be obtained, which suffices for the stability proof as well. Note that since we are considering the case where $\overrightarrow{\lambda} \in \Lambda$, there must exist some constant $\nu > 0$ such that $\overrightarrow{\lambda} + \nu\overrightarrow{1} \in \Lambda$. From Corollary 3.9 of [26], we know that there exists a stationary randomized policy that makes decision based only on the current channel states and independent of queue backlogs and

yields

$$E\left[\sum_{l\in\mathcal{O}_n}\mu_{l,c}(t)-\sum_{l\in\mathcal{I}_n}\mu_{l,c}(t)|\overrightarrow{Q}(t)\right]=\lambda_{n,c}+\nu$$

Since, by definition, the backpressure policy minimizes the RHS of Eq. (5.2) than any other policy including the class of stationary randomized policies, it follows that

$$\Delta(\overrightarrow{Q}(t))\leq NB_1-2\sum_{n,c}(\lambda_{n,c}+\nu)Q_{n,c}(t)+2\sum_{n,c}Q_{n,c}(t)E\left[A_{n,c}(t)|\overrightarrow{Q}(t)\right] \quad (5.4)$$

For the case with i.i.d. arrivals, the relation $E[A_{n,c}(t)|\overrightarrow{Q}(t)]=\lambda_{n,c}$ holds and this simplifies the rest of the analysis. However, if arrivals are correlated, $Q_{n,c}(t)$ is also correlated through the queueing dynamics, and $A_{n,c}(t)$ and $Q_{n,c}(t)$ are no longer independent of each other. The multislot Lyapunov drift technique proposed in [88] and elaborated in [25] can be envisioned; since the technique uses the fact that the non-i.i.d. behavior of the system would be eventually averaged out over sufficiently long interval, the results obtained using this technique do not explicitly contain the correlation structure of the arrival process. Thus, we take a different approach as below. We note from the queueing dynamics that

$$Q_{n,c}(t)\leq Q_{n,c}(t-T)+\sum_{k=1}^{T}\left(\sum_{l\in\mathcal{I}_n}\mu_{l,c}(t-k)+A_{n,c}(t-k)\right)$$

By multiplying $A_{n,c}(t)$ on both sides and taking expectation, we have

$$\begin{aligned}E[Q_{n,c}(t)A_{n,c}(t)]\leq\ & E\left[Q_{n,c}(t-T)A_{n,c}(t)\right]\\ &+E\left[\sum_{k=1}^{T}\left(\sum_{l\in\mathcal{I}_n}\mu_{l,c}(t-k)+A_{n,c}(t-k)\right)A_{n,c}(t)\right] \quad (5.5)\end{aligned}$$

Because all the arrival processes are assumed to have finite memory of at most length T,

we have

$$E\left[Q_{n,c}(t-T)A_{n,c}(t)\right] = E\left[Q_{n,c}(t-T)E\left[A_{n,c}(t)|\,\overrightarrow{Q}(t-T)\right]\right]$$
$$= \lambda_{n,c}E\left[Q_{n,c}(t-T)\right] \quad (5.6)$$

For the remaining of the RHS of Eq. (5.5), we obtain

$$E\left[\sum_{k=1}^{T}\left(\sum_{l\in\mathcal{I}_n}\mu_{l,c}(t-k)+A_{n,c}(t-k)\right)A_{n,c}(t)\right] \leq \sigma_{n,c}^2\sum_{k=1}^{T}\rho_{n,c}(k)$$
$$+ T\lambda_{n,c}\left(\mu_{\max}^{\text{in}}+\lambda_{n,c}\right) \quad (5.7)$$

Substituting Eqs. (5.6) and (5.7) into the RHS of Eq. (5.5) yields an upper bound on $E[Q_{n,c}(t)A_{n,c}(t)]$. Taking the expectation of Eq. (5.4) with respect to the distribution of queue backlogs and applying the bound yields the unconditional Lyapunov drift satisfying

$$E[L(\overrightarrow{Q}(t+1)) - L(\overrightarrow{Q}(t))] \leq NB_1 - 2\sum_{n,c}(\lambda_{n,c}+\nu)E\left[Q_{n,c}(t)\right]$$
$$+ 2\sum_{n,c}\lambda_{n,c}E\left[Q_{n,c}(t-T)\right] + 2\sum_{n,c}\left(\sigma_{n,c}^2\sum_{k=1}^{T}\rho_{n,c}(k) + T\lambda_{n,c}\left(\mu_{\max}^{\text{in}}+\lambda_{n,c}\right)\right)$$

Summing the inequality over $t \in \{\,0,\ldots,M-1\,\}$ yields

$$E[L(\overrightarrow{Q}(M)) - L(\overrightarrow{Q}(0))] \leq NMB_1 - 2\sum_{\tau=0}^{M-1}\sum_{n,c}(\lambda_{n,c}+\nu)E\left[Q_{n,c}(\tau)\right]$$
$$+ 2\sum_{\tau=0}^{M-1}\sum_{n,c}\lambda_{n,c}E\left[Q_{n,c}(\tau-T)\right] + 2M\sum_{n,c}\left(\sigma_{n,c}^2\sum_{k=1}^{T}\rho_{n,c}(k) + T\lambda_{n,c}\left(\mu_{\max}^{\text{in}}+\lambda_{n,c}\right)\right)$$

where $E[Q_{n,c}(t)] = 0$ for $t \leq 0$. Dividing both sides by $2M$, rearranging terms, and using the fact that the system starts with empty queues and non-negativity of the Lyapunov

function, we obtain

$$\frac{1}{M}\sum_{\tau=0}^{M-1}\sum_{n,c}(\lambda_{n,c}+\nu)E\left[Q_{n,c}(\tau)\right]-\frac{1}{M}\sum_{\tau=0}^{M-1}\sum_{n,c}\lambda_{n,c}E\left[Q_{n,c}(\tau-T)\right]$$
$$\leq\frac{NB_1}{2}+\sum_{n,c}\left(\sigma_{n,c}^2\sum_{k=1}^{T}\rho_{n,c}(k)+T\lambda_{n,c}\left(\mu_{\max}^{\text{in}}+\lambda_{n,c}\right)\right)$$

Taking a $\limsup$ as $M\to\infty$, and noting that

$$\limsup_{M\to\infty}\frac{1}{M}\sum_{\tau=0}^{M-1}E[Q_{n,c}(\tau-T)]=\limsup_{M\to\infty}\frac{1}{M}\sum_{\tau=0}^{M-1}E[Q_{n,c}(\tau)] \tag{5.8}$$

and optimizing over ν yields the result. □

Theorem 5.3.1 guarantees the stability of the network under the backpressure policy when the arrival rate vector is inside the stability region and the arrival processes are time-correlated over fixed length of interval. This is done by explicitly showing that the sum of average queue backlogs in the network is upper bounded by some finite number. However, if the condition $E[A_{n,c}(t)|H(t-k)]=\lambda_{n,c}$ for $k\geq T$ is not satisfied with any finite integer T, the theorem fails simply because the upper bound becomes infinite. The arrivals with short-range dependence might be dealt similarly with the arrivals with finite memory using the fact that their autocorrelations decrease exponentially fast as the time-lag increases. Our following theorem, on the other hand, is applicable for both short-range and long-range dependent arrivals as it only requires very mild conditions on the arrival process such as the monotonicity of its absolute autocorrelation function.

Theorem 5.3.2. *If arrival rate vector $\overrightarrow{\lambda}$ is strictly interior to stability region Λ and the absolute autocorrelation functions $|\rho_{nc}(k)|$ of the arrival processes are monotonically decreasing for all (n,c) pairs, the backpressure policy stabilizes the network and guarantees*

bounded average queue backlog as

$$\limsup_{t\to\infty}\frac{1}{t}\sum_{\tau=0}^{t-1}\sum_{n,c}E[Q_{n,c}(\tau)]\leq\frac{1}{2(\nu_{\max}-\delta)}\left(NB_1+2\sum_{n,c}\phi_{n,c}(T_\delta)\right)$$

where δ is an arbitrary constant satisfying $0<\delta<\nu_{\max}$ and T_δ is the minimum of T such that $|E[A_{n,c}(t)|H(t-k)]-\lambda_{n,c}|\leq\delta$ for $k\geq T$ and for all (n,c) pairs.

Proof. As in the proof of Theorem 5.3.1, the main difficulty of analyzing the Lyapunov drift is due to the correlation between $Q_{n,c}(t)$ and $A_{n,c}(t)$. Assume that δ and corresponding T_δ are chosen such that the conditions described in the theorem are met. Then, for $T\geq T_\delta$, we have

$$\begin{aligned}E\left[Q_{n,c}(t-T)A_{n,c}(t)\right]&=E\left[Q_{n,c}(t-T)E\left[A_{n,c}(t)|\,\overrightarrow{Q}(t-T)\right]\right]\\&\leq(\lambda_{n,c}+\delta)E\left[Q_{n,c}(t-T)\right]\end{aligned}$$

for all (n,c) pairs and inequality in Eq. (5.7) holds for any $T>0$. Therefore, the unconditional Lyapunov drift satisfies

$$\begin{aligned}&E[L(\overrightarrow{Q}(t+1))-L(\overrightarrow{Q}(t))]\leq NB_1-2\sum_{n,c}(\lambda_{n,c}+\nu)E\left[Q_{n,c}(t)\right]\\&+2\sum_{n,c}(\lambda_{n,c}+\delta)E\left[Q_{n,c}(t-T)\right]+2\sum_{n,c}\left(\sigma_{n,c}^2\sum_{k=1}^{T}\rho_{n,c}(k)+T\lambda_{n,c}\left(\mu_{\max}^{\text{in}}+\lambda_{n,c}\right)\right)\end{aligned}$$

for $T\geq T_\delta$. The rest of the proof is identical with that of Theorem 5.3.1. □

Theorem 5.3.2 can be applied to any long memory arrivals but with monotonically decreasing absolute autocorrelation functions. It is expected that long-range dependent arrivals would induce longer T_δ satisfying the condition when compared to short-range dependent arrivals due to the hyperbolic shape of the autocorrelation function. Once the

autocorrelation functions are given, one can compute T_δ deterministically. From Theorem 5.3.1 and Theorem 5.3.2, we know that the backpressure policy stabilizes the network whenever the arrival rate vector is inside the stability region no matter whether arrival processes are i.i.d. or time-correlated. Specifically, in Theorem 5.3.1, the upper bound on the sum of average queue backlogs is always finite whenever $\nu_{\max} > 0$, which corresponds to the condition that the arrival rate vector is strictly inside the stability region. In Theorem 5.3.2, there must exist δ such that $0 < \delta < \nu_{\max}$ because $\nu_{\max} > 0$ and T_δ must be finite for given δ because the autocorrelation functions are assumed to be monotonically decreasing. Therefore, the upper bound on the sum of average queue backlogs is always finite. Note that in case of i.i.d. arrivals, the upper bound is given by $NB_1/2\nu_{\max}$ [26]. Thus, apart from the stability issue, the upper bound on average network delay will increase if arrivals are time-correlated. This follows from the Little's law which states that the average network delay is proportional to average network backlog [89].

5.4 Network with Arbitrary Input Traffic

In this chapter, we consider an arrival rate vector $\overrightarrow{\lambda}$ that is possibly outside the stability region Λ as shown in Fig. 5.3. If $\overrightarrow{\lambda} \notin \Lambda$, no policy can stabilize the network unless we have a set of flow controllers in front of queues as shown in Fig. 5.4. Denote by $R_{n,c}(t)$ the amount of data that is admitted into the queue at node n for commodity c at time slot t, and define $r_{n,c} \triangleq \lim_{t\to\infty} \frac{1}{t} \sum_{\tau=0}^{t-1} E[R_{n,c}(\tau)]$. The role of flow controllers is to keep the average admission rate vector $\overrightarrow{r} = (r_{n,c})$ to be inside the stability region. If then, the stability can be achieved by the backpressure policy in Algorithm 1. With the

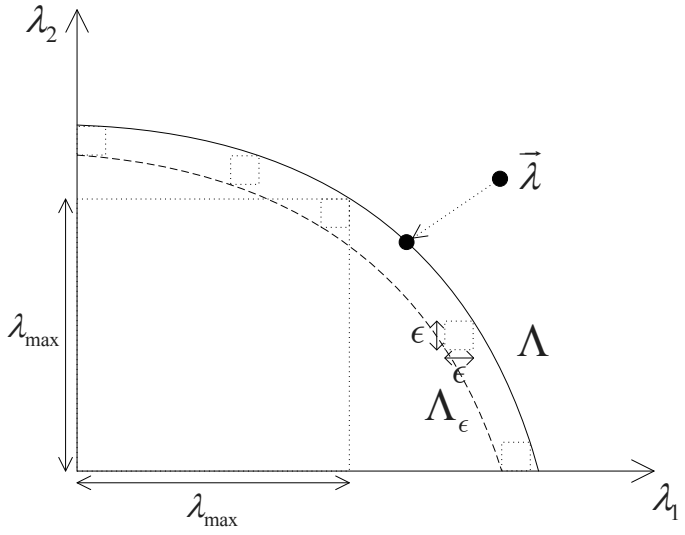

Figure 5.3: Illustration of the ϵ-stripped stability region Λ_ϵ with an arrival rate vector outside the stability region Λ

flow-controlled input, the queue size evolves as

$$Q_{n,c}(t+1) \leq \max\left[Q_{n,c}(t) - \sum_{l\in\mathcal{O}_n} \mu_{l,c}(t), 0\right] + \sum_{l\in\mathcal{I}_n} \mu_{l,c}(t) + R_{n,c}(t)$$

where the exogenous arrival $A_{n,c}(t)$ is replaced by $R_{n,c}(t)$ from Eq. (5.1).

The flow controllers need to be designed in some optimum way, which is fundamentally about how to choose the operating point of the network on the boundary of the stability region Λ. This is often modeled as a network utility maximization problem, where the utility is a measure of relative satisfaction of the users at a given rate [9,33–36].

$$\begin{aligned} \text{maximize} \quad & \sum_{n,c} U_{n,c}(r_{n,c}) \\ \text{subject to} \quad & \overrightarrow{r} \in \Lambda \\ & 0 \leq r_{n,c} \leq \lambda_{n,c},\ \forall (n,c) \end{aligned} \tag{5.9}$$

where $U_{n,c}(\cdot)$ is the utility function associated with the input stream described by (n,c)

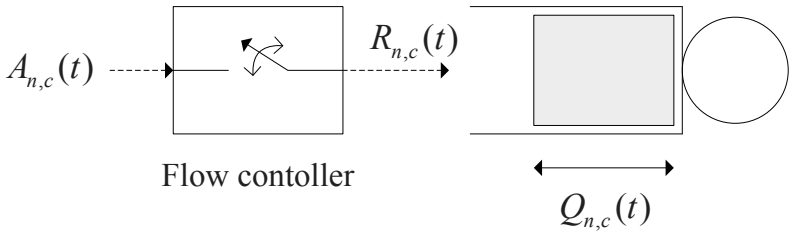

Figure 5.4: An input-controlled queueing model

pair. The first constraint in the formulation states that the average admitted rate vector must be stabilizable and the next set of constraints state that the admission rate of each stream cannot exceed its incoming rate. Those constraints are automatically satisfied under any stabilizing policy. It is often assumed that utility functions are strictly concave, non-decreasing, and continuously differentiable. As a result, the first derivative of the utility function is monotonically decreasing with maximum at $r = 0$. We assume that the maximum is bounded by some finite value $\theta_{n,c}$. It is further assumed that the utility achieved at a node is bounded by some finite value $U_{\max}$. The joint flow control and backpressure policy described in Algorithm 2 and originally derived in [26,27] was shown for i.i.d. arrivals to achieve arbitrarily close to the optimal solution of Eq. (5.9) with a corresponding tradeoff in average network delay.

Theorem 5.4.1. *If there exists finite integer $T > 0$ such that $E[A_{n,c}(t)|H(t-k)] = \lambda_{n,c}$ for $k \geq T$ and for all (n, c) pairs, the joint flow control and backpressure policy stabilizes the network and yields bounds on time average queue backlog as*

$$\limsup_{t\to\infty} \frac{1}{t} \sum_{\tau=0}^{t-1} \sum_{n,c} E[Q_{n,c}(\tau)] \leq \frac{1}{2\lambda_{\max}} \left(NB_2 + VNU_{\max} + 2 \sum_{n,c} \psi_{n,c}(T) \right)$$

Algorithm 2 Joint Flow Control and Backpressure Policy [27]

- *Flow Control* — Every time slot and for each input stream (n, c), observe $Q_{n,c}(t)$ and $Y_{n,c}(t)$ and choose:

$$R_{n,c}(t) \;=\; \begin{cases} A_{n,c}(t), & \text{if } \; Y_{n,c}(t) \geq Q_{n,c}(t) \\ \\ 0, & \text{otherwise} \end{cases}$$

where $Y_{n,c}(t)$ is updated according to

$$Y_{n,c}(t+1) = \max\left[Y_{n,c}(t) - R_{n,c}(t), 0\right] + \gamma_{n,c}(t) \tag{5.10}$$

which is called the *virtual* flow state queue in which we set $\gamma_{n,c}(t) = \gamma_{n,c}$ where $\gamma_{n,c}$ is the solution to

$$\begin{aligned} \text{maximize} \quad & VU_{n,c}(\gamma_{n,c}) - 2Y_{n,c}(t)\gamma_{n,c} \\ \text{subject to} \quad & 0 \leq \gamma_{n,c} \leq A_{\max} \end{aligned} \tag{5.11}$$

where $V > 0$ is a design parameter which affects the utility-delay tradeoff of the algorithm.

- Routing/scheduling and resource allocation are performed as in Algorithm 1.

and network utility as

$$\liminf_{t\to\infty} \sum_{n,c} U_{n,c}(\bar{r}_{n,c}(t)) \geq \sum_{n,c} U_{n,c}\left(r^*_{n,c}\right) - \frac{1}{V}\left(NB_2 + 2\sum_{n,c}\psi_{n,c}(T)\right)$$

where $\bar{r}_{n,c}(t) \triangleq \frac{1}{t}\sum_{\tau=0}^{t-1} E[R_{n,c}(\tau)]$ *and*

$$\psi_{n,c}(T) \triangleq \left\{2\sigma^2_{n,c}\sum_{k=1}^{T}\rho_{n,c}(k) + T\lambda_{n,c}\left(\mu^{\text{in}}_{\max} + \lambda_{n,c}\right)\right\}$$

and $B_2 \triangleq B_1 + 2A^2_{\max}$, $\lambda_{\max}$ *is the largest scalar such that* $(\lambda_{\max}) \in \Lambda$, *and* $(r^*_{n,c})$ *is the utility-optimal rate allocation vector.*

Proof. We begin by noting that problem Eq. (5.9) is equivalent to maximize $\sum_{n,c} U_{n,c}(\gamma_{n,c})$ with an additional set of constraints, $0 \leq \gamma_{n,c} \leq r_{n,c}$ for all (n,c) pairs because utility functions are non-decreasing. The constraints are satisfied by stabilizing the virtual flow state queues in Eq. (5.10)[1]. Define $L(\overrightarrow{\Theta}(t)) \triangleq \sum_{n,c}(Q_{n,c}(t)^2 + Y_{n,c}(t)^2)$ as a Lyapunov function whose conditional drift is written as

$$\Delta(\overrightarrow{\Theta}(t)) \triangleq E[L(\overrightarrow{\Theta}(t+1)) - L(\overrightarrow{\Theta}(t))|\overrightarrow{\Theta}(t)]$$

where $\overrightarrow{\Theta}(t) \triangleq [\overrightarrow{Q}(t); \overrightarrow{Y}(t)]$. Omitting the drift computation details for brevity, the con-

[1]The notion of virtual queueing was originally introduced in [27] and it is often used as a means of ensuring long-term average constraints.

ditional Lyapunov drift can be shown to satisfy

$$\begin{aligned}\Delta(\overrightarrow{\Theta}(t)) - V\sum_{n,c} E\left[U_{n,c}(\gamma_{n,c}(t))|\,\overrightarrow{\Theta}(t)\right] \leq NB_2 \\ - 2\sum_{n,c} Q_{n,c}(t)E\left[\sum_{l\in\mathcal{O}_n}\mu_{l,c}(t) - \sum_{l\in\mathcal{I}_n}\mu_{l,c}(t)\middle|\,\overrightarrow{\Theta}(t)\right] \\ + 2\sum_{n,c}\left(Q_{n,c}(t) - Y_{n,c}(t)\right)E\left[R_{n,c}(t)|\,\overrightarrow{\Theta}(t)\right] \\ + 2\sum_{n,c} Y_{n,c}(t)E\left[\gamma_{n,c}(t)|\,\overrightarrow{\Theta}(t)\right] - V\sum_{n,c} E\left[U_{n,c}(\gamma_{n,c}(t))|\,\overrightarrow{\Theta}(t)\right] \quad (5.12)\end{aligned}$$

where the optimization metric $V\sum_{n,c} E\left[U_{n,c}\left(\gamma_{n,c}(t)\right)|\,\overrightarrow{\Theta}(t)\right]$ was subtracted on both sides. It is apparent that the joint flow control and backpressure policy in Algorithm 2 is designed to minimize the RHS of Eq. (5.12) among all other policies.

Define for some $\epsilon > 0$, $\Lambda_\epsilon \triangleq \{\,\overrightarrow{r} \mid \overrightarrow{r} + \epsilon\,\overrightarrow{1} \in \Lambda\,\}$ and let $(r^*_{n,c}(\epsilon))$ be the optimal solution to Eq. (5.9) with the reduced stability region Λ_ϵ as illustrated in Fig. 5.3. From Corollary 3.9 of [26], we know that there exists a stationary randomized policy that makes decision based only on the current channel states and independent of queue backlogs such that

$$E\left[\sum_{l\in\mathcal{O}_n}\mu_{l,c}(t) - \sum_{l\in\mathcal{I}_n}\mu_{l,c}(t)\middle|\,\overrightarrow{\Theta}(t)\right] = r^*_{n,c}(\epsilon) + \epsilon$$

for all (n,c) pairs. We further fix $\gamma_{n,c}(t)$ to $r^*_{n,c}(\epsilon)$ for all t and consider a randomized policy for $R_{n,c}(t)$ such that $R_{n,c}(t) = A_{n,c}(t)$ with probability $r^*_{n,c}(\epsilon)/\lambda_{n,c}$ and $R_{n,c}(t) = 0$ with probability $1 - r^*_{n,c}(\epsilon)/\lambda_{n,c}$. Because the joint flow control and backpressure policy in Algorithm 2 outperforms any other policy, which follows from the construction of the

algorithm, the conditional Lyapunov drift satisfies

$$\Delta(\overrightarrow{\Theta}(t)) - V\sum_{n,c} E\left[U_{n,c}(\gamma_{n,c}(t))|\,\overrightarrow{\Theta}(t)\right] \leq NB_2$$
$$- 2\sum_{n,c}\left(r^*_{n,c}(\epsilon)+\epsilon\right)Q_{n,c}(t) + 2\sum_{n,c}\frac{r^*_{n,c}(\epsilon)}{\lambda_{n,c}}\left(Q_{n,c}(t)-Y_{n,c}(t)\right)E\left[A_{n,c}(t)|\,\overrightarrow{\Theta}(t)\right]$$
$$+ 2\sum_{n,c} r^*_{n,c}(\epsilon)Y_{n,c}(t) - V\sum_{n,c}U_{n,c}\left(r^*_{n,c}(\epsilon)\right) \quad (5.13)$$

Note that because the arrivals are time-correlated, $A_{n,c}(t)$ is not independent with $Q_{n,c}(t)$ and $Y_{n,c}(t)$ and, thus, we take a similar approach as the one used in Chapter 5.3. From the proof of Theorem 5.3.1, we know that

$$E[Q_{n,c}(t)A_{n,c}(t)] \leq \lambda_{n,c}E\left[Q_{n,c}(t-T)\right] + \sigma^2_{n,c}\sum_{k=1}^{T}\rho_{n,c}(k) + T\lambda_{n,c}\left(\mu^{\text{in}}_{\max}+\lambda_{n,c}\right) \quad (5.14)$$

Furthermore, from Eq. (5.10), we note

$$Y_{n,c}(t) \geq Y_{n,c}(t-T) - \sum_{k=1}^{T}R_{n,c}(t-k) + \sum_{k=1}^{T}\gamma_{n,c}(t-k)$$

and, thus, it follows that

$$\begin{aligned}
E\left[Y_{n,c}(t)A_{n,c}(t)\right] &\geq E\left[Y_{n,c}(t-T)A_{n,c}(t)\right] - E\left[\sum_{k=1}^{T}R_{n,c}(t-k)A_{n,c}(t)\right] \\
&\quad + E\left[\sum_{k=1}^{T}\gamma_{n,c}(t-k)A_{n,c}(t)\right] \\
&= \lambda_{n,c}E\left[Y_{n,c}(t-T)\right] - \frac{r^*_{n,c}(\epsilon)}{\lambda_{n,c}}\left(\sigma^2_{n,c}\sum_{k=1}^{T}\rho_{n,c}(k) + T\lambda^2_{n,c}\right) \\
&\quad + Tr^*_{n,c}(\epsilon)\lambda_{n,c} \\
&= \lambda_{n,c}E\left[Y_{n,c}(t-T)\right] - \frac{r^*_{n,c}(\epsilon)\sigma^2_{n,c}}{\lambda_{n,c}}\sum_{k=1}^{T}\rho_{n,c}(k) \qquad (5.15)
\end{aligned}$$

Taking the expectation of Eq. (5.13) with respect to the distribution of $\overrightarrow{\Theta}(t)$ and applying the inequalities in Eqs. (5.14) and (5.15) yields the unconditional Lyapunov drift

satisfying

$$E[L(\overrightarrow{\Theta}(t+1))-L(\overrightarrow{\Theta}(t))]-V\sum_{n,c}E\left[U_{n,c}(\gamma_{n,c}(t))\right]\leq NB_2-2\sum_{n,c}\left(r^*_{n,c}(\epsilon)+\epsilon\right)E[Q_{n,c}(t)]$$
$$+2\sum_{n,c}\left\{r^*_{n,c}(\epsilon)E\left[Q_{n,c}(t-T)\right]+\frac{r^*_{n,c}(\epsilon)\sigma^2_{n,c}}{\lambda_{n,c}}\sum_{k=1}^{T}\rho_{n,c}(k)+Tr^*_{n,c}(\epsilon)\left(\mu^{\text{in}}_{\max}+\lambda_{n,c}\right)\right\}$$
$$-2\sum_{n,c}\left\{r^*_{n,c}(\epsilon)E\left[Y_{n,c}(t-T)\right]-\left(\frac{r^*_{n,c}(\epsilon)\sigma_{n,c}}{\lambda_{n,c}}\right)^2\sum_{k=1}^{T}\rho_{n,c}(k)\right\}$$
$$+2\sum_{n,c}r^*_{n,c}(\epsilon)E[Y_{n,c}(t)]-V\sum_{n,c}U_{n,c}\left(r^*_{n,c}(\epsilon)\right) \quad (5.16)$$

Summing the inequalities over $t\in\{0,\ldots,M-1\}$, dividing by M, and taking limit as $M\to\infty$ results into

$$-V\lim_{M\to\infty}\frac{1}{M}\sum_{\tau=0}^{M-1}\sum_{n,c}E\left[U_{n,c}(\gamma_{n,c}(\tau))\right]\leq NB_2-2\epsilon\lim_{M\to\infty}\frac{1}{M}\sum_{\tau=0}^{M-1}\sum_{n,c}E[Q_{n,c}(\tau)]$$
$$+2\sum_{n,c}\left\{\left(\frac{r^*_{n,c}(\epsilon)}{\lambda_{n,c}}+\left(\frac{r^*_{n,c}(\epsilon)}{\lambda_{n,c}}\right)^2\right)\sigma^2_{n,c}\sum_{k=1}^{T}\rho_{n,c}(k)+Tr^*_{n,c}(\epsilon)\left(\mu^{\text{in}}_{\max}+\lambda_{n,c}\right)\right\}$$
$$-V\sum_{n,c}U_{n,c}\left(r^*_{n,c}(\epsilon)\right) \quad (5.17)$$

where we used the fact that the system starts with empty queues, i.e., $L(\overrightarrow{\Theta}(0))=0$, the non-negativity of the Lyapunov function, and the $\lim$ version of identity of Eq. (5.8), and the fact that

$$\lim_{M\to\infty}\frac{1}{M}\sum_{\tau=0}^{M-1}E[Y_{n,c}(\tau-T)]=\lim_{M\to\infty}\frac{1}{M}\sum_{\tau=0}^{M-1}E[Y_{n,c}(\tau)] \quad (5.18)$$

Rearranging Eq. (5.17) and dividing by 2ϵ, we have

$$\lim_{M\to\infty}\frac{1}{M}\sum_{\tau=0}^{M-1}\sum_{n,c}E[Q_{n,c}(\tau)]\leq\frac{NB_2+VNU_{\max}}{2\epsilon}$$
$$+\frac{1}{\epsilon}\sum_{n,c}\left\{2\sigma^2_{n,c}\sum_{k=1}^{T}\rho_{n,c}(k)+T\lambda_{n,c}\left(\mu^{\text{in}}_{\max}+\lambda_{n,c}\right)\right\} \quad (5.19)$$

where we used the fact that $r^*_{n,c}(\epsilon)/\lambda_{n,c} \leq 1$ and the non-negativity of the utility function. Rearranging Eq. (5.17) differently, dividing by V, and using the facts that $r^*_{n,c}(\epsilon)/\lambda_{n,c} \leq 1$ and the non-negativity of queue backlogs yields

$$\lim_{M\to\infty} \frac{1}{M} \sum_{\tau=0}^{M-1} \sum_{n,c} E\left[U_{n,c}(\gamma_{n,c}(\tau))\right] \geq \sum_{n,c} U_{n,c}\left(r^*_{n,c}(\epsilon)\right) - \frac{NB_2}{V} - \frac{2}{V} \sum_{n,c} \left\{ 2\sigma^2_{n,c} \sum_{k=1}^{T} \rho_{n,c}(k) + T\lambda_{n,c}\left(\mu^{\text{in}}_{\max} + \lambda_{n,c}\right) \right\} \quad (5.20)$$

Applying Jensen's inequality based on the concavity of the utility functions, we have $\frac{1}{M}\sum_{\tau=0}^{M-1} E\left[U_{n,c}\left(\gamma_{n,c}(\tau)\right)\right] \leq U_{n,c}(\frac{1}{M}\sum_{\tau=0}^{M-1} E\left[\gamma_{n,c}(\tau)\right])$. On the other hand, we can show that virtual flow queues $Y_{n,c}(t)$ are always stable under the joint flow control and backpressure policy implying $\overline{\gamma}_{n,c}(t) \leq \overline{r}_{n,c}(t)$, which are time averages up to slot t. The stability of the virtual queues can be established via a simple argument. Suppose that $Y_{n,c}(t) > \frac{1}{2}V\theta_{n,c}$, where $\theta_{n,c}$ is the bound on the first derivative of $U_{n,c}$. Then, the solution to Eq. (5.11) is always $\gamma_{n,c} = 0$ until $Y_{n,c}(t)$ drops below $\frac{1}{2}V\theta_{n,c}$. Suppose now that $Y_{n,c}(t) \leq \frac{1}{2}V\theta_{n,c}$. Then, the virtual queue can grow at most by $A_{\max}$ but, after that, it cannot grow further because $Y_{n,c}(t)$ exceeds $\frac{1}{2}V\theta_{n,c}$. Therefore, the virtual queue $Y_{n,c}(t)$ is always bounded below $\frac{1}{2}V\theta_{n,c} + A_{\max}$. Further note that taking $\limsup$ or $\liminf$ instead of $\lim$ does not change the results because the inequality in Eq. (5.16) holds for every t. Finally, optimizing ϵ for Eqs. (5.19) and (5.20) separately over $(0, \lambda_{\max}]$ completes the proof. □

Theorem 5.4.1 shows that the joint flow control and backpressure policy stabilizes the network even when the arrival rate vector is outside the stability region and the arrival processes are time-correlated over fixed length of interval. The theorem also shows that

the joint policy yields admission rate vector that is arbitrarily close to the utility-optimal operating point with a corresponding tradeoff in average network delay, where parameter V enables to exploit the tradeoff. We now proceed to a general case where arrivals may have infinite-length of memory such as short/long-range dependent processes.

Theorem 5.4.2. *If the absolute autocorrelation functions $|\rho_{n,c}(k)|$ of the arrival processes are monotonically decreasing for all (n,c) pairs, the joint flow control and backpressure policy stabilizes the network and yields bounds on time average queue backlog as*

$$\limsup_{t\to\infty} \frac{1}{t}\sum_{\tau=0}^{t-1}\sum_{n,c} E[Q_{n,c}(\tau)] \leq \frac{1}{2(\lambda_{\max}-\delta)} \times \left(NB_2 + VNU_{\max} + V\delta\sum_{n,c}\theta_{n,c} + 2\sum_{n,c}\psi_{n,c}(T_\delta) + 2\delta NA_{\max} \right)$$

and network utility as

$$\liminf_{t\to\infty} \sum_{n,c} U_{n,c}(\bar{r}_{n,c}(t)) \geq \sum_{n,c} U_{n,c}\left(r^*_{n,c}\right) - \delta\sum_{n,c}\theta_{n,c} - \frac{1}{V}\left(NB_2 + 2\sum_{n,c}\psi_{n,c}(T_\delta) + 2\delta NA_{\max} \right)$$

where δ is an arbitrary constant satisfying $0 < \delta < \lambda_{\max}$ and T_δ is the minimum of T such that $|E[A_{n,c}(t)|H(t-k)] - \lambda_{n,c}| \leq \delta$ for $k \geq T$ and for all (n,c) pairs.

Proof. As in the proof of Theorem 5.4.1, the main difficulty of the analysis is due to the correlations between $Q_{n,c}(t)$ and $A_{n,c}(t)$ and between $Y_{n,c}(t)$ and $A_{n,c}(t)$. Assume that δ and T_δ are chosen such that the conditions described in the theorem are met. Then, for $T \geq T_\delta$, we have

$$E[Q_{n,c}(t)A_{n,c}(t)] \leq (\lambda_{n,c}+\delta)E\left[Q_{n,c}(t-T)\right] + \sigma^2_{n,c}\sum_{k=1}^{T}\rho_{n,c}(k) + T\lambda_{n,c}\left(\mu^{\text{in}}_{\max} + \lambda_{n,c}\right) \tag{5.21}$$

and

$$E\left[Y_{n,c}(t)A_{n,c}(t)\right] \geq (\lambda_{n,c}-\delta)E\left[Y_{n,c}(t-T)\right] - \frac{r^*_{n,c}(\epsilon)\sigma^2_{n,c}}{\lambda_{n,c}}\sum_{k=1}^{T}\rho_{n,c}(k) \tag{5.22}$$

Taking the expectation of Eq. (5.13) with respect to the distribution of $\overrightarrow{\Theta}(t)$ and applying the inequalities in Eqs. (5.21) and (5.22) yields the unconditional Lyapunov drift satisfying

$$\begin{aligned}
&E[L(\overrightarrow{\Theta}(t+1)) - L(\overrightarrow{\Theta}(t))] - V\sum_{n,c}E\left[U_{n,c}(\gamma_{n,c}(t))\right] \leq NB_2 \\
&\quad - 2\sum_{n,c}\left(r^*_{n,c}(\epsilon)+\epsilon\right)E[Q_{n,c}(t)] + 2\sum_{n,c}\Bigg\{\left(r^*_{n,c}(\epsilon)+\frac{r^*_{n,c}(\epsilon)\delta}{\lambda_{n,c}}\right)E\left[Q_{n,c}(t-T)\right] \\
&\qquad\qquad + \frac{r^*_{n,c}(\epsilon)\sigma^2_{n,c}}{\lambda_{n,c}}\sum_{k=1}^{T}\rho_{n,c}(k) + Tr^*_{n,c}(\epsilon)\left(\mu^{\text{in}}_{\max}+\lambda_{n,c}\right)\Bigg\} \\
&\quad - 2\sum_{n,c}\left\{\left(r^*_{n,c}(\epsilon)-\frac{r^*_{n,c}(\epsilon)\delta}{\lambda_{n,c}}\right)E\left[Y_{n,c}(t-T)\right] - \left(\frac{r^*_{n,c}(\epsilon)\sigma_{n,c}}{\lambda_{n,c}}\right)^2\sum_{k=1}^{T}\rho_{n,c}(k)\right\} \\
&\qquad\qquad + 2\sum_{n,c}r^*_{n,c}(\epsilon)E[Y_{n,c}(t)] - V\sum_{n,c}U_{n,c}\left(r^*_{n,c}(\epsilon)\right)
\end{aligned} \tag{5.23}$$

Summing the inequalities over time slots $t \in \{0,\ldots,M-1\}$, dividing by M, and taking limit as $M\to\infty$ results

$$\begin{aligned}
&-V\lim_{M\to\infty}\frac{1}{M}\sum_{\tau=0}^{M-1}\sum_{n,c}E\left[U_{n,c}(\gamma_{n,c}(\tau))\right] \leq NB_2 \\
&\quad - 2(\epsilon-\delta)\lim_{M\to\infty}\frac{1}{M}\sum_{\tau=0}^{M-1}\sum_{n,c}E[Q_{n,c}(\tau)] + 2\delta\lim_{M\to\infty}\frac{1}{M}\sum_{\tau=0}^{M-1}\sum_{n,c}E[Y_{n,c}(\tau)] \\
&\quad + 2\sum_{n,c}\left\{2\sigma^2_{n,c}\sum_{k=1}^{T}\rho_{n,c}(k) + T\lambda_{n,c}\left(\mu^{\text{in}}_{\max}+\lambda_{n,c}\right)\right\} - V\sum_{n,c}U_{n,c}\left(r^*_{n,c}(\epsilon)\right)
\end{aligned} \tag{5.24}$$

where we used the fact that the the system starts with empty queues, $r^*_{n,c}(\epsilon)/\lambda_{n,c} \leq 1$, the non-negativity of Lyapunov function, and the $\lim$ version of identity of Eqs. (5.8) and (5.18). Rearranging terms, dividing by $2(\epsilon-\delta)$, and using non-negativity of utility

function, we obtain

$$\lim_{M\to\infty}\frac{1}{M}\sum_{\tau=0}^{M-1}\sum_{n,c}E[Q_{n,c}(\tau)] \leq \frac{NB_2+VNU_{\max}}{2(\epsilon-\delta)} + \frac{1}{\epsilon-\delta}\sum_{n,c}\left\{2\sigma_{n,c}^2\sum_{k=1}^{T}\rho_{n,c}(k)+T\lambda_{n,c}\left(\mu_{\max}^{\text{in}}+\lambda_{n,c}\right)\right\} + \frac{\delta}{\epsilon-\delta}\lim_{M\to\infty}\frac{1}{M}\sum_{\tau=0}^{M-1}\sum_{n,c}E[Y_{n,c}(\tau)] \quad (5.25)$$

Rearranging Eq. (5.24) differently, dividing by V, and using non-negativity of queue backlogs, we have

$$\lim_{M\to\infty}\frac{1}{M}\sum_{\tau=0}^{M-1}\sum_{n,c}E\left[U_{n,c}(\gamma_{n,c}(\tau))\right] \geq \sum_{n,c}U_{n,c}\left(r_{n,c}^{*}(\epsilon)\right)-\frac{NB_2}{V} -\frac{2}{V}\sum_{n,c}\left\{2\sigma_{n,c}^2\sum_{k=1}^{T}\rho_{n,c}(k)+T\lambda_{n,c}\left(\mu_{\max}^{\text{in}}+\lambda_{n,c}\right)\right\}-\frac{2\delta}{V}\lim_{M\to\infty}\frac{1}{M}\sum_{\tau=0}^{M-1}\sum_{n,c}E[Y_{n,c}(\tau)] \quad (5.26)$$

The rest of the proof follows closely that of Theorem 5.4.1 and the result is obtained by optimizing ϵ for Eqs. (5.25) and (5.26) separately over $(0,\lambda_{\max}]$ and using the fact that $Y_{n,c}(t)$ is always bounded below $\frac{1}{2}V\theta_{n,c}+A_{\max}$ from the proof of Theorem 5.4.1. Finally, note that because inequality in Eq. (5.23) holds for all t, taking $\limsup$ or $\liminf$ instead of $\lim$ does not change the results. □

In the case of i.i.d. arrivals, it was shown that the sum of average queue backlogs is at most $(NB_2+VNU_{\max})/2\lambda_{\max}$ and the achieved network utility is at worst NB_2/V apart from the value at the utility-optimal operating point [27]. Therefore, the additional terms in the tradeoff of network utility and sum of average queue backlog in Theorem 5.4.1 and Theorem 5.4.2 can be viewed as a penalty due to the correlations on the arrival processes. In Theorem 5.4.1, we needed to increase V to achieve performance that is

arbitrarily close to that of the optimal utility value with a corresponding increase in the sum of average queue backlogs. In case of Theorem 5.4.2, as V goes to infinity, the achieved network utility approaches a point that is at most $\delta \sum_{n,c} \theta_{n,c}$ apart from the optimal network utility.

5.5 Chapter Summary

The performance of backpressure-based stochastic network controls in wireless multi-hop networks with time-correlated arrivals was studied using the Lyapunov drift technique. The impact of input correlations appears in the upper bound on the average network delay when the arrival rate vector is inside the stability region and the tradeoff between the average network delay and utility when the arrival rate vector is possibly outside the stability region. To handle the Lyapunov drift with correlated terms, we first expressed the evolution of the system dynamics over multiple slots and used the fact that the conditional expectation of the arrival process given the past history falls within arbitrarily small constant range around its unconditional expectation if the time-lag between the arrival process and the past history becomes sufficiently large. This is true for both finite memory and infinite memory arrivals with monotonically decreasing autocorrelation functions. On the other hand, usual sum-of-queue-squares-type Lyapunov function was used in which no cross-terms between different links are emerging. Therefore, in order to incorporate the explicit form of the cross-correlation between the different links, the Lyapunov function needs to be modified.

Chapter 6

Neighbor Discovery in a Wireless Sensor Network with Physical-Layer Considerations

6.1 Background

Neighbor discovery in wireless networks is defined to be the process to identify a set of nodes with which a node can communicate, and it has been addressed by several authors [42–45]. In [42], a simple ALOHA-like neighbor discovery algorithm was proposed in which each node randomly transmit/listen in each time slot and analyzed for both synchronous and asynchronous timing cases. This type of discovery algorithm based on the random access protocol is well suited for randomly distributed wireless networks. In [43], similar neighbor discovery algorithm was considered and the expected time to find neighbors was obtained. In [44], a *gossip-based algorithm* was proposed in which each node transmits a table of *gossip* data (which is the list of neighbors that it has discovered so far and their locations) in a random direction using directional antennas. In [45], a family of probabilistic protocols, called birthday protocols, have been proposed to initiate the randomly deployed wireless networks. From a physical-layer point of view, however, the previous works are extremely limited due to the use of collision channel model. Under this model, if more than one nodes transmit at the same time, none of them are successful. However, it is too pessimistic in the sense that a transmission may succeed even in the

presence of interference which is called *capture effect* [47–51]. We, thus, claim that the performance of neighbor discovery algorithm has been quite underestimated so far due to the use of unrealistic channel model, and correct reassessment of the discovery algorithm is required.

Two main topics concerning with the neighbor discovery in a wireless sensor network is covered in this chapter. The first part of the chapter is devoted to an analysis of the performance of the chosen neighbor discovery algorithm under realistic physical layer conditions. For this, we consider a shared channel and nodes with multipacket reception capability in which a transmission is successful if the received signal-to-interference-plus-noise-ratio (SINR) exceeds a certain threshold. Specifically, under the discovery algorithm proposed in [42], we obtain the expression for the expected number of successful receptions *per slot* at a given SINR threshold and find the optimal transmission probability which maximizes the expected number of successful receptions. We note, however, that for a given modulation scheme and target bit error rate (BER), the data rate is an increasing function of the SINR threshold. Therefore, we derive the expected number of successful receptions *per second* rather than per slot under certain modulation scheme for a fair comparison. Finally, the performance of the discovery algorithm is evaluated over multiple slots which is important in deciding the run-time of the discovery process.

In the second part of the chapter, we consider the problem of the actual detection of transmitting neighbors. Note that the received signal at each time slot is the superposition of the signals transmitted from random set of nodes and noise. Therefore, determining the existence of a signal from a particular node itself is not an easy task. For this problem, we first present the classical matched filter method which fundamentally treats the

interference as noise. As an alternative, a more accurate method can be envisioned in an additional cost of complexity. Since the number of transmitters and their entities are all unknown, we adopt the viewpoint of random set theory (RST: see Chapter Appendix 6.A and references therein) and propose RST-based method for detecting the transmitting nodes in each time slot [46, 90–95]. Besides, it is also possible with RST to estimate additional parameters of transmitted signals such as signal amplitudes and phase.

6.2 Network Model

We consider a time-slotted wireless sensor network which is deployed over a region of interest such as large tactical area for target detection or vast rural area for environmental observation. In such scenarios, a large number of sensor nodes are released from an airplane. For a large number of nodes over a large area, the locations of nodes are modeled by a homogeneous, two-dimensional Poisson point process with intensity λ which is the average number of nodes per unit area. Therefore, the number of nodes in a unit area follows Poisson distribution with parameter λ. As is well known, a spatial Poisson process on the plane, conditioned on a given number of nodes within a given area, yields the uniform distribution of these nodes in that area. As a result, for example, if a node's discovery region is modeled as a circle of radius R_0, the cumulative probability distribution on the distance from the node to the other nodes in the region is given by

$$F_r(x) = \begin{cases} 0, & \text{if } x < 0 \\ \left(\dfrac{x}{R_0}\right)^2, & \text{if } 0 \le x \le R_0 \\ 1, & \text{if } x > R_0 \end{cases} \tag{6.1}$$

The signal received by a node at time slot t (if the node is listening) is given by

$$\mathbf{y}_t = \sum_{k \in \mathbf{I}_t} g_t^k \mathbf{s}_t^k + \mathbf{n}_t \tag{6.2}$$

where $\mathbf{I}_t$ is the set of transmitting neighbors, g_t^k is the complex amplitude of the signal received from the k-th node, $\mathbf{s}_t^k$ is the signal transmitted from the k-th node which is the message multiplied by the signature sequence bitwise, and $\mathbf{n}_t$ is a random noise. We assume that the signatures of all nodes are known to each other by assuming that they share an identical key generator which can be implemented using a linear feedback shift register. If the length of signature is L and each node transmits a 1-bit known message, then $\mathbf{y}_t = \{y_{t,1}, ..., y_{t,L}\}^T$, $\mathbf{s}_t^k = \{s_{t,1}^k, ..., s_{t,L}^k\}^T$ which is equal to the signature sequence, and $\mathbf{n}_t = \{n_{t,1}, ..., n_{t,L}\}^T$, where the symbol T denotes vector transpose. The noise samples in $\mathbf{n}_t$ are assumed to be independent and identically distributed (i.i.d.) with the normal distribution $\mathcal{N}(0, N)$ where N is the noise power which is the product of noise spectral density N_0 and bandwidth B. The complex amplitude g_t^k is of the form $g_t^k = \sqrt{G(1 + r_k)^{-\eta}}\psi_t^k$, where G is the transmission power, r_k is the distance from the k-th node to the receiver, η is the path loss exponent, and ψ_t^k is the channel fading coefficient which is modeled by i.i.d. standard circular symmetric Gaussian random process [55].

Denote by $\mathcal{J}$ and J the set of neighbors and the number of neighbors of a node, respectively, and we suppressed the particular node index for notational brevity. The SINR of node k at time slot t (if the k-th node is transmitting) is given by

$$\text{SINR}_t^k = \frac{P_{rx,k}}{\sum_{i \in \mathbf{I}_t, i \neq k} P_{rx,i} + N}$$

where $P_{rx,k}$ is the received signal power from the k-th transmitter. Note that the distances r_k $(k = 1, \ldots, J)$ are i.i.d. under the Poisson point process modeling. Also the channel

fading coefficients ψ_t^k are i.i.d., and by further assuming that r_k and ψ_t^k are mutually independent, the received signal powers $P_{rx,k}$ $(k = 1, \ldots, J)$ are i.i.d. as well, and the common cumulative distribution function of the received signal power is obtained by [48]

$$F_P(x) = 1 - \int_0^\infty F_r\left(\left(\frac{\omega G}{x}\right)^{\frac{1}{\eta}} - 1\right) f_{|\psi|^2}(\omega) d\omega \tag{6.3}$$

where $f_{|\psi|^2}(\cdot)$ is the probability density of the squared magnitude of the stationary fading process which is an exponential with unit mean. The transmission of the k-th node is said to be successful if

$$\mathrm{SINR}_t^k \geq \tau \tag{6.4}$$

where the threshold τ depends on parameters such as data rate and target BER [56].

6.3 The Neighbor Discovery Algorithm

6.3.1 Description of the Algorithm

An ALOHA-like neighbor discovery algorithm proposed in [42] is considered again in which each node transmits with probability p_{T} or listens with probability $1 - p_{\mathrm{T}}$. The transmission probability p_{T} and the transmission power G are identical for all nodes; all these simplifying assumptions were made to reduce non-essential complexities. Notice that a plain method such as the periodic beaconing can be thought but such a static approach would certainly fail in a randomly deployed network which has irregular node density. Under the chosen discovery algorithm, in order for a node to be discovered by some other node, the former should transmit and the other should listen at the same time. On top of that, the transmission must be successful which requires a certain criterion; in

the collision channel, the criterion is that there is only one transmission at that time slot. However, we adopt a more realistic SINR criterion for success and optimize the transmission probability which has been quite underestimated so far due to the use of collision channel model.

6.3.2 Considerations on Early Termination

Obviously, the marginal revenue of running the discovery algorithm diminishes as time goes and, because sensors are usually assumed to be battery-powered, it is needed to consider an early termination of the discovery process to prolong the lifetime of the network. Several metrics can be envisioned as a criterion for the early termination. A simple criterion is to terminate when a node has discovered a predetermined number of neighbors. In the case of nodes located at the sparsely populated areas, however, this may not be satisfied until the end of the discovery process (even if all the neighbors are discovered early). Alternatively, one may want to allow an early termination if a node has discovered a predetermined fraction of neighbors. However, because each node does not know *a priori* how many neighbors it has, this criterion is untestable. As will be seen in the next chapter, as time goes, the set of discovered neighbors in each time slot will overlap with the previously discovered ones. Therefore, if a node do not find any new neighbors for a sufficiently large number of slots, then it can be regarded that all the neighbors have been discovered. Hence, an early termination can be declared if a node does not receive any new messages during a predetermined number of time slots.

6.4 Analysis with the Multipacket Reception Capability

6.4.1 Optimal Transmission Probability

We start by deriving the expected number of successful receptions in each time slot as a function of SINR threshold τ. After that the transmission probability p_{T} is set to maximize it. We first denote by $\mathbf{I}_t^s (\subseteq \mathbf{I}_t)$ the set of transmitting neighbors satisfying the SINR criterion in Eq. (6.4). Then, the expected number of successful receptions by one node is expressed as[1]

$$\begin{aligned} E[|\mathbf{I}_t^s|] &= \Pr\{\text{a node is listening}\} \sum_{n=1}^{J} \Pr\{|\mathbf{I}_t| = n\} S_n \\ &= \sum_{n=1}^{J} \binom{J}{n} {p_{\mathrm{T}}}^n (1-p_{\mathrm{T}})^{J-n+1} S_n \end{aligned}$$

where S_n is the expected number of successful receptions given $n(\geq 1)$ simultaneous transmissions and is obtained by

$$S_n = n \Pr\left\{ \mathrm{SINR}_t^1 > \tau \;\middle|\; |\mathbf{I}_t| = n, 1 \in \mathbf{I}_t \right\} \tag{6.5}$$

where SINR_t^1 is the SINR of the first transmitter [48]. Note that Eq. (6.5) follows from the assumption that the received signal powers $P_{rx,k}$ $(k = 1, \ldots, J)$ are i.i.d. and, thus, the first transmitter needs not be the closest one to the receiver. It is computed as

$$\begin{aligned} \Pr\left\{ \mathrm{SINR}_t^1 > \tau \;\middle|\; |\mathbf{I}_t| = n, 1 \in \mathbf{I}_t \right\} &= 1 \\ &\quad - \int_0^\infty \cdots \int_0^\infty F_P\left(\tau \sum_{i=2}^{n} x_i\right) dF_P(x_2) \cdots dF_P(x_n) \end{aligned} \tag{6.6}$$

[1] $|\cdot|$ is the cardinality of a set.

where the noise effect was neglected for simplicity. Consequently, in principle, we can find the optimal transmission probability that maximizes the expected number of successful receptions.

Example 6.4.1. *As an illustration of the use of above equations, consider a simple example in which there are three nodes and they are within the radio range of each other. Since all three nodes have two neighbors, the expected number of successful receptions by one node is given by*

$$E[|\mathbf{I}_t^s|] = 2p_{\mathrm{T}}(1-p_{\mathrm{T}})^2 \mathrm{Pr}\left\{ \mathrm{SINR}_t^1 > \tau \;\middle|\; |\mathbf{I}_t| = 1, 1 \in \mathbf{I}_t \right\} + 2{p_{\mathrm{T}}}^2(1-p_{\mathrm{T}})\mathrm{Pr}\left\{ \mathrm{SINR}_t^1 > \tau \;\middle|\; |\mathbf{I}_t| = 2, 1 \in \mathbf{I}_t \right\}$$

Let us further consider a simplified path loss model in which the received signal power is given by $P_{rx,k} = r_k^{-\eta}$. Then, it can be easily shown that for $\tau < 1$,

$$E[|\mathbf{I}_t^s|] = \tau^{\frac{2}{\eta}} {p_{\mathrm{T}}}^3 - \left(2 + \tau^{\frac{2}{\eta}}\right) {p_{\mathrm{T}}}^2 + 2p_{\mathrm{T}} \tag{6.7}$$

and for $\tau \geq 1$,

$$E[|\mathbf{I}_t^s|] = \left(2 - \tau^{-\frac{2}{\eta}}\right) {p_{\mathrm{T}}}^3 + \left(\tau^{-\frac{2}{\eta}} - 4\right) {p_{\mathrm{T}}}^2 + 2p_{\mathrm{T}} \tag{6.8}$$

Note that Eqs. (6.7) and (6.8) are (strictly) concave over the feasible region. Thus, differentiating them with respect to p_{T}, and setting the derivatives to 0, we find the optimal transmission probability p_{T}^* which maximizes the expected number of successful receptions in each slot as

$$p_{\mathrm{T}}^* = \begin{cases} \dfrac{\tau^{\frac{2}{\eta}} + 2 - \sqrt{(\tau^{\frac{2}{\eta}} - 1)^2 + 3}}{3\tau^{\frac{2}{\eta}}}, & \text{if } \tau < 1 \\ \dfrac{\tau^{-\frac{2}{\eta}} - 4 + \sqrt{(\tau^{-\frac{2}{\eta}} - 1)^2 + 3}}{3(\tau^{-\frac{2}{\eta}} - 2)}, & \text{if } \tau \geq 1 \end{cases} \tag{6.9}$$

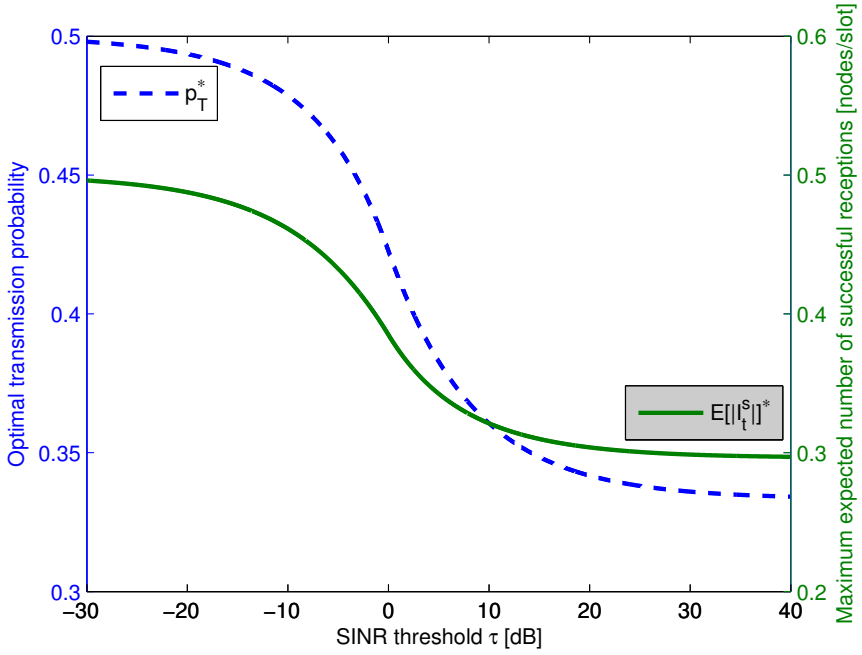

Figure 6.1: Optimal transmission probability p_{T}^* and corresponding maximum expected number of successful receptions $E[|\mathbf{I}_t^s|]^*$ for the three node example

In Fig. 6.1, we plot Eq. (6.9) as a function of τ with path loss exponent $\eta = 4$. It can be seen that as threshold τ increases, p_{T}^* decreases. This is because at a higher threshold, it becomes more difficult for multiple transmitters to simultaneously satisfy the SINR criterion. We can also see that the maximum expected number of successful receptions $E[|\mathbf{I}_t^s|]^*$ decreases as the threshold τ increases. However, it does not necessarily mean that we will have a reduced number of successful receptions in a unit time, because the transmission duration will also become shorter. We will look at this issue in the subsequent chapter.

Remark 6.4.1. *In [42], the optimal transmission probability under the collision channel model was derived, and was given by the inverse of the total number of nodes as in the*

original slotted ALOHA system. Recall that as τ goes to ∞, our model accommodates the collision channel model. In Eq. (6.9), we have $p_{\mathrm{T}}^{*} = 1/3$ as τ goes to ∞, which is consistent with the quoted result. Therefore, we conclude that the optimal transmission probability derived under collision channel model is fundamentally assuming the worst prior on the channel conditions by neglecting all the possibilities of succeeding in the presence of interference.

6.4.2 Controlling the Threshold for the Successful Decoding

For a given modulation scheme and target BER, the data rate is an increasing function of the SINR threshold τ [56]. Hence, if the number of bits to be transmitted is fixed and we increase τ, the slot duration must be shortened due to the increased rate. However, as we have seen in the previous chapter, the transmission probability p_{T} needs to be lowered. To investigate this, let us consider the M-PSK modulation scheme[2] whose symbol rate [symbols/sec/Hz] at a given target BER z is given by

$$R_s \approx \begin{cases} \min\left\{\frac{2\tau}{[Q^{-1}(z)]^2}, R_s^{\mathrm{m}}\right\}, & M = 2(\mathrm{BPSK}) \\ \min\left\{\frac{\tau}{2[Q^{-1}(z)]^2}, R_s^{\mathrm{m}}\right\}, & M = 4(\mathrm{QPSK}) \\ \min\left\{\frac{2\tau \sin^2(\pi/M)}{\left[Q^{-1}\left(\frac{z \log_2 M}{2}\right)\right]^2}, R_s^{\mathrm{m}}\right\}, & M = 2^n, n > 2 \end{cases}$$

where $Q(z)$ is the probability that the standard normal random variable is greater than z. The maximum symbol rate R_s^{m} is given by $R_s^{\mathrm{m}} = 1/k_g$, where k_g is the constant that depends on the pulse shape of the analog signal. Without loss of generality, we set $k_g = 1$ (i.e., the raised cosine pulse with roll-off factor of 1). Denote by W the

[2]We could use the Shannon capacity formula but it would not make practical sense since it gives an asymptotic limit of the rate with arbitrarily small probability of error and arbitrarily long block length.

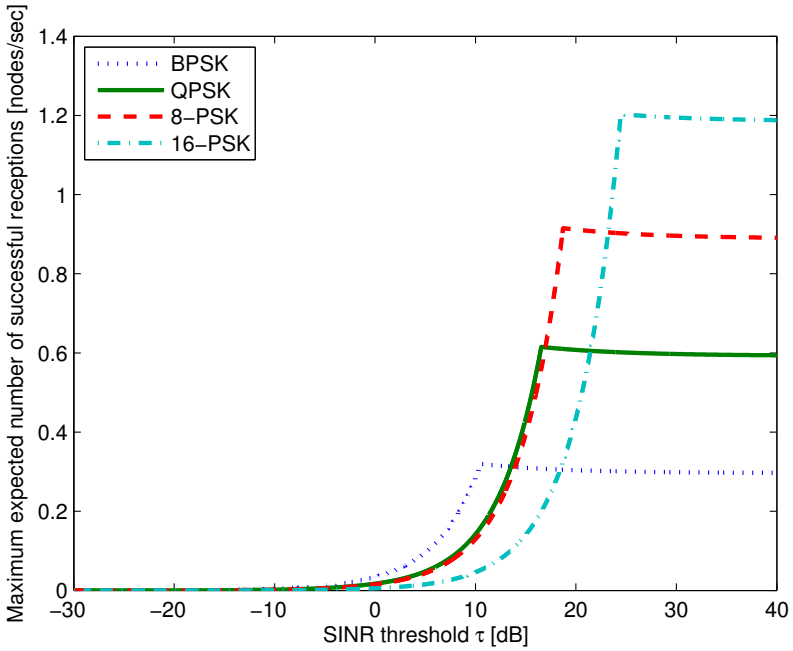

Figure 6.2: The maximum expected number of successful receptions per second under the M-PSK modulation scheme

number of bits to be transmitted in each time slot. Then, the transmission duration is given by $T_{\text{slot}} = \frac{W}{R_s B \log_2 M}$. Consequently, we can redraw the maximum expected number of successful receptions as in Fig. 6.2, where we set $\eta = 4$, $z = 10^{-6}$, $W = 1$ bit, and $B = 1$ Hz, respectively. Note that in the figure, the units were changed from [nodes/slot] to [nodes/sec].

6.4.3 Performance over Multiple Slots

Because as time goes on, the set of discovered neighbors in each time slot will overlap with the previously discovered ones, it is important to know the performance of the discovery algorithm over multiple slots. We start with a simplifying assumption that the set of successful transmitters $\mathbf{I}_t^s$ is independent from slot to slot. This is a hypothetical

scenario because the set $\mathbf{I}_t^s$ is indeed correlated since a node closer to the receiver has a better chance of being discovered in any slots. The scenario where $\mathbf{I}_t^s$ is correlated over slots will also be studied later in this chapter.

Assuming that the set of successful transmitters $\mathbf{I}_t^s$ is independent from slot to slot implies that each neighboring node has equal probability of success. Therefore, for a given number of successful receptions h_t and the total number of neighbors J, the probability that a certain neighboring node belongs to the set $\mathbf{I}_t^s$ is given by h_t/J and, over D multiple slots, the probability is obtained by

$$\Pr\left\{ k \in \bigcup_{t=1}^{D} \mathbf{I}_t^s \;\middle|\; |\mathbf{I}_1^s| = h_1, \ldots, |\mathbf{I}_D^s| = h_D \right\} = 1 - \prod_{t=1}^{D} \left(1 - \frac{h_t}{J}\right) \tag{6.10}$$

We call Eq. (6.10) a slot-basis prediction to distinguish from the Bernoulli approximation which will be given in the sequel.

Note that the event that a particular neighboring node belongs to the set $\mathbf{I}_t^s$ can be approximated by the Bernoulli trial with success probability $E[|\mathbf{I}_t^s|]/J$. Thus, the approximated number of discovering the particular node over D multiple slots is a binomial random variable with success probability $E[|\mathbf{I}_t^s|]/J$ and the total number of trials D. For large D and small $E[|\mathbf{I}_t^s|]/J$, it can be further approximated by the Poisson random variable with parameter $DE[|\mathbf{I}_t^s|]/J$ [96, p. 435]. Hence, the probability that the particular node has been discovered over D multiple slots is approximately $1 - \exp(-DE[|\mathbf{I}_t^s|]/J)$, which is equal to the probability that the Poisson random variable is non-zero. Note that the slot-basis prediction in Eq. (6.10) and the above approximation do not depend on the particular node index because we assumed that $\mathbf{I}_t^s$ is independent from slot to slot. Therefore, it can be viewed as the predicted fraction of neighbors discovered up to time

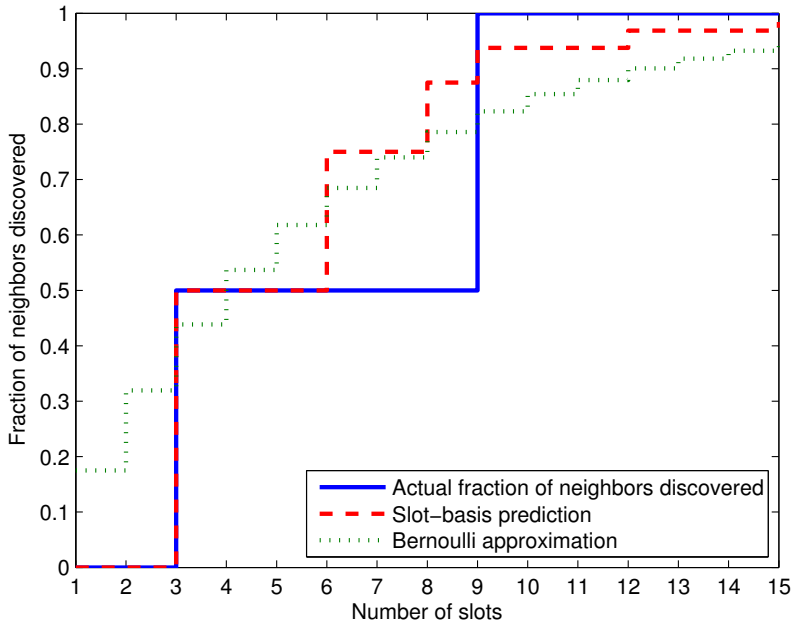

Figure 6.3: The fraction of neighbors discovered by node A for the example transmit/listen pattern in Table 6.1

slot D. In Fig. 6.3, we plot the actual/predicted fraction of neighbors discovered for the example transmit/listen pattern in Table 6.1. For the figure, the SINR threshold τ is set to 1 (in linear scale), and the transmission probability p_{T} is set to 0.4226, which is the optimal value by Eq. (6.9) with path loss exponent $\eta = 4$. Note that this is the optimal transmission probability which maximizes the expected number of successful receptions at that threshold value. Consequently, we obtain the expected number of successful receptions per slot as 0.3849 by Eq. (6.8), and this value was used to plot the Bernoulli approximation.

In practice, the probability that a particular node belongs to the set of successful transmitters $\mathbf{I}_t^s$ depends on the distance between the node and the receiver and, thus, $\mathbf{I}_t^s$ is correlated over time slots. Therefore, we first obtain the conditional probability that a

Table 6.1: An example transmit/listen pattern of three nodes (the letters T and L stand for transmit and listen, respectively.)

Time slot	1	2	3	4	5	6	7	8	9	10	11	12	13	14	15
Node A	T	T	L	L	T	L	T	L	L	T	T	L	T	T	L
Node B	L	L	T	L	T	T	L	T	L	L	L	L	T	T	T
Node C	L	T	T	L	T	L	L	T	T	T	T	T	T	T	L

particular node at the specific distance from the receiver belongs to the set $\mathbf{I}_t^s$ given the total number of successful receptions h_t as (see Chapter Appendix 6.B)

$$\Pr\{\, k \in \mathbf{I}_t^s \mid |\mathbf{I}_t^s| = h_t, r_k = r' \,\} = \frac{\sum_{n=h_t}^{J} \binom{J-1}{n-1} {p_{\mathrm{T}}}^n (1-p_{\mathrm{T}})^{J-n} \zeta_n}{\sum_{n=h_t}^{J} \binom{J}{n} {p_{\mathrm{T}}}^n (1-p_{\mathrm{T}})^{J-n} \left(\frac{n}{J}\left(\zeta_n + \gamma_n - \xi_n\right) + \xi_n\right)} \tag{6.11}$$

where ζ_n, γ_n, and ξ_n are defined as

$$\begin{aligned}
\zeta_n &= \binom{n-1}{h_t-1} f_{1,n} f_{2,n}^{h_t-1} (1-f_{2,n})^{n-h_t} \\
\gamma_n &= \binom{n-1}{h_t} f_{2,n}^{h_t} (1-f_{2,n})^{n-h_t-1} (1-f_{1,n}) \\
\xi_n &= \binom{n}{h_t} f_n^{h_t} (1-f_n)^{n-h_t}
\end{aligned}$$

and $f_{1,n}$ is the probability that a transmitter located at distance r' from the receiver will succeed among $n(\geq 1)$ simultaneous transmissions and $f_{2,n}$ is the probability that a transmitter at an arbitrary distance will succeed among $n(> 1)$ simultaneous transmissions given that one of the other transmitter is located at distance r' from the receiver. The expressions for $f_{1,n}$ and $f_{2,n}$ are given in Chapter Appendix 6.B. The function f_n is the shorthand notation for Eq. (6.6). Using the conditional probability in Eq. (6.11), the probability that a particular node at distance r' has been discovered over multiple slots

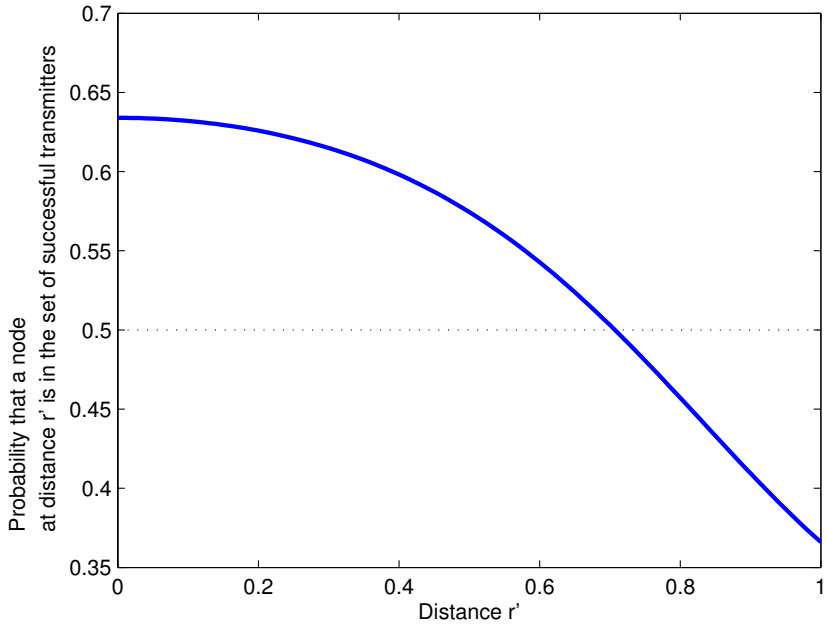

Figure 6.4: The probability that a node at distance r' from the reference node is in the set of successful transmitters for the three node example given the number of successful transmissions $h_t = 1$

can be obtained similarly with Eq. (6.10). To get a better understanding on the conditional probability in Eq. (6.11), let us consider the following example which is in line with the Example 6.4.1.

Example 6.4.2. *Since each node has two neighbors,* $\Pr\{\, k \in \mathbf{I}_t^s \mid |\mathbf{I}_t^s| = 0, r_k = r' \,\} = 0$ *and* $\Pr\{\, k \in \mathbf{I}_t^s \mid |\mathbf{I}_t^s| = 2, r_k = r' \,\} = 1$. *For* $h_t = 1$, *we obtain*

$$\Pr\{\, k \in \mathbf{I}_t^s \mid |\mathbf{I}_t^s| = 1, r_k = r' \,\} = \frac{1 - p_{\mathrm{T}} + p_{\mathrm{T}} \left(1 - r'^2\right)^2}{2(1 - p_{\mathrm{T}}) + \left(\left(1 - r'^2\right)^2 + r'^4\right) p_{\mathrm{T}}}$$

where the discovery range R_0 *in Eq.* (6.1) *is normalized to 1 and the threshold* τ *is set to 1. We plot the result in Fig. 6.4 where all other parameters are set identical with those used for Fig 6.3. Note that even if* $r' = 0$, *the probability is not equal to 1 because of the*

random transmit/listen pattern of a node.

6.5 Detection of the Transmitting Neighbors

6.5.1 Classical Approach Using a Bank of Matched Filters

To decide the existence of a signal from a particular node, we require the use of matched filters in which the outputs of the filters are compared to a certain threshold. Note that such a decision is subject to probabilistic errors such as the *false alarm* and *miss* and, thus, the threshold needs to be chosen in some optimum way. Since the set of transmitting neighbors and their signal amplitudes are all unknown and hard to be tracked, we simplify it by assuming that the sum of interfering signals and the noise act as another noise process $\mathbf{n}'_t = \{n'_{t,1}, ..., n'_{t,L}\}^T$ whose samples are i.i.d. with $\mathcal{N}(0, N')$. The average noise power N' can be computed as

$$N' = N + \sum_{n=1}^{\bar{J}-1} \binom{\bar{J}-1}{n} {p_{\mathrm{T}}}^n (1-p_{\mathrm{T}})^{\bar{J}-1-n} n \bar{P}_{rx} \tag{6.12}$$

where $\bar{J}$ and $\bar{P}_{rx}$ is the average number of neighbors and the received signal power, respectively. Note that this is a reasonable approximation if there is a large number of nodes, and it is commonly applied to the analysis of cellular code division multiple access (CDMA) systems [56].

Based on the above approximation, we formulate the binary hypothesis testing

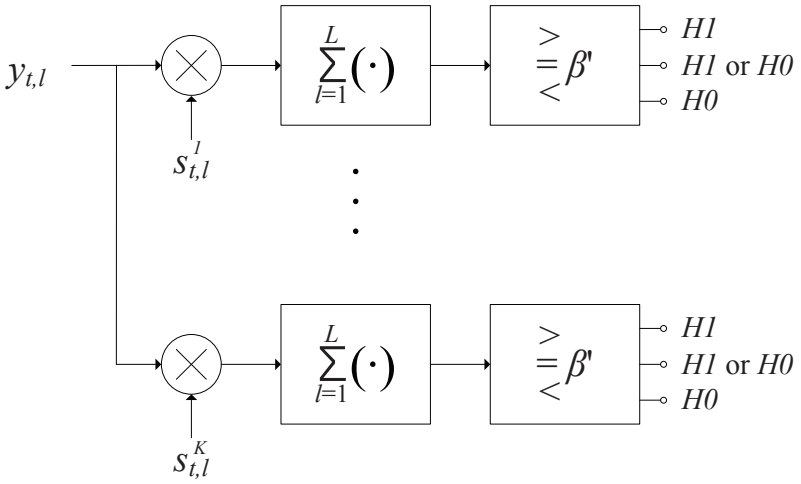

Figure 6.5: Bank of matched filters

problem for the transmission of a particular node k as

$$H_0 : \mathbf{y}_t = \mathbf{n}'_t$$

versus

$$H_1 : \mathbf{y}_t = g_t^k \mathbf{s}_t^k + \mathbf{n}'_t$$

which is a *composite* hypothesis testing because the signal $\mathbf{s}_t^k$ is known but still not its amplitude. For the problem, a *generalized likelihood ratio test* method would provide a simple decision rule as[3] [71, p. 51]

$$\frac{1}{N'} \sum_{l=1}^{L} y_{t,l} s_{t,l}^k \underset{H_0}{\overset{H_1}{\gtrless}} \beta \tag{6.13}$$

This structure is depicted in Fig. 6.5, where $\beta' = \beta N'$. Note that each node transmits with probability p_{T} and listens with probability $1 - p_{\mathrm{T}}$, and they are the *prior* probabilities for each hypothesis.

[3]Note that the decision rule in Eq. (6.13) is optimal for g_t^k near 0 which holds for most of the practical situations.

Given the cost structure C_{ij} which is the cost incurred by choosing hypothesis H_i when hypothesis H_j is true, the optimum threshold for the minimum average cost is given by $\beta = \frac{\pi_0(C_{10}-C_{00})}{\pi_1(C_{01}-C_{11})}$, where π_i is the *prior* probability of hypothesis H_i. Under the *minimum-probability-of-error* criterion where the cost assignment is done by $C_{ij} = 0$ for $i = j$, and $C_{ij} = 1$ for $i \neq j$, the threshold is obtained by $\beta = \pi_0/\pi_1 = (1 - p_{\mathrm{T}})/p_{\mathrm{T}}$.

6.5.2 Random Set Theory-based Approach

The classical approach using a bank of matched filters holds a certain desired property; that is, its complexity does not scale with the number of nodes by averaging out the effect of random interferences. However, the performance would be worse than the class of decorrelator detectors. On the other hand, total number of transmitting neighbors and their entities are all random in our problem setting and, thus, standard decorrelator detectors are not directly applicable because they fundamentally assume a fixed number of transmitters with known entities. This problem naturally falls in the purview of RST which generalizes standard probability theory by assigning *sets*, rather than values, to random outcomes (see Chapter Appendix 6.A and references therein). RST has been applied before in the context of multi-source data fusion and multi-target identification problems [46, 90–94] and, recently, multi-user detection problem in a dynamic environment [95]. The utility of RST mostly comes from the fact that we can readily treat the random behavior of a random number of entities as a single random set having likelihood.

Mathematically, a random set $\mathbf{X}$ is defined as a mapping from a sample space Ω to a power set $\mathcal{P}(\mathbb{S})$ of a hybrid space $\mathbb{S}$. It is referred to as a random *finite* set, if for all

$\omega \in \Omega$, the set is finite (i.e., $|\mathbf{X}(\omega)| < \infty$). The hybrid space $\mathbb{S} \triangleq \mathbb{R}^d \times U$ is the Cartesian product of a d-dimensional Euclidean space $\mathbb{R}^d$ and a finite discrete space U. To illustrate the use of the RST-based method, we focus on the case where the hybrid space $\mathbb{S}$ is given by a finite discrete space as $\mathbb{S} = \{1, ..., K\}$, i.e., the random set $\mathbf{X}_t$ is simply equal to the *unknown* set of transmitting neighbors at that time slot, which was previously denoted by $\mathbf{I}_t$ in Eq. (6.2). Additionally, if the amplitudes of the signals from transmitting neighbors are of interest, we can define it as $\mathbb{S} = \{1, \ldots, K\} \times \mathbb{R}_+$, where $\mathbb{R}_+$ is the non-negative real space. In the following, we estimate the random set $\mathbf{X}_t$ based on the observed signal $\mathbf{y}_t$ in each time slot.

Since the number of transmitting neighbors in each time slot depends on the total number of neighbors, both the random set $\mathbf{X}_t$ and the total number of neighbors J need to be jointly estimated as

$$\arg \max_{(\mathbf{X}'_t, J')} f_{\mathbf{X}_t, J|\mathbf{Y}_t}(\mathbf{X}'_t, J'|\mathbf{y}_t)$$

where $f_{\mathbf{X}_t, J|\mathbf{Y}_t}(\cdot)$ is the likelihood of random set $\mathbf{X}_t$ and J neighbors given the received signal $\mathbf{Y}_t = \mathbf{y}_t$. By Bayes rule, $f_{\mathbf{X}_t, J|\mathbf{Y}_t}(\mathbf{X}'_t, J'|\mathbf{y}_t)$ is proportional to

$$f_{\mathbf{Y}_t|\mathbf{X}_t, J}(\mathbf{y}_t|\mathbf{X}'_t, J')\, f_{\mathbf{X}_t|J}(\mathbf{X}'_t|J') f_J(J')$$

where $f_{\mathbf{Y}_t|\mathbf{X}_t, J}(\cdot)$ is the likelihood of received signal $\mathbf{Y}_t$ given $\mathbf{X}_t = \mathbf{X}'_t$ and $J = J'$, $f_{\mathbf{X}_t|J}(\cdot)$ is the likelihood of random set $\mathbf{X}_t$ given $J = J'$, and $f_J(\cdot)$ is the likelihood of having J neighbors. Consequently, the joint MAP estimator of the random set $\mathbf{X}_t$ and the total number of neighbors J is obtained by

$$\arg \max_{(\mathbf{X}'_t, J')} f_{\mathbf{Y}_t|\mathbf{X}_t, J}(\mathbf{y}_t|\mathbf{X}'_t, J')\, f_{\mathbf{X}_t|J}(\mathbf{X}'_t|J') f_J(J')$$

In order to run the above estimator, it is required to specify the densities $f_{\mathbf{Y}_t|\mathbf{X}_t,J}(\cdot)$, $f_{\mathbf{X}_t|J}(\cdot)$, and $f_J(\cdot)$. We outline how these densities are obtained.

The received signal $\mathbf{y}_t$ not only depends on the set of transmitting neighbors $\mathbf{X}_t$, but also depends on their signal amplitudes $\mathbf{g}_t = \{g_t^k, \forall k \in \mathbf{X}_t\}$. Since the amplitudes are all random, we take average by assuming that the amplitudes of the nodes are independent of each other as

$$f_{\mathbf{Y}_t|\mathbf{X}_t,J}(\mathbf{y}_t|\mathbf{X}_t', J') = \int_0^\infty \cdots \int_0^\infty f_{\mathbf{Y}_t|\mathbf{X}_t,\mathbf{g}_t,J}(\mathbf{y}_t|\mathbf{X}_t', \mathbf{g}_t', J') dF_g(g_1') \cdots dF_g(g_{|\mathbf{X}_t'|}') \tag{6.14}$$

where $f_{\mathbf{Y}_t|\mathbf{X}_t,\mathbf{g}_t,J}(\mathbf{y}_t|\mathbf{X}_t', \mathbf{g}_t', J')$ is the likelihood of received signal $\mathbf{Y}_t$ given $\mathbf{X}_t = \mathbf{X}_t'$, $\mathbf{g}_t = \mathbf{g}_t'$, and $J = J'$. The set $\mathbf{g}_t' = \{g_1', \ldots, g_{|\mathbf{X}_t'|}'\}$ and $F_g(\cdot)$ denote the realization of $\mathbf{g}_t$ and the common cumulative distribution of the received signal amplitude, respectively. Note that by further conditioning the received signal $\mathbf{y}_t$ on the set of transmitting neighbors and their signal amplitudes, the only randomness remaining is in the noise $\mathbf{n}_t$. Therefore, it is given by

$$f_{\mathbf{Y}_t|\mathbf{X}_t,\mathbf{g}_t,J}(\mathbf{y}_t|\mathbf{X}_t', \mathbf{g}_t', J') = \frac{1}{(2\pi N)^{L/2}} \exp\left(-\frac{1}{2N} \sum_{l=0}^{L} \left(y_{t,l} - \sum_{k \in \mathbf{X}_t'} g_{m(k)}' s_{t,l}^k \right)^2 \right)$$

where the bijective function $m(k)$ has been introduced to map the elements in $\mathbf{X}_t'$ to the elements in the set $\{1, \ldots, |\mathbf{X}_t'|\}$. For example, if $\mathbf{X}_t' = \{2, 5\}$, then $m(2) = 1$ and $m(5) = 2$.

In order to obtain $f_{\mathbf{X}_t|J}(\mathbf{X}_t'|J')$, we first obtain the *belief mass* of a random set $\mathbf{X}_t$ for a given number of neighbors $J = J'$ as (see Chapter Appendix 6.A)

$$\beta_{\mathbf{X}_t|J}(\mathbf{C}|J') = \sum_{n=0}^{J'} \sum_{\mathbf{B}:\mathbf{B}\subseteq\mathbf{C},|\mathbf{B}|=n} \Pr\{\mathbf{X}_t = \mathbf{B}|J = J'\}$$

where $\mathbf{C}$ is a closed subset of the space $\mathbb{S}$, and $\mathbf{B}$ is a realization of the random set $\mathbf{X}_t$. Let us first derive $\beta_{\mathbf{X}_t|J}(\mathbf{C}|J')$ for a particular example as follows.

Example 6.5.1. *Set* $\mathbb{S} = \{1, 2, 3\}$, $\mathbf{C} = \mathbb{S}$, *and* $J' = 2$. *1) The set* $\{\mathbf{B} : \mathbf{B} \subseteq \mathbf{C}, |\mathbf{B}| = 0\}$ *is given by* $\{\emptyset\}$ *and, thus,* $\sum_{\mathbf{B}:\mathbf{B}\subseteq\mathbf{C},|\mathbf{B}|=0} \Pr\{\mathbf{X}_t = \mathbf{B}|J = 2\} = (1 - p_{\mathrm{T}})^2$. *2) The set* $\{\mathbf{B} : \mathbf{B} \subseteq \mathbf{C}, |\mathbf{B}| = 1\}$ *is given by* $\{\{1\}, \{2\}, \{3\}\}$ *and, thus,* $\sum_{\mathbf{B}:\mathbf{B}\subseteq\mathbf{C},|\mathbf{B}|=1} \Pr\{\mathbf{X}_t = \mathbf{B}|J = 2\} = 3p_{\mathrm{T}}\,(1 - p_{\mathrm{T}})$. *3) The set* $\{\mathbf{B} : \mathbf{B} \subseteq \mathbf{C}, |\mathbf{B}| = 2\}$ *is given by* $\{\{1, 2\}, \{1, 3\}, \{2, 3\}\}$ *and, thus,* $\sum_{\mathbf{B}:\mathbf{B}\subseteq\mathbf{C},|\mathbf{B}|=2} \Pr\{\mathbf{X}_t = \mathbf{B}|J = 2\} = 3{p_{\mathrm{T}}}^2$. *4) Since* $J' = 2$, *the probability that a random set* $\mathbf{X}_t$ *is equal to* $\mathbf{B}$ *for* $|\mathbf{B}| > 2$ *is zero. Summing over all possible* $\mathbf{B}$*'s yields* $\beta_{\mathbf{X}_t|J}(\mathbf{C}|J') = \sum_{n=0}^{2} \binom{3}{n} {p_{\mathrm{T}}}^n\,(1 - p_{\mathrm{T}})^{2-n}$.

For general cases, we have

$$\beta_{\mathbf{X}_t|J}(\mathbf{C}|J') = \sum_{n=0}^{J'} \binom{|\mathbf{C}|}{n} {p_{\mathrm{T}}}^n\,(1 - p_{\mathrm{T}})^{J'-n}$$

The *belief density* $f_{\mathbf{X}_t|J}(\mathbf{X}'_t|J')$ is obtained by taking the *set derivative* of the *belief mass* obtained above. For the case where the hybrid space $\mathbb{S}$ is comprised only of the discrete space, it can be readily obtained through the following Möbius inversion formula as (see Chapter Appendix 6.A)

$$f_{\mathbf{X}_t|J}(\mathbf{X}'_t|J') = \sum_{\mathbf{C}\subseteq\mathbf{X}'_t} (-1)^{|\mathbf{X}'_t\setminus\mathbf{C}|}\beta_{\mathbf{X}_t|J}(\mathbf{C}|J')$$

Example 6.5.2. *Take* $\mathbf{X}'_t = \{1, 3\}$ *and* $J' = 2$, *then the set* $\{\mathbf{C} : \mathbf{C} \subseteq \mathbf{X}'_t\}$ *is given by* $\{\emptyset, \{1\}, \{3\}, \{1, 3\}\}$. *1) For* $\mathbf{C} = \emptyset$, $\beta_{\mathbf{X}_t|J}(\mathbf{C}|J') = (1 - p_{\mathrm{T}})^2$. *2) For* $\mathbf{C} = \{1\}$, $\beta_{\mathbf{X}_t|J}(\mathbf{C}|J') = (1 - p_{\mathrm{T}})^2 + p_{\mathrm{T}}\,(1 - p_{\mathrm{T}})$. *3) For* $\mathbf{C} = \{3\}$, $\beta_{\mathbf{X}_t|J}(\mathbf{C}|J') = (1 - p_{\mathrm{T}})^2 + p_{\mathrm{T}}\,(1 - p_{\mathrm{T}})$. *4) For* $\mathbf{C} = \{1, 3\}$, $\beta_{\mathbf{X}_t|J}(\mathbf{C}|J') = (1 - p_{\mathrm{T}})^2 + 2p_{\mathrm{T}}\,(1 - p_{\mathrm{T}}) + {p_{\mathrm{T}}}^2$. *Summing over all the possible* $\mathbf{C}$*'s by considering the sign of the terms yields* $f_{\mathbf{X}_t|J}(\mathbf{X}'_t|J') = {p_{\mathrm{T}}}^2$.

Similarly, for general cases, we have

$$f_{\mathbf{X}_t|J}(\mathbf{X}'_t|J') = \begin{cases} {p_{\mathrm{T}}}^{|\mathbf{X}'_t|}\left(1-p_{\mathrm{T}}\right)^{J'-|\mathbf{X}'_t|}, & \text{for } |\mathbf{X}'_t| \leq J' \\ 0, & \text{otherwise} \end{cases}$$

Note that the scenario in which $\mathbf{X}_t$ contains only the identity of the transmitters is the simplest case that can be solved by standard probability theory as well. The usefulness of RST comes when we extend the set $\mathbf{X}_t$ so that additional parameters, such as signal amplitudes, can be estimated at the same time.

The density $f_J(J')$ is the probability that there are J' number of neighbors. By defining the discovery region as the circle of radius R_0, from Chapter 6.2, the number of nodes inside the discovery region follows a Poisson random variable with parameter $\lambda\pi{R_0}^2$. Notice that there is no definite way of choosing R_0 because the decisions on whether a particular node is my neighbor are inconclusive due to the continuity of signal strength together with the random effect of noise and fading. However, as will be shown in the numerical example, the estimator gives more weights to an appropriate size of the set which is likely to be occurred at that size of discovery region.

6.6 Numerical Results

Here, we focus on the comparison of the physical layer signal processing methods for the detection of transmitting neighbors. For the simulation, a total of 8 wireless sensor nodes are uniformly deployed over the region of interest which is modeled as a circle of radius R which is set to 1 km as shown in Fig. 6.6. The reference node denoted by index 0 is assumed to be located at the center of the circle. For the wireless channel, we consider

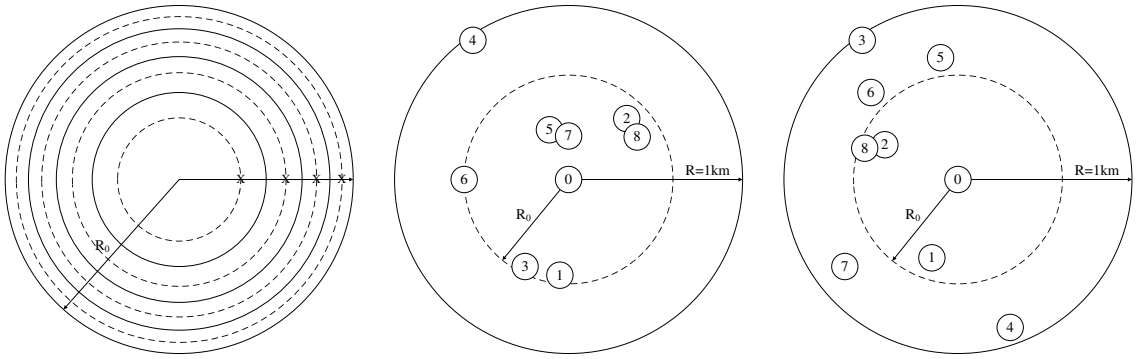

(a) Discretization of the distance (b) Deployment scenario 1 (c) Deployment scenario 2

Figure 6.6: Discretization of the distance for fast computation of Eq. (6.14) and example deployment scenarios

a simple path loss model which only depends on the transmitter-receiver distance, and the path loss exponent η is set to 4. The transmission power G is set to -24 dBm[4], and the noise spectral density N_0 is set to -173 dBm/Hz as commonly done. The effect of fading was intentionally ignored to clearly reveal the effect of the distance between nodes in detection outcomes. The bandwidth B is set to 100 Hz (which is artificially low but really irrelevant for our purposes here). The transmission probability p_{T} is set to 0.5 (to better observe the effect of the multiple access). For the signatures of the nodes, we used length 15 maximal-length sequences [98]. Gold and Kasami sequences which have better correlation property can be used, but comparing the performance of different codes is beyond the scope of this work.

Note that the computation of $f_{\mathbf{Y}_t|\mathbf{X}_t,J}(\cdot)$ in Eq. (6.14) is tedious because of the multiple integrals. Hence, we transform the integrals to a finite summation by discretizing the distance. To do this, we first divide the discovery region of the reference node into a finite

[4]For example, the transmission power of the MICAz Mote, a commercial wireless sensor node by Crossbow Technology, Inc., is programmable in 8 steps from -24 to 0 dBm [97].

number of strips having the same area and, after that, each strip is further divided into two having the same area as shown in Fig. 6.6(a). By doing so, the probability that a node is on either one of those radii becomes uniform. For the numerical examples, we used 7 discrete points and, obviously, the accuracy will improve as the number of points increases. Also note that, since a total of 8 nodes are uniformly deployed over the specified region of interest, the density $f_J(\cdot)$ on the number of nodes inside the discovery region of radius R_0 can be more accurately described by the binomial distribution $B(8, \frac{{R_0}^2}{R^2})$, rather than the Poisson approximation. For the classical approach, it is computed by $\beta' = \beta N'$ where $\beta = (1-p_{\rm T})/p_{\rm T} = 1$ and $N' = N_0 B + 3.5\bar{P}_{rx}$ by Eq. (6.12) with $\bar{P}_{rx} = 3.3333 \times 10^{-7} G$ using the cumulative distribution function of the received signal power in Eq. (6.3) without fading.

Table 6.2 and 6.3 show the detection results for deployment scenario 1 and 2 in Fig. 6.6(b)-(c), respectively. Note that the objective of the neighbor discovery is to identify the *correct set of neighbors* which is difficult to be measured with a single parameter, and it is the reason why we simply listed the detection outcomes as shown in the tables. The letters H, C, F, and M stand for *hit*, *correct rejection*, *false alarm*, and *miss*, respectively. Note that F and M are the erroneous detections. From Table 6.2, it can be seen that a total of 1 *miss* and 3 *false alarms* are induced under the RST-based approach with $R_0 = 1$ km (which is the entire region of interest), and 2 *misses* and 1 *false alarm* are occurred with $R_0 = 0.5$ km. Under the classical approach, however, a total of 6 *misses* and 10 *false alarms* occur, which is 4 times more than the RST-based approach with $R_0 = 1$ km and 5.3 times more than that with $R_0 = 0.5$ km.

From Table 6.3, we can see that a total of 2 *misses* and 4 *false alarms* are induced

Table 6.2: Detection results for deployment scenario 1 in Fig. 6.6(b) (the letters H, C, F, and M stand for *hit*, *correct rejection*, *false alarm*, and *miss*, respectively.)

(a) RST-based approach ($R_0 = 1$ km)

Time slot	1	2	3	4	5	6	7	8	9	10	11	12	13	14	15	16	17	18	19	20
Node 1	C	H	C	C	C	C	H	C	H	C	H	C	H	C	C	H	H	C	C	H
Node 2	H	H	H	H	H	C	C	C	H	C	C	H	C	C	C	C	H	H	C	H
Node 3	H	H	C	C	C	C	C	H	H	F	H	H	H	H	C	C	C	C	C	C
Node 4	C	C	C	F	H	C	H	H	C	C	C	C	H	C	C	H	M	C	C	H
Node 5	H	C	H	H	H	C	C	C	C	C	C	H	C	C	H	C	C	H	C	H
Node 6	H	C	C	H	H	C	C	C	H	C	C	C	H	H	C	H	H	H	H	C
Node 7	H	H	C	C	H	C	H	C	C	C	H	C	H	F	C	C	H	H	H	C
Node 8	C	H	H	H	H	H	H	H	C	C	H	H	H	C	H	C	H	H	H	H

(b) RST-based approach ($R_0 = 0.5$ km)

Time slot	1	2	3	4	5	6	7	8	9	10	11	12	13	14	15	16	17	18	19	20
Node 1	C	H	C	C	C	C	H	C	H	C	H	C	H	C	C	H	H	C	C	H
Node 2	H	H	H	H	H	C	C	C	H	C	C	H	C	C	C	C	H	H	C	H
Node 3	H	H	C	C	C	C	C	H	H	F	H	H	H	H	C	C	C	C	C	C
Node 4	C	C	C	C	M	C	H	H	C	C	C	C	H	C	C	H	M	C	C	H
Node 5	H	C	H	H	H	C	C	C	C	C	C	H	C	C	H	C	C	H	C	H
Node 6	H	C	C	H	H	C	C	C	H	C	C	C	H	H	C	H	H	H	H	C
Node 7	H	H	C	C	H	C	H	C	C	C	H	C	H	C	C	C	H	H	H	C
Node 8	C	H	H	H	H	H	H	H	C	C	H	H	H	C	H	C	H	H	H	H

(c) Classical approach using a bank of matched filters

Time slot	1	2	3	4	5	6	7	8	9	10	11	12	13	14	15	16	17	18	19	20
Node 1	C	H	C	C	C	F	H	C	H	F	H	C	H	C	C	H	H	C	C	H
Node 2	H	H	H	H	H	C	C	C	H	F	C	H	C	C	C	C	H	H	C	H
Node 3	H	H	C	C	C	C	C	H	H	F	H	H	H	H	C	C	C	C	C	C
Node 4	C	C	C	C	M	C	H	H	C	F	C	C	M	C	C	H	M	C	C	M
Node 5	H	C	H	H	H	C	C	C	C	C	C	H	C	C	H	C	C	H	C	H
Node 6	M	C	C	H	M	C	C	F	H	F	C	C	H	H	C	H	H	H	H	C
Node 7	H	H	C	C	H	C	H	C	C	F	H	C	H	F	C	C	H	H	H	C
Node 8	C	H	H	H	H	H	H	H	C	C	H	H	H	F	H	C	H	H	H	H

Table 6.3: Detection results for deployment scenario 2 in Fig. 6.6(c)

(a) RST-based approach ($R_0 = 1$ km)

Time slot	1	2	3	4	5	6	7	8	9	10	11	12	13	14	15	16	17	18	19	20
Node 1	C	C	C	C	C	C	H	C	H	H	C	H	H	C	H	H	H	H	C	H
Node 2	H	C	H	H	C	**F**	C	H	C	C	H	C	C	**F**	H	C	C	H	C	C
Node 3	H	C	H	H	H	H	H	**M**	C	C	C	C	H	H	C	C	H	C	C	C
Node 4	H	C	H	H	H	H	C	C	H	H	C	**M**	C	C	H	H	C	C	C	H
Node 5	H	C	C	H	H	H	**F**	H	H	C	H	H	C	H	C	C	H	C	H	H
Node 6	H	C	C	H	C	H	H	H	H	H	H	H	H	C	C	**F**	C	H	C	C
Node 7	C	H	C	H	H	C	C	C	H	H	H	C	C	C	H	H	H	C	C	C
Node 8	H	C	H	C	C	H	C	H	C	C	H	H	H	C	H	H	H	H	H	H

(b) RST-based approach ($R_0 = 0.5$ km)

Time slot	1	2	3	4	5	6	7	8	9	10	11	12	13	14	15	16	17	18	19	20
Node 1	C	C	C	C	C	C	H	C	H	H	C	H	H	C	H	H	H	H	C	H
Node 2	H	C	H	H	C	C	C	H	C	C	H	C	C	C	H	C	C	H	C	C
Node 3	H	C	H	**M**	**M**	H	H	**M**	C	C	C	C	H	H	C	C	**M**	C	C	C
Node 4	H	C	H	**M**	**M**	**M**	C	C	H	H	C	**M**	C	C	H	**M**	C	C	C	H
Node 5	H	C	C	H	H	H	**F**	H	H	C	H	H	C	H	C	C	H	C	H	H
Node 6	H	C	C	H	C	H	H	H	H	H	H	H	H	C	C	C	C	H	C	C
Node 7	C	H	C	H	H	C	C	C	H	H	H	C	C	C	H	H	H	C	C	C
Node 8	H	C	H	C	C	H	C	H	C	C	H	H	H	C	H	H	H	H	H	H

(c) Classical approach using a bank of matched filters

Time slot	1	2	3	4	5	6	7	8	9	10	11	12	13	14	15	16	17	18	19	20
Node 1	C	C	C	C	C	C	H	C	H	H	C	H	H	C	H	H	H	H	C	H
Node 2	H	C	H	H	C	**F**	C	H	C	C	H	C	C	**F**	H	C	C	H	C	C
Node 3	H	C	H	H	H	H	H	**M**	C	C	C	C	H	H	C	C	H	C	C	C
Node 4	H	C	H	H	H	H	C	C	H	H	C	**M**	C	C	H	H	C	C	C	H
Node 5	H	C	C	H	H	H	**F**	H	H	C	H	H	C	H	C	C	H	C	H	H
Node 6	H	**F**	C	H	C	H	H	H	H	H	H	H	H	C	C	**F**	C	H	C	C
Node 7	C	H	C	H	H	C	C	C	H	H	H	C	C	**F**	H	H	H	C	C	C
Node 8	H	**F**	H	C	C	H	C	H	C	C	H	H	H	C	H	H	H	H	H	H

under the RST-based approach with $R_0 = 1$ km, and 9 *misses* and 1 *false alarm* are occurred with $R_0 = 0.5$ km. Overall, by reducing the discovery range R_0, the occurrence of *false alarm* is reduced, whereas that of *miss* is increased. Note, however, that most of the *misses* are due to the nodes outside the discovery region (i.e., node 3 and 4). In fact, the detection of the nodes inside the discovery region is more accurate than before. These are because the density $f_J(\cdot)$ gives more weight to the smaller size of the set $\mathbf{X}_t$ during the decision process. Also, it should be mentioned that the nodes outside the discovery region can be detected in a particular reception since there is no absolute and deterministic boundary for a node detection. On the other hand, under the classical approach, a total of 2 *misses* and 7 *false alarms* occur, which is 1.5 times more than the RST-based approach with $R_0 = 1$ km and is tantamount to that with $R_0 = 0.5$ km. Note again that most of the errors under the RST-based approach, specifically the *misses*, come from detecting the nodes outside the discovery region which is actually a *preferred* error.

6.7 Chapter Summary

In this work, we studied the problem of neighbor discovery in a wireless sensor network. By incorporating physical layer parameters, we enabled a more accurate and realistic performance assessment of the chosen neighbor discovery algorithm. Unlike the collision channel, such incorporation required us to explicitly specify the set of transmitting neighbors in each time slot based on the received signal. With the aid of the theory of random set, we were able to present an alternative method to the classical approach using a bank of matched filters for detecting the set of transmitting neighbors. The performance

gain of using this new method comes in an additional cost of complexity. Several steps are still needed to complete our work. To fully validate the advantages of the alternative method, the performance evaluation needs to be supplemented with additional simulations. Also, it should be noted that we focused on discovering unidirectional links as in most of the previous work. However, for routing and other important functions of a network, bidirectional links simplify the network operation. Therefore, it is of interest to develop a self-organizing protocol which establishes bidirectional links in a distributed manner.

Chapter Appendix 6.A – Fundamentals of the Theory of Random Set

Random set theory (RST) and its associated finite-set statistics (FISST) are extensively studied in the book *Mathematics of Data Fusion* [46]. This appendix briefly introduces the essentials of RST, and refer to [46] and other companion publications [90–94] for more details. In RST, the *belief mass* of a random finite set $\mathbf{X}$ plays a similar role to that of the cumulative distribution function of a random variable, and is defined as

$$\beta_{\mathbf{X}}(\mathbf{C}) \triangleq \Pr\{\mathbf{X} \subseteq \mathbf{C}\} \tag{6.15}$$

where $\mathbf{C}$ is a closed subset of the space $\mathbb{S}$. For example [92], if $\mathbf{X} = \{\mathbf{x}\}$, i.e., a singleton, where $\mathbf{x}$ is a random vector, $\beta_{\mathbf{X}}(\mathbf{C}) = \Pr\{\mathbf{X} \subseteq \mathbf{C}\} = \Pr\{\mathbf{x} \in \mathbf{C}\}$ where $\Pr\{\mathbf{x} \in \mathbf{C}\}$ is the probability measure on $\mathbb{S}$. From this, it can be conjectured that the belief mass generalizes the ordinary probability measure. It is straightforward to write the belief

mass in Eq. (6.15) as

$$\beta_{\mathbf{X}}(\mathbf{C}) = \sum_{\mathbf{B}\subseteq\mathbf{C}} \Pr\{\mathbf{X} = \mathbf{B}\} = \sum_{\mathbf{B}\subseteq\mathbf{C}} f_{\mathbf{X}}(\mathbf{B}) \tag{6.16}$$

where $f_{\mathbf{X}}(\cdot)$ is the *belief density* of a random set $\mathbf{X}$, and it plays the role of a probability density function. One natural question is how to derive $f_{\mathbf{X}}(\cdot)$ from $\beta_{\mathbf{X}}(\cdot)$ which will be answered in the sequel.

Consider the case where the hybrid space $\mathbb{S}$ is comprised only of a finite discrete space U. Then, the belief density $f_{\mathbf{X}}(\cdot)$ of a random finite set $\mathbf{X}$ can be obtained via the Möbius inverse transform of $\beta_{\mathbf{X}}(\cdot)$ as

$$f_{\mathbf{X}}(\mathbf{B}) = \sum_{\mathbf{C}\subseteq\mathbf{B}} (-1)^{|\mathbf{B}\setminus\mathbf{C}|} \beta_{\mathbf{X}}(\mathbf{C}) \tag{6.17}$$

by viewing sets as points in another space.

Example 6.7.1. *Take* $\mathbb{S} = U = \{a, b\}$. *Then,* $\mathcal{P}(\mathbb{S}) = \{\emptyset, \{a\}, \{b\}, \{a, b\}\}$. *Assign probability to each element of the power set so that the sum is equal to 1:*

$$f_{\mathbf{X}}(\emptyset) = 0.1, f_{\mathbf{X}}(\{a\}) = 0.4, f_{\mathbf{X}}(\{b\}) = 0.3, f_{\mathbf{X}}(\{a, b\}) = 0.2$$

Then, we can obtain the values of the belief mass using Eq. (6.16). For example, $\beta_{\mathbf{X}}(\{b\}) = f_{\mathbf{X}}(\emptyset) + f_{\mathbf{X}}(\{b\}) = 0.4$. *Likewise, we have*

$$\beta_{\mathbf{X}}(\emptyset) = 0.1, \beta_{\mathbf{X}}(\{a\}) = 0.5, \beta_{\mathbf{X}}(\{a, b\}) = 1$$

We can also retrieve the values of the belief density from the belief mass using Eq. (6.17). For example, $f_{\mathbf{X}}(\{b\}) = -\beta_{\mathbf{X}}(\emptyset) + \beta_{\mathbf{X}}(\{b\}) = 0.3$.

For a general case where $\mathbb{S} \triangleq \mathbb{R}^d \times U$ with $d > 0$, the Möbius inverse transform is not applicable because it applies only for a finite partially ordered set [46]. The continuous

analog of the Möbius inverse transform, which is often called the *set derivative*, at $\mathbf{Z} = \{\mathbf{z}_1, \ldots, \mathbf{z}_n\}$ with $\mathbf{z}_1 \neq \cdots \neq \mathbf{z}_n$, is defined by [93]

$$\frac{\delta F(\mathbf{C})}{\delta \mathbf{Z}} \triangleq \frac{\delta^n F}{\delta \mathbf{z}_n \cdots \delta \mathbf{z}_1}(\mathbf{C}) \triangleq \frac{\delta}{\delta \mathbf{z}_n} \frac{\delta^{n-1} F}{\delta \mathbf{z}_{n-1} \cdots \delta \mathbf{z}_1}(\mathbf{C})$$

where

$$\frac{\delta F(\mathbf{C})}{\delta \mathbf{z}_i} \triangleq \lim_{\nu(E_{\mathbf{z}_i}) \to 0} \frac{F(\mathbf{C} \cup E_{\mathbf{z}_i}) - F(\mathbf{C})}{\nu(E_{\mathbf{z}_i})}$$

where $E_{\mathbf{z}_i}$ is a small neighborhood of $\mathbf{z}_i$ and $\nu(\cdot)$ is the hyper-volume (i.e., Lebesgue measure) of a given set, and $\frac{\delta F(\mathbf{C})}{\delta \emptyset} \triangleq F(\mathbf{C})$.

Chapter Appendix 6.B – Derivation of Eq. (6.11)

The details in deriving Eq. (6.11) is delivered in this appendix. By applying Bayes rule to the conditional probability, we have

$$\Pr\{\, k \in \mathbf{I}_t^s \mid |\mathbf{I}_t^s| = h_t, r_k = r' \,\} = \frac{\Pr\{k \in \mathbf{I}_t^s, |\mathbf{I}_t^s| = h_t, r_k = r'\}}{\Pr\{|\mathbf{I}_t^s| = h_t, r_k = r'\}}$$

whose numerator and denominator are specified one by one in the following. Conditioning the numerator on the number of transmitters and applying Bayes rule once again yields

$$\Pr\{k \in \mathbf{I}_t^s, |\mathbf{I}_t^s| = h_t, r_k = r'\} = \sum_{n=h_t}^{J} \Pr\{|\mathbf{I}_t^s| = h_t | k \in \mathbf{I}_t^s, r_k = r', |\mathbf{I}_t| = n\}$$
$$\times \Pr\{k \in \mathbf{I}_t^s, r_k = r', |\mathbf{I}_t| = n\}$$

Define $f_{1,n}$ as the probability that a transmitter located at distance r' from the receiver will succeed among $n(\geq 1)$ simultaneous transmissions and it is given by

$$f_{1,n} = 1 - \int_0^\infty \cdots \int_0^\infty F_P\left(\tau \sum_{i=2}^{n} x_i \middle| r'\right) dF_P(x_2) \cdots dF_P(x_n)$$

Also, define $f_{2,n}$ as the probability that a transmitter at an arbitrary distance will succeed among $n(>1)$ simultaneous transmissions given that one of the other transmitters is known to be located at distance r' from the receiver which is obtained by

$$f_{2,n} = 1 - \int_0^\infty \cdots \int_0^\infty F_P\left(\tau \sum_{i=2}^{n} x_i\right) dF_P(x_2|r') dF_P(x_3) \cdots dF_P(x_n)$$

and $f_{2,1} = 0$. Using these probabilities, we can compute the numerator as

$$\Pr\{k \in \mathbf{I}_t^s, |\mathbf{I}_t^s| = h_t, r_k = r'\} = \sum_{n=h_t}^{J} \binom{n-1}{h_t-1} f_{2,n}^{h_t-1}(1-f_{2,n})^{n-h_t} \times \binom{J-1}{n-1} p_{\mathrm{T}}^n (1-p_{\mathrm{T}})^{J-n} f_{1,n} f_r(r')$$

Similarly, the denominator can be expanded as

$$\Pr\{|\mathbf{I}_t^s| = h_t, r_k = r'\} = \sum_{n=h_t}^{J} \Pr\{|\mathbf{I}_t^s| = h_t | r_k = r', |\mathbf{I}_t| = n\} \cdot \Pr\{r_k = r', |\mathbf{I}_t| = n\} \tag{6.18}$$

Denote by $\mathcal{J}_n$ the set of elements in the power set $\mathcal{P}(\mathcal{J})$ whose cardinality is equal to n, and $\mathcal{J}_n^k (\subseteq \mathcal{J}_n)$ the set of elements containing a specific node index k. For example, if $\mathcal{J} = \{1,2,3\}$, then $\mathcal{P}(\mathcal{J}) = \{\emptyset, \{1\}, \{2\}, \{3\}, \{1,2\}, \{1,3\}, \{2,3\}, \{1,2,3\}\}$, $\mathcal{J}_2 = \{\{1,2\}, \{1,3\}, \{2,3\}\}$, and $\mathcal{J}_2^1 = \{\{1,2\}, \{1,3\}\}$. Using these notations, the first probability in the summation of Eq. (6.18) can be split into

$$\begin{aligned}\Pr\{|\mathbf{I}_t^s| = h_t | r_k = r', |\mathbf{I}_t| = n\} = &\sum_{\mathcal{S} \in \mathcal{J}_n^k} \Pr\{k \in \mathbf{I}_t^s, |\mathbf{I}_t^s| = h_t, \mathbf{I}_t = \mathcal{S} | r_k = r', |\mathbf{I}_t| = n\} \\ &+ \sum_{\mathcal{S} \in \mathcal{J}_n^k} \Pr\{k \notin \mathbf{I}_t^s, |\mathbf{I}_t^s| = h_t, \mathbf{I}_t = \mathcal{S} | r_k = r', |\mathbf{I}_t| = n\} \\ &+ \sum_{\mathcal{S} \in \mathcal{J}_n \setminus \mathcal{J}_n^k} \Pr\{|\mathbf{I}_t^s| = h_t, \mathbf{I}_t = \mathcal{S} | r_k = r', |\mathbf{I}_t| = n\} \end{aligned} \tag{6.19}$$

Since nodes are randomly transmitting with equal probability, each realization of the set of transmitters having same cardinality are equiprobable, i.e., $\Pr\{\, \mathbf{I}_t = \mathcal{S} \mid |\mathbf{I}_t| = n \,\} = 1/\binom{J}{n}$, for all $\mathcal{S} \in \mathcal{J}_n$, and the set of transmitters $\mathbf{I}_t$ itself is independent over time slots (but the set of successful transmitters $\mathbf{I}_t^s$ is not). Therefore, the probability in the first summation of Eq. (6.19) is computed as

$$\Pr\{k \in \mathbf{I}_t^s, |\mathbf{I}_t^s| = h_t, \mathbf{I}_t = \mathcal{S} | r_k = r', |\mathbf{I}_t| = n\} = \binom{n-1}{h_t-1} f_{2,n}^{h_t-1}(1-f_{2,n})^{n-h_t} f_{1,n} \frac{1}{\binom{J}{n}}$$

for all $\mathcal{S} \in \mathcal{J}_n^k$. Likewise, we can specify the remaining probabilities in Eq. (6.19). By noting that $|\mathcal{J}_n| = \binom{J}{n}$ and $|\mathcal{J}_n^k| = \binom{J-1}{n-1}$ and after some manipulation, Eq. (6.19) becomes

$$\begin{aligned}\Pr\{|\mathbf{I}_t^s| = h_t | r_k = r', |\mathbf{I}_t| = n\} &= \frac{n}{J}\binom{n-1}{h_t-1} f_{2,n}^{h_t-1}(1-f_{2,n})^{n-h_t} f_{1,n} \\ &+ \frac{n}{J}\binom{n-1}{h_t} f_{2,n}^{h_t}(1-f_{2,n})^{n-h_t-1}(1-f_{1,n}) + \left(1-\frac{n}{J}\right)\binom{n}{h_t} f_n^{h_t}(1-f_n)^{n-h_t} \quad (6.20)\end{aligned}$$

where f_n is the shorthand notation for Eq. (6.6). The second probability in Eq. (6.18) is simply

$$\Pr\{r_k = r', |\mathbf{I}_t| = n\} = \binom{J}{n} {p_{\mathrm{T}}}^n (1-p_{\mathrm{T}})^{J-n} f_r(r') \quad (6.21)$$

By substituting Eqs. (6.20) and (6.21) into Eq. (6.18), the denominator becomes

$$\Pr\{|\mathbf{I}_t^s| = h_t, r_k = r'\} = \sum_{n=h_t}^{J} \left(\frac{n}{J}(\zeta_n + \gamma_n - \xi_n) + \xi_n\right) \binom{J}{n} {p_{\mathrm{T}}}^n (1-p_{\mathrm{T}})^{J-n} f_r(r')$$

where the shorthand notations ζ_n, γ_n and ξ_n are defined in Chapter 6.4.3.

Chapter 7

Conclusion

7.1 Summary of Contributions

In the first part of this dissertation, we studied the stability property of cognitive radio systems. Interestingly, we showed that even with non-zero sensing error rates, there exists a condition for which we can achieve the identical stability region that is achieved with perfect sensing. This is remarkable because the spectrum sensing itself becomes unnecessary in terms of the achieved stability region. The problem on how to control the operating point of sensing device over its receiver operating characteristics was also discussed. We next studied the hybrid access for cognitive radio systems with time-varying connectivity and showed that the hybrid access policy does not always outperform the interweave-only mode, and the condition for which there is a gain from using the hybrid access policy was specified.

In the second part of this dissertation, we studied the stability property of random access systems. Specifically, the effect of limited, but renewable, energy availability due to harvesting on the stability region was precisely analyzed. The effect of finite capacity batteries was studied. We then considered the channel-aware random access, in which each node adapts its transmission probability based on the local channel state information which is erroneous. It was shown that the stability region of the channel-aware random access is not necessarily a proper subset of that of the centralized optimal policy, specifi-

cally, as the multipacket reception capability improves.

In the third part of this dissertation, we studied the performance of backpressure-based stochastic control for wireless multi-hop networks with time-correlated arrivals using the Lyapunov drift technique. It was shown that the original backpressure policy is still throughput-optimal even with time-correlated arrivals but with increased average network delay. The case when the arrival rate vector is possibly outside the stability region was also studied and the performance of the joint flow control and backpressure policy was derived in terms of the average network delay and the achieved network utility for the case with time-correlated arrivals.

In the last part of this dissertation, we studied the problem of neighbor discovery in a wireless sensor network. By incorporating physical layer parameters, we provided more accurate and realistic performance assessment of the chosen neighbor discovery algorithm. For the actual detection of the set of transmitting neighbors in each time slot, we applied the theory of random set and showed its superiority over the classical approach using a bank of matched filters. The performance gain of using this new method, however, comes in an additional cost of computational complexity.

7.2 Additional Contributions and Collaborations

7.2.1 Cognitive Radio with a Rechargeable Primary Source

In [99] and its conference version [60], we considered two source-destination pairs and applied the concept of cognitive radio in sharing the shared medium. The high-priority communication pair is assumed to harvest energy from the environment as in

Chapter 4.2, whereas the low-priority communication pair is plugged to a reliable power supply and, thus, free from the energy availability constraint. For the considered model, we obtained the two-dimensional stability region separately for both cases when the capacity of the battery is infinite and finite.

7.2.2 Wireless Network-Level Partial Relay Cooperation

Cooperative communication helps overcome fading and attenuation in wireless networks. Its main purpose is to increase the communication rates across the network and to increase reliability of time-varying links. It is known that wireless communication from a source to a destination can benefit from the cooperation of a node that overhear the transmission. The classical single relay channel [100] exemplifies this situation. On the other hand, it was shown that additional gains can be achieved with *network-layer* cooperation (or packet-level cooperation), that is plain relaying without any physical layer considerations [101, 102]. In [63], we introduced the notion of partial network-level cooperation by adding a flow controller for the traffic from source to relay and showed that the system with the flow controller always performs better than or at least equal to the system without the flow controller by optimally choosing the traffic admission rate.

Bibliography

[1] FCC. Spectrum policy task force. *Technical Report*, Nov. 2002.

[2] Simon Haykin. Cognitive radio: Brain-empowered wireless communications. *IEEE Journal on Selected Areas in Communications*, 23:201–220, Feb. 2005.

[3] Simon Haykin, D. J. Thomson, and J. H. Reed. Spectrum sensing for cognitive radio. *Proceedings of the IEEE*, 97(5):849–877, May 2009.

[4] Q. Zhao and B. M. Sadler. A survey of dynamic spectrum access. *IEEE Signal Processing Magazine*, 24(3):79–89, May 2007.

[5] J. A. Paradiso and T. Starner. Energy scavenging for mobile and wireless electronics. *IEEE Pervasive Computing*, 4(1):18–27, Jan.-Mar. 2005.

[6] S. Chalasani and J. M. Conrad. A survey of energy harvesting sources for embedded systems. In *Proceedings of IEEE Southeastcon*, Apr. 2008.

[7] Scott Meninger, Jose Oscar Mur-Miranda, Rajeevan Amirtharajah, Anantha P. Chandrakasan, and Jeffrey H. Lang. Vibration-to-electric energy conversion. *IEEE Transactions On Very Large Scale Integration (VLSI) Systems*, 9:64–76, Feb. 2001.

[8] R. Knopp and P. Humblet. Information capacity and power control in single-cell multiuser communications. In *Proceedings of IEEE ICC*, Jun. 1995.

[9] Mung Chiang. Balancing transport and physical layers in wireless multihop networks: Jointly optimal congestion control and power control. *IEEE Journal on Selected Areas in Communications*, 23(1):104–116, Jan. 2005.

[10] I. F. Akyildiz, W. Su, Y. Sankarasubramaniam, and E. Cayirci. A survey on sensor networks. *IEEE Communications Magazine*, pages 102–114, Aug. 2002.

[11] S. Srinivasa and S. A. Jafar. The throughput potential of cognitive radio: A theoretical perspective. *IEEE Communications Magazine*, 45:73–79, May 2007.

[12] N. Abramson. The aloha system – another alternative for computer communications. In *Proceedings of AFIPS Conference*, 1970.

[13] Anthony Ephremides and Bruce Hajek. Information theory and communication networks: An unconsummated union. *IEEE Trans. Inform. Theory*, 44:2416–2434, 1998.

[14] Gaurav S. Kasbekar, Yigal Bejerano, and Saswati Sarkar. Lifetime and coverage guarantees through distributed coordinate-free sensor activation. In *Proceedings of ACM MobiCom*, Sep. 2009.

[15] J. Jeon and A. Ephremides. Neighbor discovery in a wireless sensor network: Multipacket reception capability and physical-layer signal processing. In *Proceedings of the Forty-Eighth Annual Allerton Conference*, Sep. 2010.

[16] P. Viswanath, D. N. C. Tse, and R. Laroia. Opportunistic beamforming using dumb antennas. *IEEE Transactions on Information Theory*, 48:1277–1294, 2002.

[17] R. Agrawal and V. Subramanian. Optimality of certain channel aware scheduling policies. In *Proceedings of the Fortieth Annual Allerton Conference*, Oct. 2002.

[18] Harold J. Kushner and Philip A. Whiting. Convergence of proportional-fair sharing algorithms under general conditions. *IEEE Trans. Wireless Communications*, 3(4):1250–1259, Jul. 2004.

[19] R. Agrawal, A. Bedekar, R. La, and V. Subramanian. A class and channel-condition based weighted proportional fair scheduler. In *Proceedings of ITC*, Sep. 2001.

[20] Xiangping Qin and Randall Berry. Distributed approaches for exploiting multiuser diversity in wireless networks. *IEEE Transactions on Information Theory*, 52(2):392–413, Feb. 2006.

[21] Srihari Adireddy and Lang Tong. Exploiting decentralized channel state information for random access. *IEEE Transactions on Information Theory*, 51(2):537–561, Feb. 2005.

[22] Y.-W. Hong, C.-K. Lin, and S.-H. Wang. On the stability of two-user slotted ALOHA with channel-aware cooperative users. In *Proceedings of 5th International Symposium on Modeling and Optimization in Mobile, Ad Hoc and Wireless Networks (WiOpt)*, Apr. 2007.

[23] A. Fanous and A. Ephremides. Transmission control of two-user slotted ALOHA over Gilbert-Elliott channel: Stability and delay analysis. In *Proceedings of IEEE International Symposium on Information Theory (ISIT)*, Aug. 2011.

[24] L. Tassiulas and A. Ephremides. Stability properties of constrained queueing systems and scheduling policies for maximum throughput in multihop radio networks. *IEEE Transactions on Automatic Control*, 37(12):1936–1948, Dec. 1992.

[25] M. J. Neely, E. Modiano, and C. E. Rohrs. Dynamic power allocation and routing for time-varying wireless networks. *IEEE Journal on Selected Areas in Communications*, 23(1):89–103, Jan. 2005.

[26] L. Georgiadis, M. J. Neely, and L. Tassiulas. Resource allocation and cross-layer control in wireless networks. *Foundations and Trends in Networking*, 1(1):1–149, 2006.

[27] M. J. Neely, E. Modiano, and Chih-Ping Li. Fairness and optimal stochastic control for heterogeneous networks. In *Proceedings of IEEE INFOCOM*, Mar. 2005.

[28] M. J. Neely. Energy optimal control for time varying wireless networks. *IEEE Transactions on Information Theory*, 52(7):2915–2934, Jul. 2006.

[29] M. J. Neely. Super-fast delay tradeoffs for utility optimal fair scheduling in wireless networks. *IEEE Journal on Selected Areas in Communications*, 24(8):1489–1501, Aug. 2006.

[30] M. J. Neely. Order optimal delay for opportunistic scheduling in multi-user wireless uplinks and downlinks. In *Proceedings of the 44th Annual Allerton Conference on Communication, Control, and Computing*, Sep. 2006.

[31] Long B. Le, Eytan Modiano, and Ness B. Shroff. Optimal control of wireless networks with finite buffers. In *Proceedings of IEEE INFOCOM*, 2010.

[32] A. Mekkittikul and N. McKeown. A practical scheduling algorithm to achieve 100% throughput in input-queued switches. In *Proceedings of IEEE INFOCOM*, 1998.

[33] Frank Kelly. Charging and rate control for elastic traffic. *European Transactions on Telecommunications*, 8:33–37, Dec. 1997.

[34] Frank Kelly, A. K. Maulloo, and D. K. H. Tan. Rate control for communication networks: shadow prices, proportional fairness and stability. *Journal of the Operational Research Society*, 49(3):237–252, Sep. 1998.

[35] S. H. Low and D. E. Lapsley. Optimization flow control-1: Basic algorithm and convergence. *IEEE/ACM Transactions on Networking*, 7(6):861–874, Dec. 1999.

[36] Jeonghoon Mo and Jean Walrand. Fair end-to-end window-based congestion control. *IEEE/ACM Transactions on Networking*, 8(5):556–567, Oct. 2000.

[37] W. Leland, M. Taqqu, W. Willinger, and D. Wilson. On the self-similar nature of ethernet traffic (extended version). *IEEE/ACM Transactions on Networking*, 2:1–15, Feb. 1994.

[38] V. Paxson and S. Floyd. Wide-area traffic: The failure of poisson modeling. *IEEE/ACM Transactions on Networking*, 3(3).

[39] M. E. Crovella and A. Bestavros. Self-similar in world wide web traffic: Evidence and possible causes. *IEEE/ACM Transactions on Networking*, 5(6).

[40] J. Beran, R. Sherman, M. S. Taqqu, and W. Willinger. Long-range dependence in viriable-bit-rate video traffic. *IEEE Transactions on Communications*, 43(2/3/4).

[41] Gennady Samorodnitsky. Long range dependence. *Foundations and Trends in Stochastic Systems*, 1(3):163–257, 2007.

[42] Steven A. Borbash, Anthony Ephremides, and Michael J. McGlynn. An asynchronous neighbor discovery algorithm for wireless sensor networks. *Ad Hoc Networks*, 5:998–1016, 2007.

[43] Sudarshan Vasudevan, Donald Towsley, Dennis Goeckel, and Ramin Khalili. Neighbor discovery in wireless networks and the coupon collector's problem. In *ACM MobiCom*, Beijing, China, Sep. 2009.

[44] S. Vasudevan, J. Kurose, and D. Towsley. On neighbor discovery in wireless networks with directional antennas. In *IEEE INFOCOM*, Miami, Florida, Mar. 2005.

[45] Michael J. McGlynn and Steven A. Borbash. Birthday protocols for low energy deployment and flexible neighbor discovery in ad hoc wireless networks. In *ACM MobiHoc*, Long Beach, California, Oct. 2001.

[46] I. R. Goodman, R. P. S. Mahler, and H. T. Nguyen. *Mathematics of Data Fusion*. Kluwer Academic Publishers, Dordrecht, The Netherlands, 1997.

[47] M. Zorzi and R. Rao. Capture and retransmission control in mobile radio. *IEEE Journal on Selected Areas in Communications*, 12(8):1289 – 1298, Oct. 1994.

[48] Gam D. Nguyen, Anthony Ephremides, and Jeffrey E. Wieselthier. On capture in random-access systems. In *IEEE ISIT*, Seattle, Washington, Jul. 2006.

[49] Christian Namislo. Analysis of mobile radio slotted aloha networks. *IEEE Journal on Selected Areas in Communications*, SAC-2(4):583 – 588, Jul. 1984.

[50] Bruce Hajek, Arvind Krishna, and Richard O. LaMaire. On the capture probability for a large number of stations. *IEEE Transactions on Communications*, 45(2):254–260, 1997.

[51] S. Ghez and S. Verdú. Stability property of slotted aloha with multipacket reception capability. *IEEE Transactions on Automatic Control*, 33(7):640 – 649, Jul. 1988.

[52] L. Tong, Q. Zhao, and G. Mergen. Multipacket reception in random access wireless networks: from signal processing to optimal medium access control. *IEEE Communications Magazine*, 39(11):108–112, Nov. 2001.

[53] V. Naware, G. Mergen, and L. Tong. Stability and delay of finite-user slotted aloha with multipacket reception. *IEEE Transactions on Information Theory*, 51(7):2636–2656, Jul. 2005.

[54] S. Verdú. *Multiuser Detection*. Cambridge University Press, 1998.

[55] David Tse and Pramod Viswanath. *Fundamentals of Wireless Communication*. Cambridge university press, Cambridge, United Kingdom, 2005.

[56] Andrea Goldsmith. *Wireless Communications*. Cambridge university press, Cambridge, United Kingdom, 2005.

[57] Wojciech Szpankowski. Stability conditions for some distributed systems: Buffered random access systems. *Advances in Applied Probability*, 26(2):498–515, Jun. 1994.

[58] R. M. Loynes. The stability of a queue with non-independent inter-arrival and service times. *Mathematical Proceedings of the Cambridge Philosophical Society*, 58(3):497–520, 1962.

[59] R. Rao and A. Ephremides. On the stability of interacting queues in a multi-access system. *IEEE Transactions on Information Theory*, 34(5):918–930, Sep. 1988.

[60] N. Pappas, J. Jeon, A. Ephremides, and A. Traganitis. Optimal utilization of a cognitive shared channel with a rechargeable primary source node. In *Proceedings of IEEE Information Theory Workshop (ITW)*, Oct. 2011.

[61] J. Jeon and A. Ephremides. On the stability of random multiple access with stochastic energy harvesting. *arXiv:1112.5995v2*, Nov. 2012.

[62] J. Jeon and A. Ephremides. Effect of channel estimation errors on the stability of channel-aware random access. In *Proceedings of IEEE ISIT*, Jul. 2012.

[63] N. Pappas, J. Jeon, A. Ephremides, and A. Traganitis. Wireless network-level partial relay cooperation. In *Proceedings of IEEE ISIT*, Jul. 2012.

[64] R. Urgaonkar and M. J. Neely. Opportunistic scheduling with reliability guarantees in cognitive radio networks. *IEEE Transactions on Mobile Computing*, 8(6):766–777, Jun. 2009.

[65] R. Urgaonkar and M. J. Neely. Opportunistic cooperation in cognitive femtocell networks. *To appear in the IEEE Journal on Selected Areas in Communications*.

[66] S. Kompella, G. D. Nguyen, J. E. Wieselthier, and A. Ephremides. Stable throughput tradeoffs in cognitive shared channels with cooperative relaying. In *Proceedings of IEEE INFOCOM*, Apr. 2011.

[67] Y.-C. Liang, Y. Zeng, E. C. Y. Peh, and A. T. Hoang. Sensing-throughput tradeoff for cognitive radio networks. *IEEE Transactions on Wireless Communications*, 7(4):1326–1337, Apr. 2008.

[68] T. Yucek and H. Arslan. A survey of spectrum sensing algorithms for cognitive radio applications. *IEEE Communications Surveys & Tutorials*, 11(1):116 – 130, First Quarter 2009.

[69] T. Zhang and D. H. K. Tsang. Optimal cooperative sensing scheduling for energy-efficient cognitive radio networks. In *Proceedings of IEEE INFOCOM*, Apr. 2011.

[70] IEEE 802.22 Wireless RAN. Funtional requirements for the 802.22 WRAN standard, IEEE 802.22-05/0007r46. Oct. 2005.

[71] H. Vincent Poor. *An Introduction to Signal Detection and Estimation*. Springer-Verlag, New York, 2 edition, 1994.

[72] J. Jeon, K. Son, and S. Chong. Spatial resource reuse in the multi-hop cellular networks: Difficulties and benefits. In *Proceedings of IEEE GLOBECOM*, Nov. 2008.

[73] J. Oh and W. Choi. A hybrid cognitive radio system: a combination of underlay and overlay approaches. In *Proceedings of IEEE VTC*, Sep. 2010.

[74] J. Hu, L.-L. Yang, and L. Hanzo. Optimal queue scheduling for hybrid cognitive radio maintaining maximum average service rate under delay constraints. In *Proceedings of IEEE GLOBECOM, Cognitive Radio and Networks Symposium*, Dec. 2012.

[75] S. Kompella, G. D. Nguyen, J. E. Wieselthier, and A. Ephremides. Impact of channel state information on the stability of cognitive shared channels. In *Proceedings of IEEE INFOCOM Mini-Conference*, Mar. 2012.

[76] B. S. Tsybakov and V. A. Mikhailov. Ergodicity of a slotted aloha system. *Problems of Information Transmission*, 15(4):301–312, 1979.

[77] W. Luo and A. Ephremides. Stability of *N* interacting queues in random-access systems. *IEEE Transactions on Information Theory*, 45(5):1579–1587, Jul. 1999.

[78] Charles Bordenave, David McDonald, and Alexandre Proutiere. Asymptotic stability region of slotted Aloha. *IEEE Transactions on Information Theory*, 58(9):5841–5855, Sep. 2012.

[79] Olivier Cappé, Eric Moulines, Jean-Christophe Pesquet, Athina Petropulu, and Xueshi Yang. Long-range dependence and heavy-tail modeling for teletraffic data. *IEEE Signal Processing Magazine*, 19(3):14 – 27, May 2002.

[80] L. Kleinrock. *Queueing Theory, Volume I: Theory*. Wiley, 1975.

[81] Sheldon M. Ross. Bounding the stationary distribution of the $M/G/1$ queue size. *Probability in the Engineering and Informational Sciences*, 20(4):571 – 574, Oct. 2006.

[82] S. H. Wang, C.-K. Lin, and Y.-W. Peter Hong. On the stability and delay of channel-aware slotted ALOHA with imperfect CSI. In *Proceedings of IEEE International Conference on Communications (ICC)*, 2008.

[83] S. H. Wang and Y.-W. Peter Hong. Transmission control with imperfect CSI in channel-aware slotted ALOHA networks. In *Proceedings of IEEE International Conference on Communications (ICC)*, 2009.

[84] L. Tassiulas and A. Ephremides. Dynamic server allocation to parallel queues with randomly varying connectivity. *IEEE Transactions on Information Theory*, 39(2):466–478, Mar. 1993.

[85] Long B. Le, K. Jagannathan, and Eytan Modiano. Delay analysis of maximum weight scheduling in wireless ad hoc networks. In *Proceedings of Conference on Information Sciences and Systems (CISS)*, 2009.

[86] M. J. Neely. Delay analysis for maximal scheduling with flow control in wireless networks with bursty traffic. *IEEE/ACM Transactions on Networking*, 17(4):1146–1159, Aug. 2009.

[87] S. Asmussen. *Applied Probability and Queues*. Springer-Velag, New York, 2003.

[88] L. Tassiulas. Scheduling and performance limits of networks with constantly changing topology. *IEEE Transactions on Information Theory*, 43(3):1067–1073, May. 1997.

[89] Dimitri Bertsekas and Robert Gallager. *Data Networks*. Prentice Hall, Saddle River, NJ, 1992.

[90] Andreas M. Ali, Ralph Hudson, Flavio Lorenzelli, and Kung Yao. *A Random Finite Set Approach to Joint Estimation/Detection/Tracking/Fusion in a Wireless Sensor Network*. Research Report, University of California, Los Angeles, 2008.

[91] Matti Vihola. *Random Sets for Multitarget Tracking and Data Fusion*. Licentiate Thesis, Tampere University of Technology, 2004.

[92] Ronald P. S. Mahler. Engineering statistics for multi-object tracking. In *IEEE Workshop on Multi-Object Tracking*, Vancouver, Canada, Jul. 2001.

[93] Ronald P. S. Mahler. Random sets: Unification and computation for information fusion–a retrospective assessment. In *The 7th International Conference on Information Fusion*, Stockholm, Sweden, Jul. 2004.

[94] Ronald P. S. Mahler. *Statistical Multisource-Multitarget Information Fusion*. Artech House, Norwood, MA, 2007.

[95] Ezio Biglieri and Marco Lops. Multiuser detection in a dynamic environment-part 1: User identification and data detection. *IEEE Transactions on Information Theory*, 53(9):3158 – 3170, Sep. 2007.

[96] Alberto Leon-Garcia. *Probability and Random Processes for Electrical Engineering*. Addison-Wesley Publishing Company, Reading, MA, 2 edition, 1994.

[97] XBOW MICAz Mote Specifications.

[98] William Stallings. *Wireless Communications and Networks*. Pearson Prentice Hall, Upper Saddle River, NJ, 2 edition, 2005.

[99] N. Pappas, J. Jeon, A. Ephremides, and A. Traganitis. Optimal utilization of a cognitive shared channel with a rechargeable primary source node. *Journal of Communications and Networks, Special Issue on Energy Harvesting in Wireless Networks*, 14(2):162–168, Apr. 2012.

[100] Edward C. Van Der Meulen. Three-terminal communication channels. *Advances in Applied Probability*, 3(1):pp. 120–154, 1971.

[101] A.K. Sadek, K.J.R. Liu, and A. Ephremides. Cognitive multiple access via cooperation: Protocol design and performance analysis. *IEEE Transactions on Information Theory*, 53(10):3677 –3696, 2007.

[102] B. Rong and A. Ephremides. Protocol-level cooperation in wireless networks: Stable throughput and delay analysis. In *In Proceedings of 7th International Symposium on Modeling and Optimization in Mobile, Ad Hoc, and Wireless Networks (WiOpt)*, 2009.